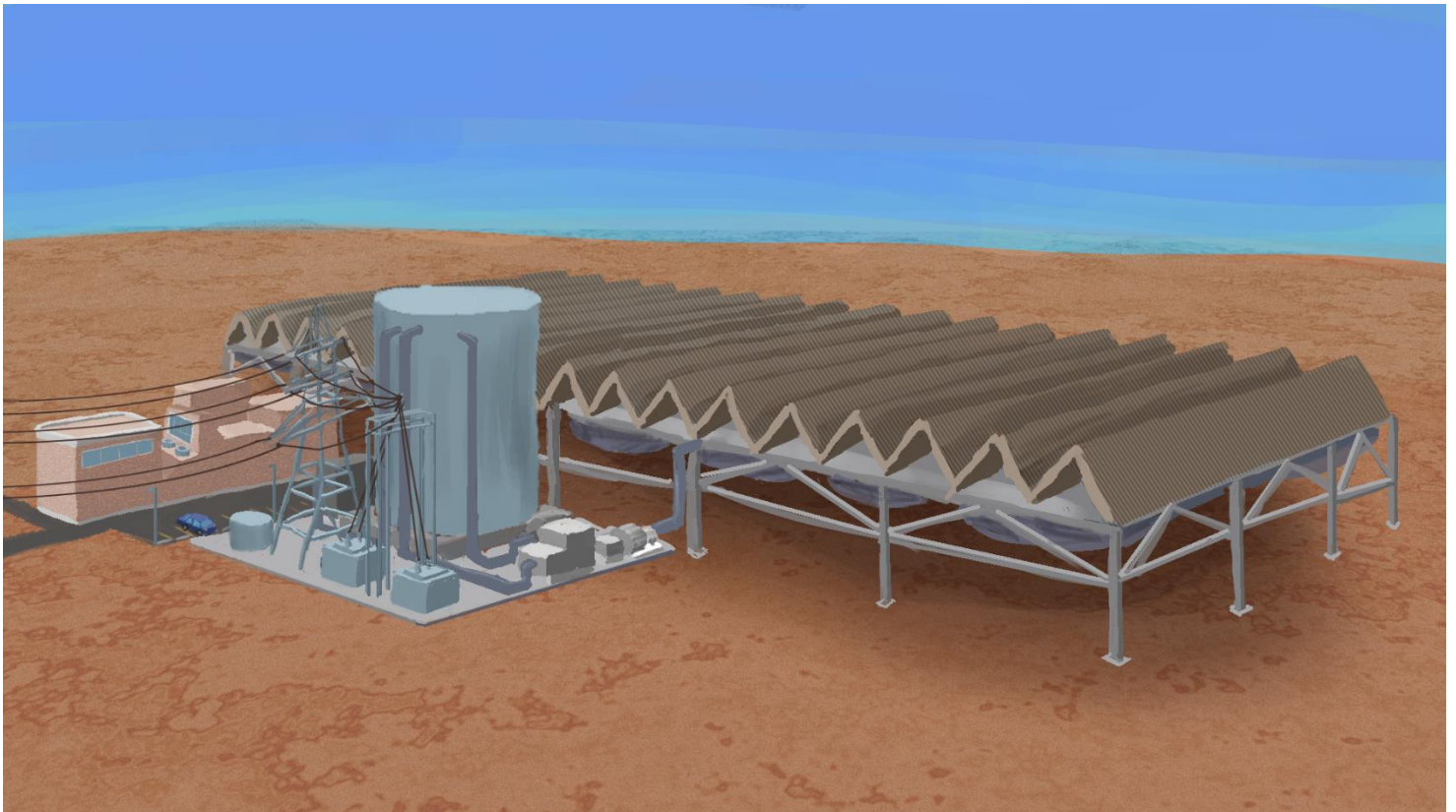


Modular Atomic Energy Reactor Device Final Design Report



DREAM Plant Layout

Andy Wolf
Eliza Mitchell
Gustave Granroth
Michael Chizhevsky

Faculty Advisors: John Murphy
Tim Bohm
Tom McGlamery

Submission Date: May 11, 2014

Acknowledgements

The authors would like to acknowledge the following individuals for their generous assistance provided to the authors in the course of completing the DREAM design.

- John Murphy: For directing the authors to design aspects needing special attention and for organizing the structure of the senior design course.
- Tim Bohm: For assisting the authors in debugging MCNP geometry errors and instructing the authors on proper use of MCNP5 and MCNP6.
- Tom McGlamery: For assistance with preparation, organization, and formatting of the reports and presentations.
- Paul Wilson: For providing MCNP support and instruction in NE 506.

The authors would also like to acknowledge their families for supporting them to this point in their careers and their teachers for providing the knowledge required to undergo this design project.

The cover image is provided courtesy of Lawrence Granroth, who donated time and effort to translate the authors' rough sketches of the DREAM plant layout into a work of art.

1	Introduction	1
	Motivation	1
	Design Objectives	2
	Proposed Design Overview	3
	Document Outline	5
2	Design Methodology	5
	Existing Designs Overview	5
	Design Modularity	8
	<i>Thermodynamic Cycle</i>	8
	<i>Steam Generator Design</i>	11
	<i>Condenser Design</i>	12
	<i>Reactor Core Design</i>	14
	<i>Reactor Pressure Vessel (RPV) Design</i>	24
	<i>Containment Design</i>	27
	Design Safety	29
	Non-Electrical Applications	30
3	Design Analysis	30
	<i>Thermodynamic Cycle Inefficiencies</i>	31
	<i>Steam Generator Sizing and Pressure Loss</i>	33
	<i>Condenser Pressure and Energy Loss</i>	36
	<i>Reactor Core Analysis</i>	37
	<i>Spent Fuel</i>	42
	<i>RPV Strength and Natural Circulation</i>	44
	<i>Removable Core Module Structure</i>	45
	<i>Containment Strength and Shielding</i>	45
	Design Safety	47
	Design Economics	48
	Design Transportation	54
4	Conclusion	55
	Proposed Design Comparisons	55
	Future Work	56
5	References	57
6	Design Specifications	64
7	Glossary	69
8	Appendices	72

Executive Summary

Although large-scale nuclear power plants provide a large portion of the baseload electricity in the United States, these power plants are tied to the electrical grid. Therefore, these power plants are unable to provide power during natural disasters when the electrical grid is inoperable and cannot be transported to provide power to remote locations of the world. In addition, these reactors are usually custom-built on-site, and refuel in a period of several weeks where each individual fuel assembly is removed and relocated.

One alternative to large-scale nuclear power plants is small modular reactors (SMRs). By definition SMRs are small, composed of at one fuel module among other modules, and capable of providing a large amount of electricity or process heat. This report details the development and analysis of the DREAM design, a SMR designed to fit in 38 semi-trailers, provide electricity to 23,000 U. S. homes for 3 years (29.2 MWe in total) without refueling, and refuel in one eight-hour work-day. In addition, the DREAM design implements several safety features not found in large-scale power plants, such as natural circulation for reactor core cooling and a passive decay heat removal system. Finally, the DREAM design can operate in remote locations without access to water through the use of a dry condenser, with the entire design fitting in 1.5 acres.

Although the DREAM design has been heavily-analyzed to verify the safety and economics of the design, the authors have several additional analyses to complete before an actual DREAM can be built. However with the analysis already performed, the authors are confident the DREAM design is economically-competitive to alternative SMRs and fossil-fuel based systems, as safe as current LWRs, and readily-transportable to remote locations. In conclusion, the DREAM design as analyzed satisfies all the requirements for a small modular reactor and merits consideration for future design work.

The Modular Atomic Energy Reactor Device (DREAM) represents the design work of the authors undertaken for Nuclear Engineering 412 (Senior Design) at the University of Wisconsin -- Madison. The DREAM outputs 29.2 MW of electricity continuously with a three-year refueling cycle, uses proliferation-resistant 4.95% low-enriched uranium, and can be used for alternative generation purposes such as desalination and localized heating and cooling applications.

Motivation

Small Modular Reactors, defined as typically producing less than 300 megawatts-electric (MWe) or less than 1,000 *megawatts-thermal*⁺ (MWth), are currently under investigation for possible use in targeted applications.¹ These reactors are constructed from standardized modules, the most important module being an easily-removable fuel assembly for quick and simple refueling. With the smallest nuclear power plant in America producing 1,500 MWth (megawatts-thermal), none of the nation's nuclear power plants can be considered small.² These reactors also typically refuel in stages by removing each reactor *fuel assembly*, instead of removing all the assemblies at once as a module. Whereas 500 to 2000 MWe nuclear power plants reach high efficiencies near 40% thermal, SMRs instead provide specialized capabilities rather than economy of scale.

In contrast to large land-based power stations, SMRs can be portable, as is the KLT-40S Russian icebreaker reactor depicted in **Figure 1**. Portable nuclear reactors provide a compact, cost-competitive electricity source in remote environments, where fossil-fuel or renewable power plants are located. Additionally, while land-based power stations are reliant upon a large-scale electrical grid, off-grid SMRs could power a medium-sized city. This capability allows SMRs to potentially function as localized power supplies after natural disasters or terrorist attacks, when transmission capabilities are impacted.

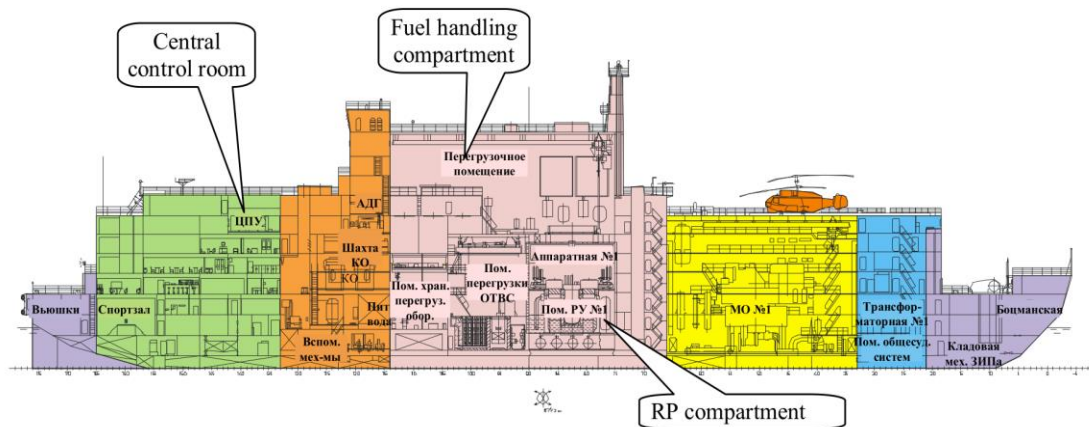


Figure 1: KLT-40S icebreaker-based SMR for electricity and steam generation.³

⁺All italicized words and phrases will be defined in the **Glossary**.

Due to the customization possible with SMRs, specialized SMRs can also be used in hydrogen production, desalination, and city-wide heating and cooling.¹ Depending on the efficiency of the designed SMR, these processes can either operate on waste heat or from generated electricity.

SMRs are designed so that large components can be easily removed and replaced. Proper modularization makes each major component of the system simpler by reducing interdependencies between modules, thereby reducing the initial capital cost for a SMR.¹ Modularization also allows for higher standardization of components, more robust modules, and easier, less frequent maintenance.⁴ NuScale's SMR design considers the reactors themselves as modules and uses 12 to form a large-scale, highly-redundant, potentially load-following facility shown in **Figure 2**. When the reactor core is a separate module, nations without nuclear enrichment capability can benefit from SMR technology by exchanging a used fuel module for a new fuel module from an enrichment-capable nation.

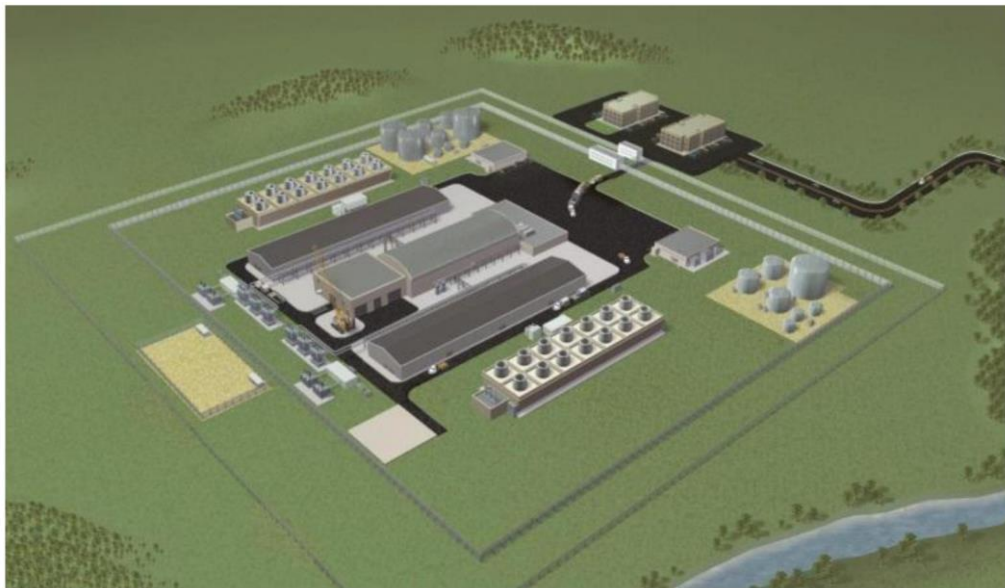


Figure 2: NuScale land-based 12 unit SMR for electricity generation.⁵

Design Objectives

With the varied usage scenarios provided by SMRs, the required design objectives are understandably broad. The objectives as specified for DREAM⁶ are as follows:

- Minimum of 100 MWth power, usable for any purpose.
- Minimum of 3 years between refueling.
- Maximum of 6 weeks for refueling in the summer months.
- Retrievable fuel module.
- Competitive design in reliability, safety, and economics.

Overall, these objectives are consistent with the motivations discussed above. However, in addition to the required objectives, the authors include the following desired objectives:

- Very Small -- DREAM design is transportable by semi-trucks.
- Completely Modular -- All major components are broken up into subsystems.

These two desired features are not necessary for designing a small modular reactor -- a “small module” may be roughly the length of a Boeing 737-100 airplane.^{7,8} But the authors used all listed constraints in designing the DREAM, so these additional objectives will be emphasized in the proposed design.

Proposed Design Overview

The authors propose the following system-level DREAM design, listed in **Figure 3** and discussed below, as a design solution to the proposed design objectives and motivations.

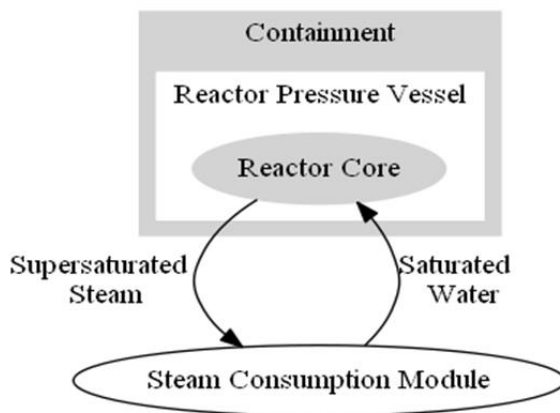


Figure 3: Block Diagram of the DREAM.

The DREAM is organized into three primary modules, with two steam consumption modules for application-specific purposes. The primary modules (reactor core, reactor pressure vessel, and containment) form a high-level steam generation module, whereas the secondary modules (for steam heating and for electrical generation) consume the steam produced. Although nesting the primary modules increases the difficulty in performing maintenance to the *reactor pressure vessel* (RPV) and *reactor core*, nesting shields each layer from the radiation emitted from the reactor core. With this design, the DREAM can either provide electricity or process heat, but not both simultaneously.

Overall, the DREAM is a *pressurized light-water reactor* (PWR) operating at 75 atm *primary-loop* pressure with *natural circulation* for reactor core cooling. To provide 100 MWth output power for three years without refueling, the DREAM operates with 4,123 *fuel pins* of 4.95% enriched *uranium oxide* arranged in 19 hexagonal assemblies, as shown in **Figure 4**. The lattice of assemblies is surrounded by a natural graphite *reflector*, bringing the total core diameter to 1.50 m. With the fuel rods having a height of 1.34 m, plus an additional 14.4 cm of graphite above and below each fuel rod, the total core height is 1.63 m. Finally, each assembly is surrounded by a *boron carbide* (B_4C) hexagonal *control blade* capable of isolating each assembly from the whole reactor core to safely control the DREAM core.

Because the DREAM uses a once-through fuel cycle, the depleted fuel leaves the reactor through a complete replacement of the removable reactor core module. Replacing the removable core module can be completed in roughly one work-day (8 hours), during an estimated one week maintenance and refueling time. The short core replacement time is made possible by the *Removable Core Module Structure* (RCMS), which supports the core during normal operation. During refueling, the control blades are locked in their all-in position to the RCMS, and the RCMS is unbolted from the main reactor pressure vessel (RPV) structure. The RCMS then guides the core out of the RPV inner shell, allowing for easy replacement of the entire core and all the control blades. This procedure is described in more detail in the *RPV Design* section.

Because the DREAM operates at a lower primary-loop pressure than typical PWRs, the electrical generation module is based upon a Rankine-with-reheat cycle operating at a high

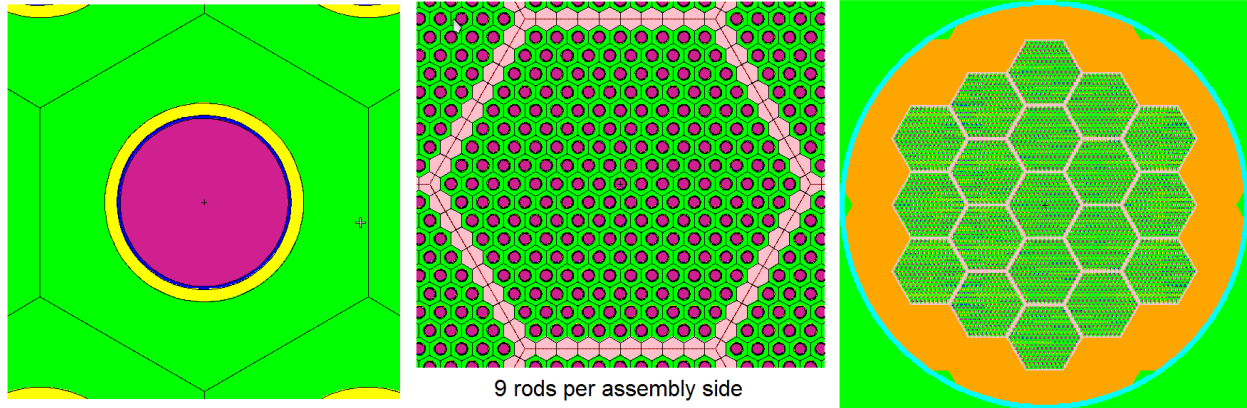


Figure 4: Top-views from left to right: DREAM fuel rod, assembly, and reactor core.

pressure of 47 atm, reheat pressure of 11.5 atm, and *condenser* pressure of 0.28 atm. To prevent deterioration of the turbines, the steam exit quality of the high-pressure turbine is 90.5% and the steam exit quality of the low-pressure turbine is 90.4%. This thermodynamic cycle provides a theoretical efficiency of 33.0%, which is reduced to 29.2% through pressure losses and component inefficiencies. In contrast to the electrical generation module, the steam generation module uses the reactor output heat without conversion and cannot be compared directly to the electrical generation module. Because the DREAM exceeds 20% electrical efficiency, performing desalination with electricity is more efficient than with waste heat.⁹ Therefore, the

steam generation module will likely be used for only localized heating and cooling.

To preclude the use of active pumps for core cooling, the authors designed the reactor pressure vessel to support natural circulation. The RPV, shown in **Figure 5**, is constructed from stainless steel 316 (SS-316) with a total height of 11.02 m and outer radius of 1.70 m. Although the RPV was designed to support the 75 atm primary-loop pressure, the RPV can withstand a maximum pressure of 112 atm under accident scenarios.

In case of a failure, the authors also designed an outer *containment* structure capable of preventing the leakage of radioactive material. The containment is also constructed from SS-316 with a total height of 15 m and outer radius of 4.16 m. Under normal conditions the containment is maintained at atmospheric pressure, with water filling the containment up to 5 m to prevent excessive radiation exposure outside of the containment. However, this fill water also helps remove *decay heat* during a loss-of-power accident. During an accident, such as an RPV structural

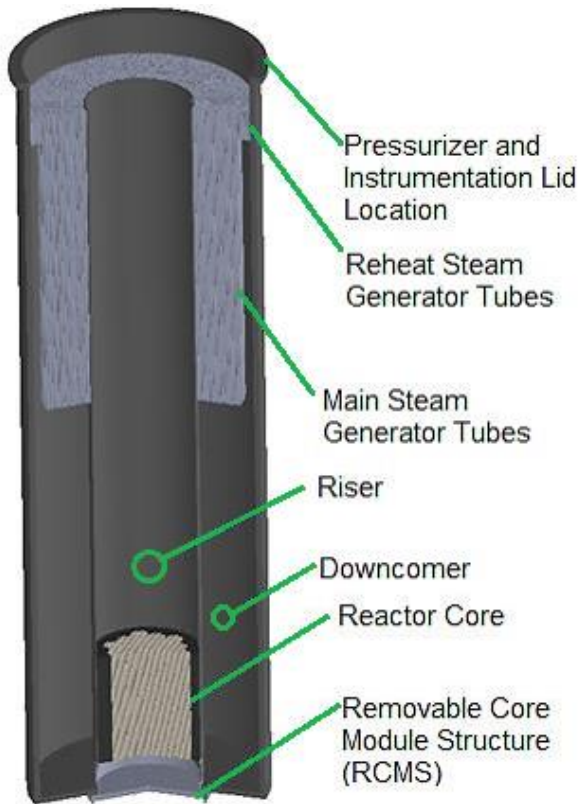


Figure 5: RPV cutout image showing the *steam generator*, reactor core, and RCMS.

breach, the containment was designed to withstand 20 atm of pressure with a maximum structural pressure of 30 atm.

The DREAM design makes economic sense, with an estimated construction cost of \$196.4 million (2013 USD), yearly operation cost of \$8.94 million, and *levelized cost of electricity* of 39 mills/kWh with 70 employees to 110 mills/kWh with 280 employees. Because the levelized cost of electricity for the DREAM design is heavily dependent upon the number of employees, the authors consider the DREAM to be economically competitive to a new light-water reactor (LWR) having a levelized cost of electricity of 86.1 mills/kWh.¹⁰ This design is also economically-comparable to other SMR designs such as Toshiba's \$80 million, 10 MWe 4S reactor.¹¹ The DREAM design is also readily-transportable, fitting in 38 semi-trailers by weight or 24 by volume. Although the entire DREAM design does not fit into a commercial airplane, the design can be transported in 11 Boeing 747-8F cargo planes.

In addition to inducing natural circulation in the primary-loop, the DREAM increases design safety and proliferation resistance through operating at a lower primary pressure, the use of *low-enriched uranium* (LEU) of less than 5% enrichment, and system modularization. The DREAM design also follows defense-in-depth principles by using an outer containment, inner RPV, and fuel cladding to prevent leakage of radioactive material. Overall, the DREAM satisfies all the required and desired design objectives.

Document Outline

The following **Design Methodology** section covers the design of the DREAM and the design process of the authors in creating the DREAM, along with minor calculations. The **Design Analysis** section covers in-depth analysis of all the DREAM components and lists the economic and transportation analyses performed for the entire DREAM design. The **Conclusion** section covers a comparison of the DREAM design to other existing designs and details future work necessary in validating the DREAM design. Finally, the **Design Specifications** section lists detailed numerical and qualitative data summarizing the DREAM design.

2 Design Methodology

After initial research, the authors began designing the DREAM by starting from the outermost system—the thermodynamic cycle—and the innermost system—the reactor core. The reactor pressure vessel (RPV) was then designed to merge the innermost and outermost designs. Finally, the containment was designed to protect against RPV failures, shield the radiation emitted from the reactor core, and hold cooling water for decay heat removal. This section's structure mirrors the design process of the authors. For reference, detailed DREAM design specifications are listed in the **Design Specifications** section.

Existing Designs Overview

The authors began designing the DREAM by reviewing literature on several variants of SMRs, including *boiling-water reactors* (BWR), pressurized-water reactors (PWR), *fast reactors*, and *high-temperature gas reactors* (HTGR).¹ Because the authors wanted to explore improvements upon current technology and not create an entirely new reactor variant, the decision was made to design a thermal, light-water PWR. Although the authors considered

designing a BWR, modularization is more difficult because BWRs normally drive the turbine from the boiled—and therefore radioactive—primary-loop water. Separating the primary-loop into a separate loop would require a steam-to-steam heat exchanger in that loop, which would be too large for practical purposes.

Research of four other PWR-based SMRs was then conducted, the results of which is summarized in **Table 1**. All of these PWRs use less than 5% LEU fuel and integrate the pressurizer, steam generator, and control rods (with drives) inside the RPV. However, IRIS is the only design which does not induce natural convection for the primary-loop, likely because its thermal output is higher than that of the other designs.

Table 1: Summary of data on the NuScale, mPower, IRIS, and MODULUS designs.^{7, 12, 13, 14}

<i>Reactor Design</i>	<i>Primary Pressure (atm)</i>	<i>Thermal Output (MWth)</i>	<i>Efficiency (MWe/MWth)</i>	<i>Fuel Design</i>
NuScale	127.6	160	28.1 %	37 17x17 bundles, ½ normal height active
mPower	139.2	530	34.0 %	69 17x17 bundles, 2.41 m active height
IRIS	153.0	1000	33.5 %	89 17x17 bundles, 4.27 m active height
MODULUS	157.9	175	26.6 %	21 17x17 bundles, 2.20 m active height

While these designs span a wide range of thermal outputs, the fuel design remains the same for all designs; only the number of bundles change. The efficiency for all these designs is also about the same, around 30%. To keep the DREAM portable, the authors decided to design DREAM for the lowest permissible thermal power output—100 MWth—which is closest to the 160 MWth NuScale design and 175 MWth MODULUS design.

The authors also noted that for all four SMR designs, the primary-loop pressure remained close to the 150 atm of a large-scale PWR. Because PWRs operate without boiling the primary-loop water, a higher pressure increases the temperature at which boiling occurs, which increases the maximum thermal efficiency. However, as is shown in **Figure 6**, each doubling in pressure only results in a nearly linear increase in efficiency. Higher pressures also require stronger and larger system components and increase the danger, should a break occur. Therefore, because operating at a lower system pressure allows for smaller components and increased safety, yet also provides a reasonable efficiency, the authors chose to operate the primary loop at 75 atm.

After reviewing the design of the reactor core, the authors realized that the DREAM core appeared similar to the SP-100 reactor core. A side-by-side visual is provided in **Figure 7**, with key feature callouts. Although there is similar hexagonal patterns visible in the SP-100 and DREAM reactor core designs, these designs are dissimilar in nearly all other features. **Table 2** lists the differences between these two designs, and purposes of each major component.

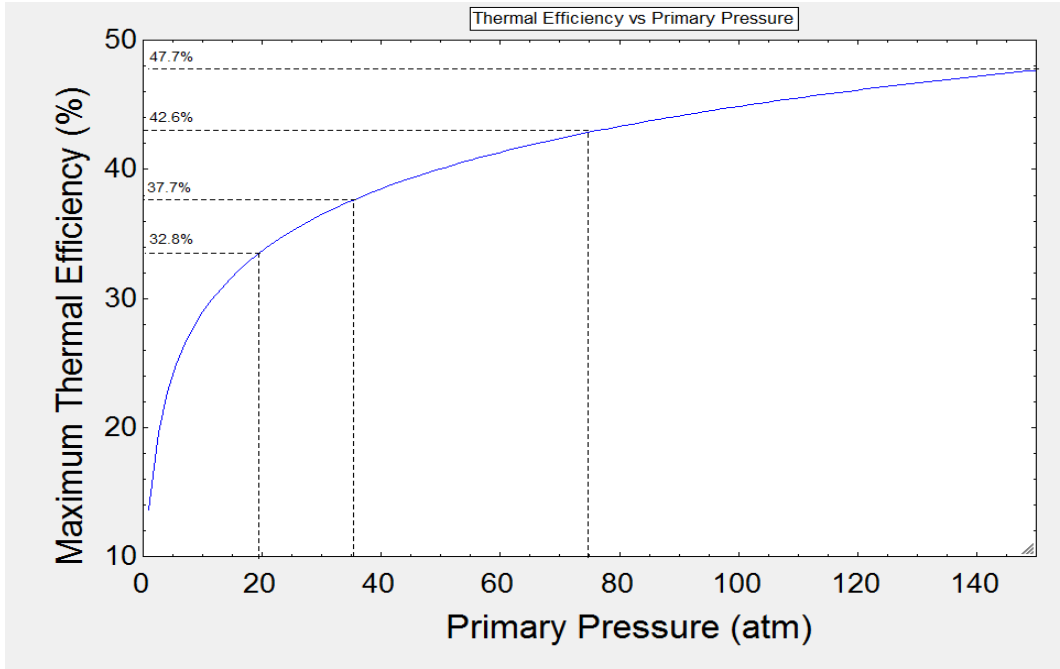


Figure 6: Maximum Thermal Efficiency versus the Primary-Loop Pressure.

Figure 7: SP-100¹⁵ and DREAM reactor cores.

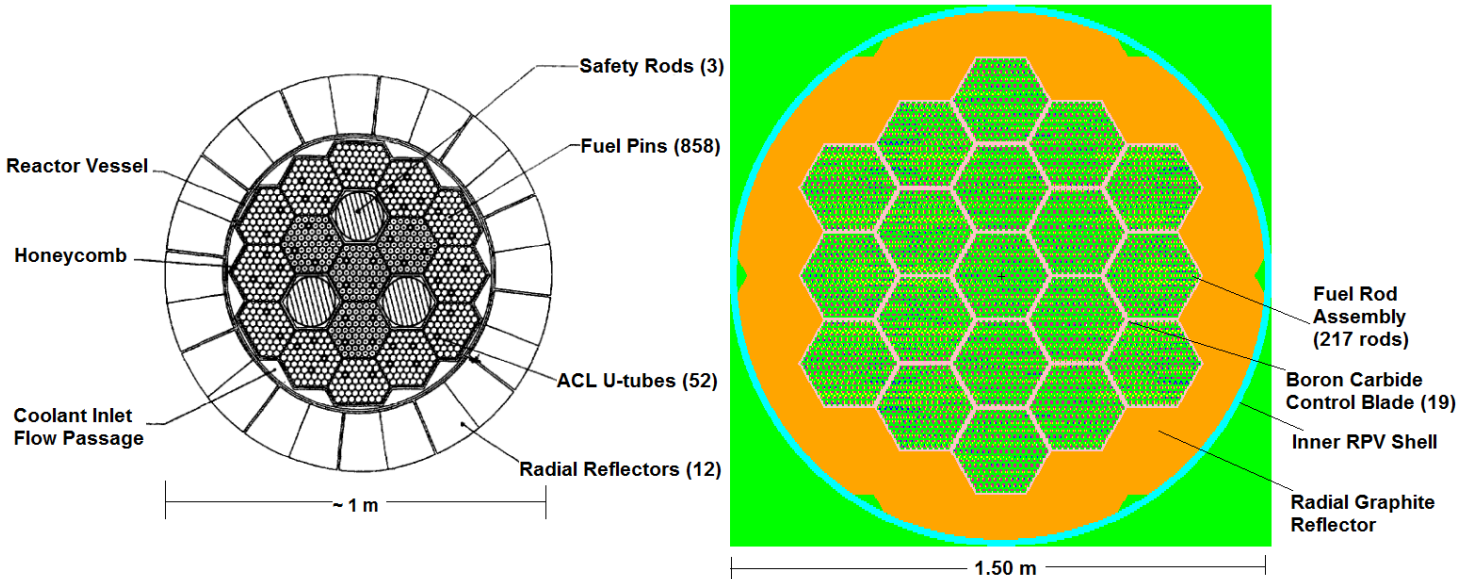


Table 2: SP-100 and DREAM reactor core differences

Parameter	SP-100 Reactor Core ¹⁵	DREAM Reactor Core
Operating Regime	Fast Reactor	Thermal Reactor
Coolant	Lithium	Light Water
Control	3 Safety Assemblies	19 Hexagonal Blades
Reflector Purpose	Removable for control, softens radial flux	Softens radial flux
Thermal Power	2.4 MWth	100 MWth

Design Modularity

Surprisingly, all four explored designs and the DREAM design consisted of closely-related modular designs shown in **Figure 8** which follow the block diagram depicted in **Figure 3**. These similarities arise in part from the desire to leverage thermodynamic effects, such as buoyancy effects, and design constraints, such as integrating common components into the RPV. In the DREAM design the steam generator and pressurizer are inside the RPV, as it is in the four existing designs. However, the control mechanisms and drives are outside of the RPV, because the lower primary-loop pressure reduces the risk of breaks occurring near punctures in the RPV.

Inside the DREAM RPV, the reactor core is located at the bottom of the RPV to harness buoyancy effects for natural circulation. By keeping the control mechanisms and drives outside of the RPV, one replaces the reactor core module by pulling it out of the bottom of the RPV, similar yet simpler than NuScale's core removal procedure which involves removing larger segments of the RPV.¹³

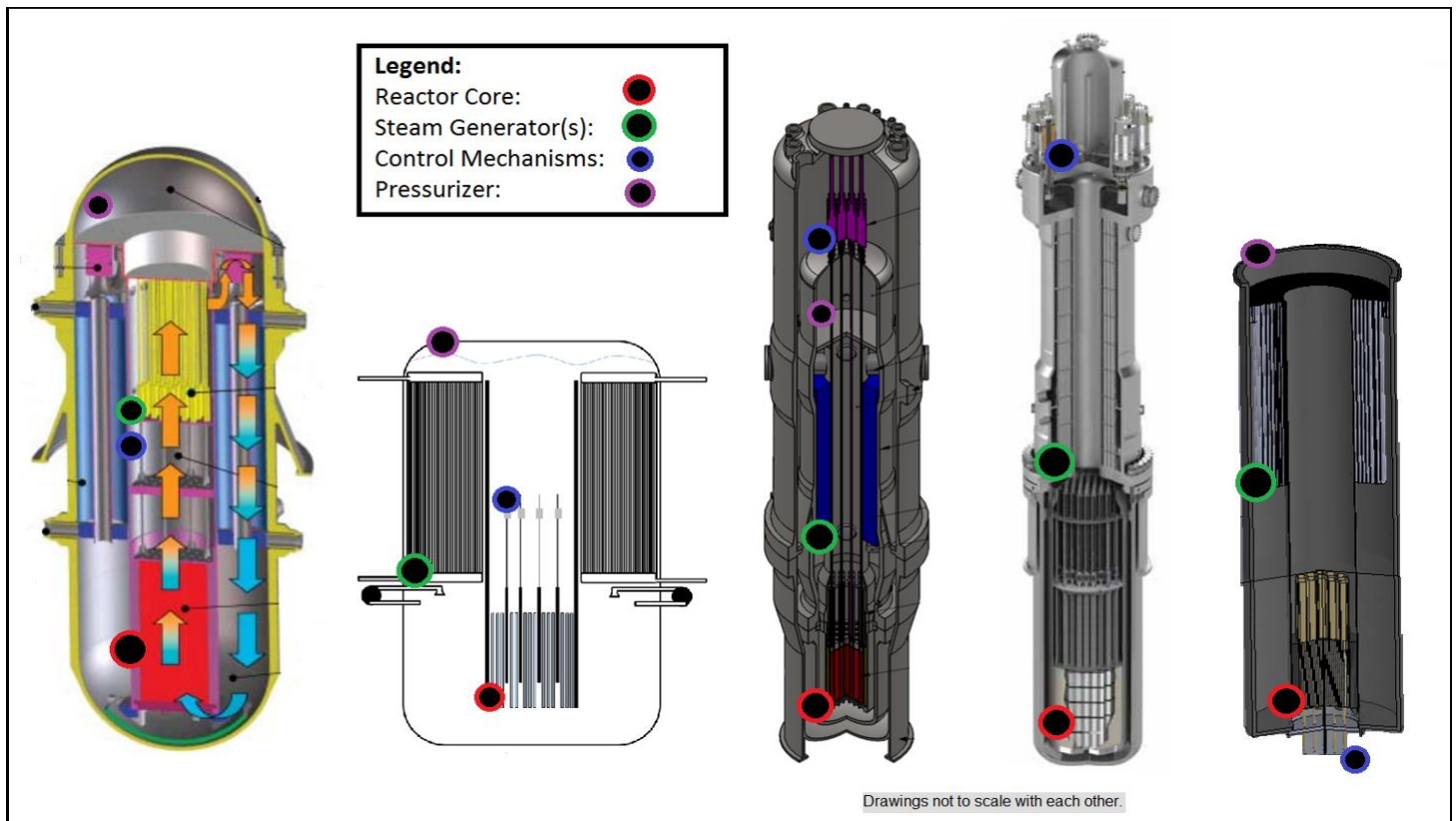


Figure 8: Left-to-Right: IRIS, MODULUS, NuScale, mPower, and DREAM RPV cutouts.^{7, 12, 13, 14}

Thermodynamic Cycle

The authors began designing the thermodynamic cycle by starting at a basic Rankine cycle, which was chosen for its efficiency, being superior to the efficiency of direct thermoelectric conversion. While direct thermoelectric conversion requires no moving parts in the thermodynamic cycle, the electrical efficiency is very low (4.2 % for the SP100¹⁵).

The authors first analyzed a simple Rankine cycle depicted in **Figure 9**, having no

additional components. With the primary-loop pressure set at 75 atm, the *saturation temperature* of water is 291.4 °C. To avoid boiling the RPV water, the author set the bulk core outlet temperature at 290 °C. For an initial analysis, the authors assumed a perfect heat exchanger for the primary-loop and therefore used 290 °C as the hot temperature for the Rankine cycle. Because the DREAM design should operate in remote locations, the cold temperature for the Rankine cycle was chosen to be 50 °C (122 °F), which is near the maximum recorded temperature in the Sahara desert.¹⁶

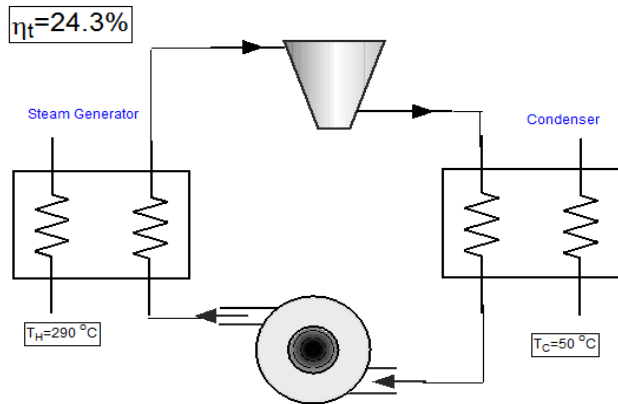
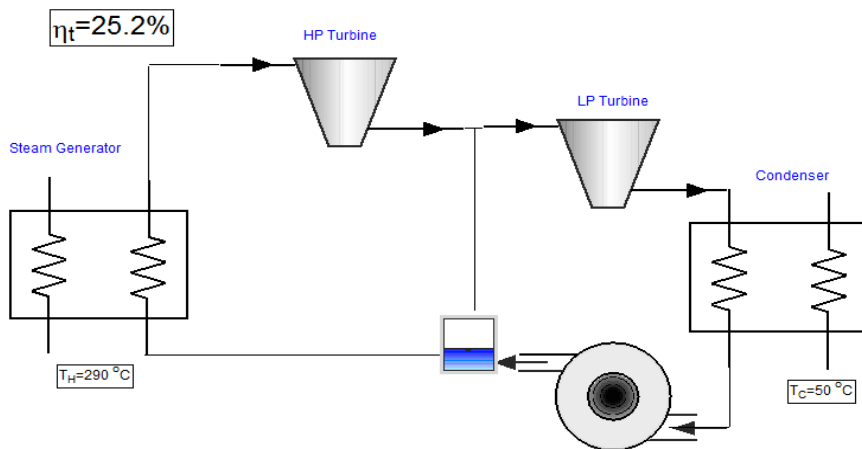


Figure 9: Simple Rankine Cycle.

With these chosen low and high temperatures, the theoretical maximum efficiency from a heat engine (Carnot cycle) was found to be 42.6 %. However, because the turbine in the Rankine cycle must have an exit quality greater than 90 % to prevent rapid deterioration¹⁷, the thermal efficiency for the simple Rankine cycle was determined to be 24.3 %.

One way to improve the Rankine cycle is to add regeneration so that a portion of the steam leaving the turbine is used to preheat the input fluid to the steam generator.¹⁷ **Figure 10** depicts the

analyzed Rankine-with-regeneration cycle. While this cycle does add the complexity and size of an additional turbine and mixing chamber, the thermal efficiency increases 0.9 % with these components when both turbines are restricted to steam with a non-destructive exit quality.



Another way to improve the Rankine cycle is to add reheat, so that the exiting high-pressure (HP) steam is sent through a secondary steam generator which feeds a low-pressure (LP) turbine.¹⁷ While this design requires an additional steam generator, Rankine-with-reheat removes the mixing chamber and

dramatically increases the efficiency to 33.0 %. The authors chose this thermodynamic cycle for its high efficiency and minimal complexity. For reference, this cycle is displayed in **Figure 11**, with detailed thermodynamic information listed in **Table 44** in **Appendix B** and the *EES code* used to analyze this cycle listed in **Appendix C**. Adding regeneration to Rankine-with-reheat increases the efficiency to 33.9 %. However, due to the added cost and size of the mixing chamber, the authors decided not to use a combined Rankine-with-regeneration-and-reheat cycle.

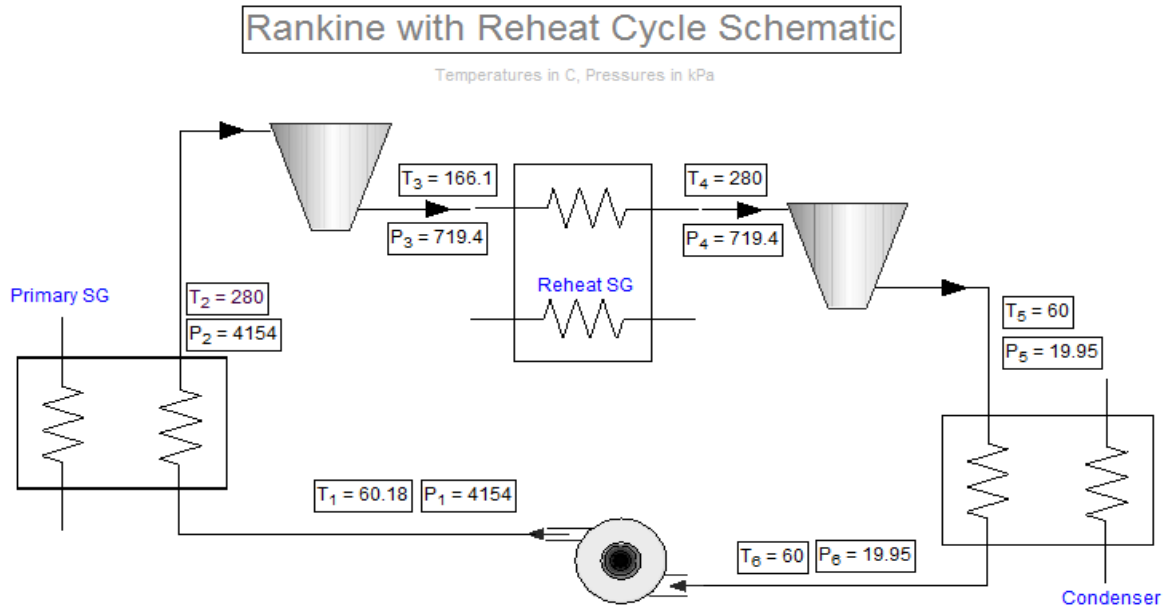


Figure 11: DREAM Electricity Generation Thermodynamic Cycle (Rankine with Reheat).

With ideal components and operation, **Figure 12** shows the temperature-entropy (T-s) diagram for the Rankine-with-reheat cycle and indicates the high and reheat pressures required for proper operation of the turbines.

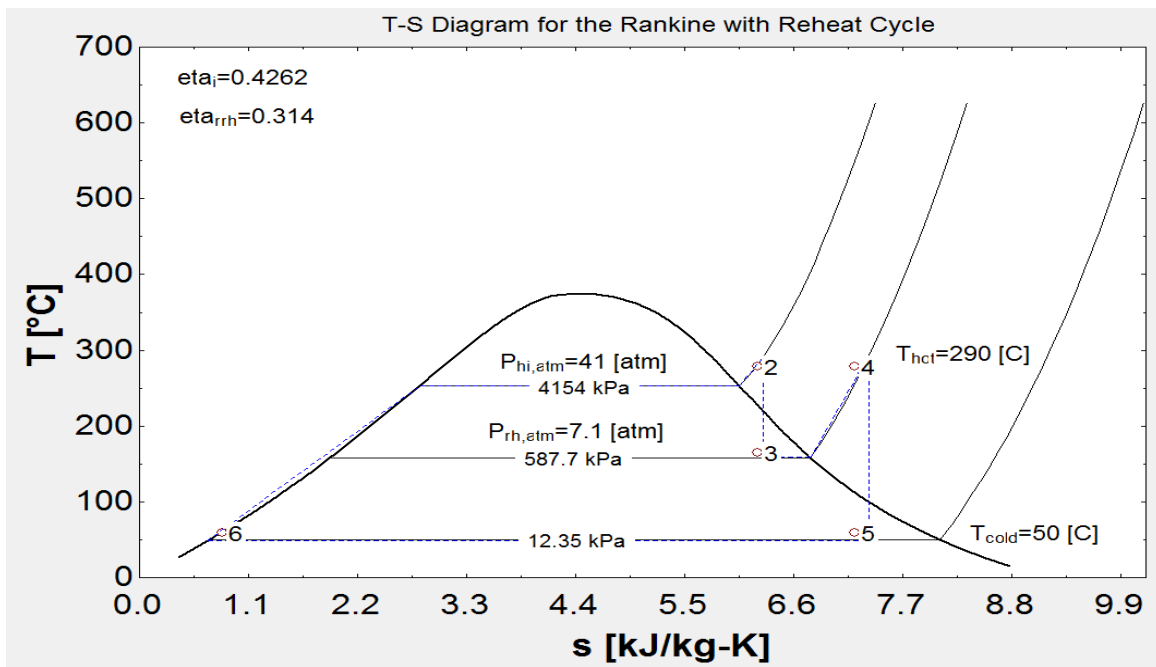


Figure 12: T-s Diagram of the DREAM's Thermodynamic Cycle

By including all the inefficiencies in the Rankine-with-reheat EES code from the *Thermodynamic Cycle Inefficiencies* section, the authors calculated the non-ideal DREAM thermodynamic cycle efficiency to be 29.2%. A temperature-entropy diagram of the non-ideal

cycle is provided in **Figure 13**.

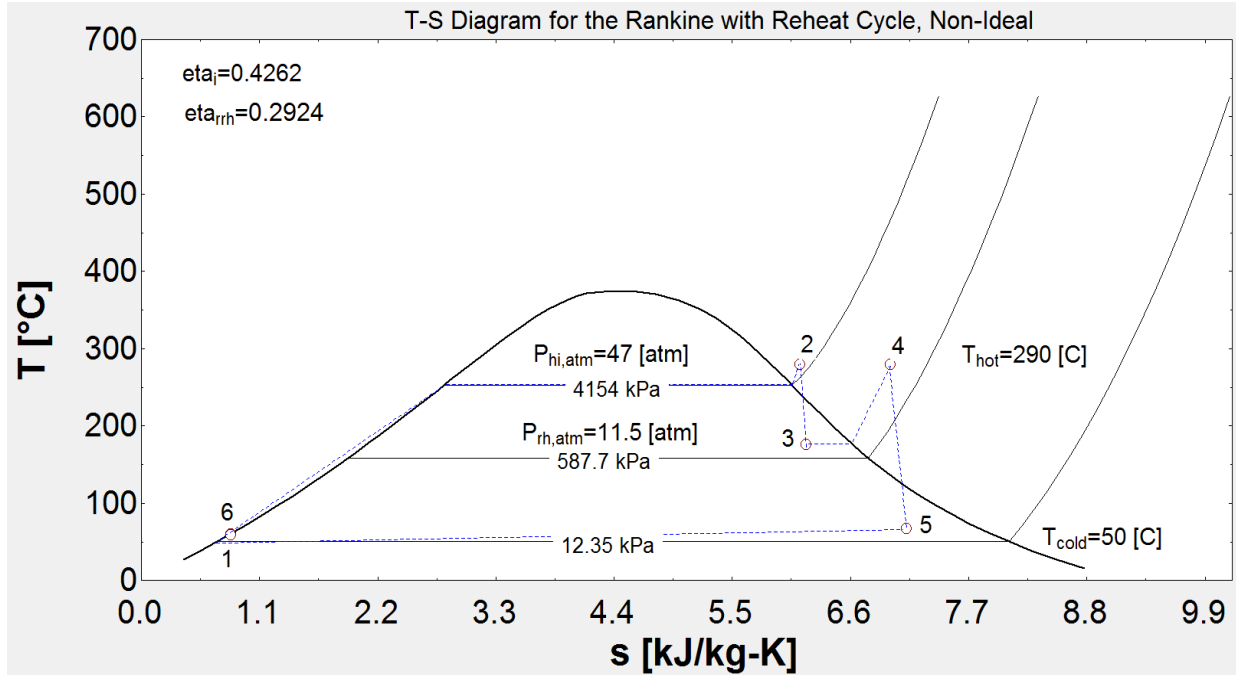


Figure 13: Non-Ideal T-s Diagram of the DREAM’s Thermodynamic Cycle.

Steam Generator Design

Unlike typical *light water reactors*, SMR’s implement an integral steam generator design, so that the steam generator is located inside of the RPV. Thus, the chances of steam line breaks and steam generator rupture accidents are minimized. However, this design brings new challenges in comparison to typical shell-and-tube heat exchangers. In particular, the authors needed to ensure that the size (surface area and volume) of the steam generator is minimized so that it can be fit between the reactor core and the RPV.

By using the EES computer calculations listed in **Appendix D**, the authors determined the minimum steam generator size to extract 100 MWth of energy from the RPV. First an initial pressure, core inlet, and core outlet temperatures were determined. By using these values in addition to our 100 MWth requirement, a flow rate through the reactor core of 666.8 kg/s was established.

By performing sizing estimates in the *Steam Generator Sizing and Pressure Loss* section using the core flow rate and thermodynamic data determined in the *Thermodynamic Cycle* section, the authors determined that 5,000 total tubes in the steam generator would balance the pressure loss and the size of the steam generator. By applying additional pressure loss analysis in the *Steam Generator Sizing and Pressure Loss* section to balance primary and secondary pressure losses, the authors determined a main/reheat pipe fraction of 62.6%.

Finally, the authors decided to use *Sanicro 69* as the material for the steam generator tubes. Sanicro 69 is an austenitic nickel-chromium-iron alloy designed for use in nuclear power steam generators¹⁸, such as the DREAM steam generator. Final steam generator parameters after all analysis are listed in **Table 3**, with the 3D model displayed in **Figure 14**.

Table 3: Final Steam Generator Parameters.

<i>Parameter</i>	<i>Specification</i>
Number of Tubes (Main / Reheat)	3,130 / 1,870
Tube Material	Sanicro 69
Tube inner radius	1 cm
Tube thickness	0.25 cm
Tube spacing	1 cm
Tube Height (Main / Reheat)	4.50 m / 0.405 m
Pressure Loss (Main / Reheat)	105.9 kPa / 243.3 kPa

Although **Figure 14** does not display the RPV penetrations for the steam generator feed tubes, nor the collector tubes combining the several small main

and reheat tubes, the authors do not anticipate adding these features to significantly affect the analysis of the steam generator or RPV.

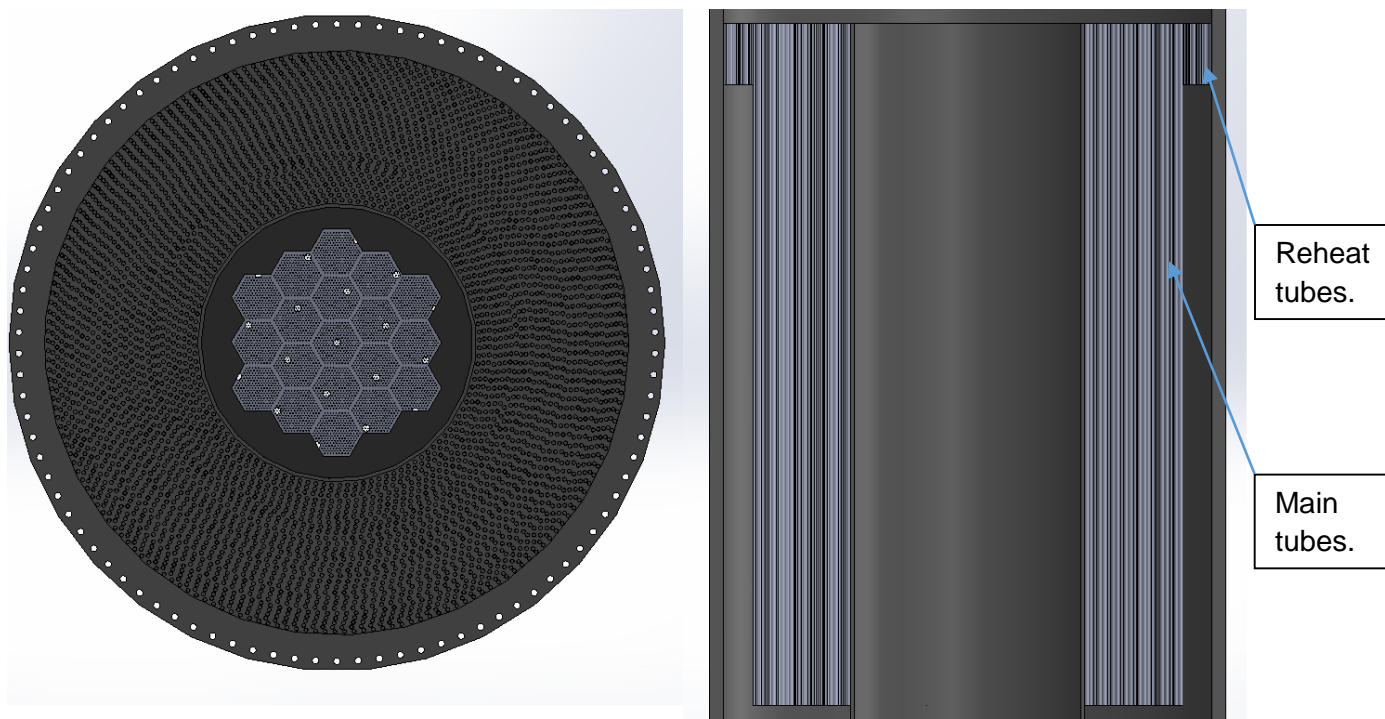


Figure 14: Top-down and side views of the steam generator in the RPV.

Condenser Design

Because the DREAM designers wanted the design to operate in geographic regions without access to nearby cooling water, the authors pursued a dry cooling condenser. Although dry condensers are less thermally efficient and more expensive than wet condensers¹⁹, the authors judged that the water savings from dry condensers offset the additional expense.

The authors initially considered designing a custom, natural convection-cooled condenser, paralleling the design process of the DREAM's custom steam generator. However, initial research revealed that forced convection dry condensers are currently used at commercial power stations in dry climates. For example, **Figure 15** shows Wygen-3, a 100 MWe coal power plant in Gillette, Wyoming, using a dry condenser system.²⁰ Therefore, to reduce costs and to permit the DREAM design to operate in arid regions, the authors decided to use a commercial

forced-convection dry condenser.

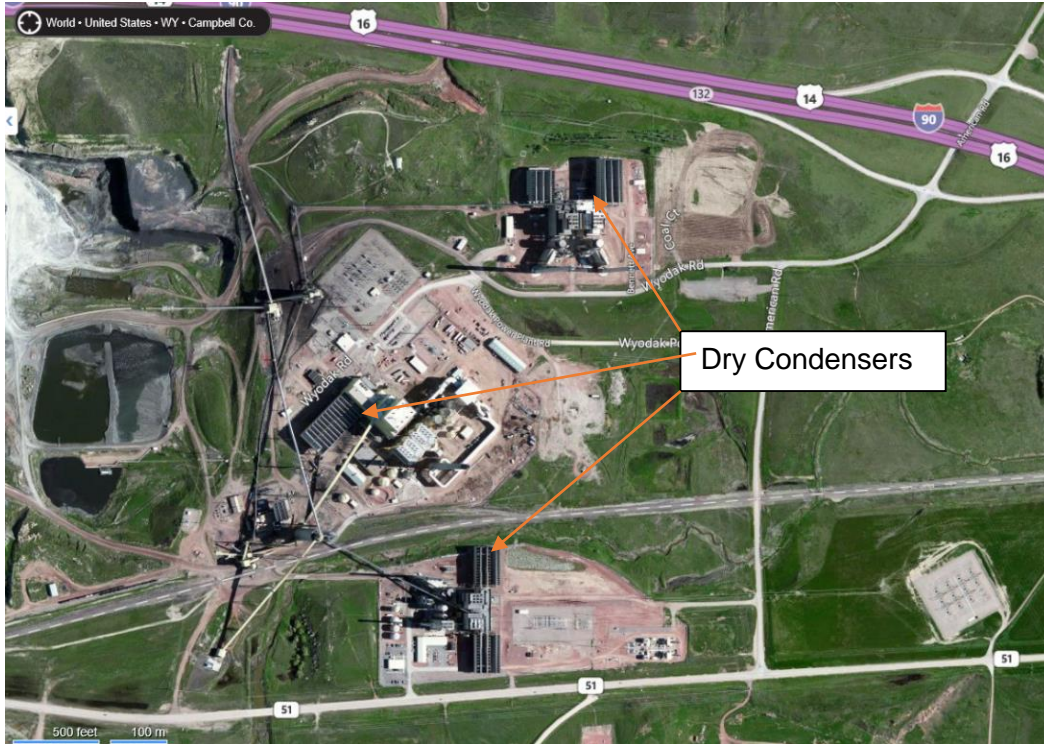


Figure 15: Wygen-3 Labeled Aerial Photo.²¹

The authors decided to use a ModuleAir™ dry condenser available from SPX Power+Energy.²² This system, shown in **Figure 16**, was chosen because each condenser can be split into separate modules and assembled in stages. Therefore, if the DREAM design is operated at lower power or in regions with lower ambient air temperatures, fewer dry condenser modules will need to be transported and assembled at the plant location.

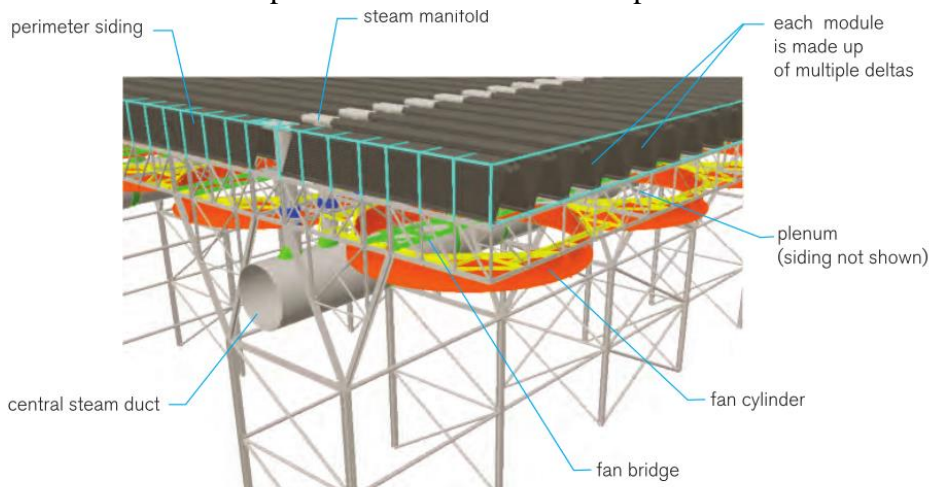


Figure 16: ModuleAir™ Dry Condenser System.²²

To estimate the maximum land area for the Dry Condenser for the DREAM design, the authors first determined the total area of the Wygen-3 condensers visible in **Figure 15**. This land area of 18,200 m² was then divided by 3 because Wygen-3 outputs 3 times the thermal power of the DREAM design and operates at a similar efficiency to the DREAM design. The resulting land area of 6,070 m²

operates at a similar efficiency to the DREAM design. The resulting land area of 6,070 m²

required for the condenser is slightly larger than an American football field, which covers 5,351 m².²³ Finally, by estimating condenser module to be 13 m per side, the authors estimated that 36 condenser modules are needed for the DREAM design.

By analyzing the condenser’s pressure and energy loss, the authors determined a frictional pressure loss of 8.64 kPa through the condenser and a power of 8.92 kWe required to run the condenser. These calculations are detailed in the *Condenser Pressure and Energy Loss* section.

Reactor Core Design

As expected from the similarities in fuel bundles, the fuel rods for each of the four analyzed reactors were rather similar—all analyzed designs used LEU fuel in a 17x17 square array. However, the authors wanted to improve upon the 17x17 LEU design with the goal to decrease the reactor core size. Therefore to determine the optimal fuel rod radius, gap size, cladding thickness, and unit cell pitch, the authors decided to run a homogeneous core calculation, a 2D core calculation, and finally a 3D core calculation in *MCNP6*.

The purpose of analyzing a homogeneous reactor core containing the isotopes in a fuel rod unit cell was to determine whether the simple core could become critical. Using a unit cell with a 0.41 cm in radius and 3% enriched UO₂ fuel pin, a 0.01 cm He gap, a 0.06 cm Zr cladding, and a pitch of 1.28 cm with light-water fill, the authors determined the number density and nuclear properties listed in **Table 4**. To improve upon the thermal conductance in the fuel pin, the authors set the initial helium pressure to 30 atm. Because higher pressure increases the thermal conductance of the fill gas,²⁴ this pressure leads to a decreased centerline fuel temperature in comparison to standard LWR fuel pins.

Table 4: Isotopes in the analyzed fuel rod and physical properties.²⁵

Isotope	N (#/cm ³)	σ_a (b)	σ_f (b)	Σ_a (cm ⁻¹)
U-235	0.0032	678	577	2.245
U-238	0.1036	2.73	101	0.293
O-16	0.4023	0.0001	N/A	4.16E-05
He-4	0.0122	0	N/A	0
Zr-90	0.0535	0.011	N/A	0.000609
Zr-94	0.0181	0.0499	N/A	0.000935
H-1	0.3735	0.3327	N/A	0.129
H ₂ O	0.0335	0.66	N/A	0.022
UO ₂ (combined)	0.0223	7.6	N/A	0.169
Zr (combined)	0.0423	0.185	N/A	0.008

The authors, assuming zero neutron leakage, used the four-factor formula, **Equation 1**, to determine reactor criticality:

$$k_{\infty} = \eta f p \epsilon$$

Equation 1: Four-Factor Formula²⁶

$$\eta = \frac{\nu \sigma_f}{\sigma_a}$$

Equation 2: Neutron fission/absorption ratio²⁶

$$f = \frac{\Sigma_{a,\text{fuel}}}{\Sigma_{a,\text{fuel}} + \Sigma_{a,\text{other}}}$$

Equation 3: Thermal Utilization²⁶

By assuming limited fast fissions and adequate neutron thermalization, the authors set the resonance absorption factor and fast fission factor to 1. Using **Equations 2 and 3** and the average number of neutrons produced per fission (ν) to be 2.3, the authors calculated k_{∞} to be 1.64—this configuration is certainly critical.

As the completed reactor core will be modeled in 3D using MCNP, the authors ran a MCNP analysis of the homogenized reactor core to compare results.²⁷ From this code, listed in **Appendix E**, the authors retrieved an effective multiplication factor of 1.260 ± 0.001 , which is still critical but much lower than the manual calculation. However, this result was expected because the resonance absorption factor is actually *less than one* due to the U-238 in the homogeneous mixture.

The authors used the same unit cell from the 1D analysis, depicted in **Figure 17**, to run a 2D MCNP calculation and perform a manual analysis. Just as in the homogeneous case, the manual calculation was intended to validate the 2D MCNP code, so that results from 3D MCNP analysis can be used with confidence. The manual calculation was performed using **Equations 1, 4, 5, 6, and 7** and setting the product of the resonance absorption and fast fission factors to 0.9 and the thermal disadvantage factor to 1.18.

$$f = \frac{\frac{\sqrt{\pi}}{2} \sqrt{\left(\frac{I_0}{I_n}\right)} N_{UO_2} (x \sigma_a^{U-235} + (1-x) \sigma_a^{U-238})}{\frac{\sqrt{\pi}}{2} \sqrt{\left(\frac{I_0}{I_n}\right)} N_{UO_2} (x \sigma_a^{U-235} + (1-x) \sigma_a^{U-238}) + \left(\Sigma_a^{H_2O} \frac{V_{H_2O}}{V_F} + \Sigma_a^{Zr} \frac{V_{Zr}}{V_F} \right) \xi}$$

Equation 4: Thermal Utilization (2)²⁶

$$V_F = \pi r^2$$

Equation 5: Volume of Fuel

$$V_{Zr} = \pi(r+t)^2 - \pi r^2$$

Equation 6: Volume of Cladding

$$V_{H_2O} = P^2 - \pi r^2$$

Equation 7: Volume of Moderator

By doing these manual criticality calculations, the authors calculated k_{∞} to be 1.34. From the 2D MCNP code in **Appendix F**, a k_{∞} of 1.330 ± 0.001 resulted. Due to the close agreement between the MCNP and manual calculations, the authors are confident in having successfully grounded MCNP's results in reality.

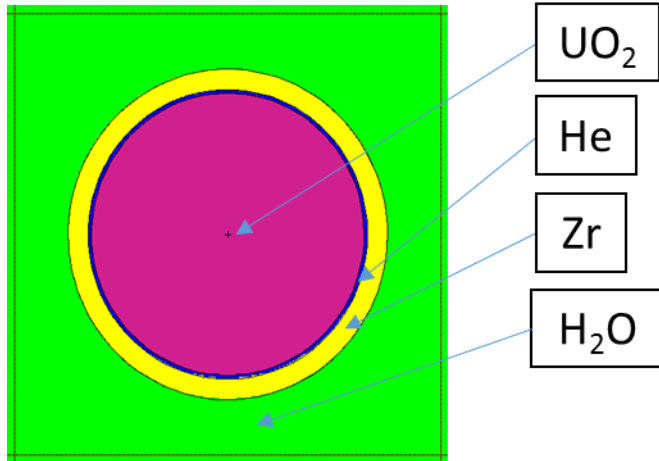


Figure 17: 2D unit cell used to link manual calculations to the MCNP analysis.

After anchoring the manual calculations to the MCNP calculations, several variations of the 2D square lattice design were run to optimize system criticality. **Table 5** lists the criticality of the variants attempted, including the chosen optimal lattice design. After determining the optimal parameters, the authors shifted to a hexagonal unit cell to enhance symmetry. The unit cell pitch was then optimized again after the geometry change, the optimal results of which are also listed in **Table 5**.

When determining the optimal cell parameters, the authors noted that increasing the cladding thickness only decreased the criticality of the system. Additionally, changing the density of the fill gas or composition of the gas between He and CO₂ had no significant effect upon the criticality of the system.

Table 5: Variations on 2D square and hexagonal lattice designs for the DREAM design.

<i>Unit Cell Change</i>	k_{∞}	σ^2	<i>Gap Thickness (cm)</i>	<i>Cladding Thickness (cm)</i>	<i>Pitch (cm)</i>	<i>Enrichment (%)</i>
<i>Square Lattice</i>						
Baseline	1.33144	0.00053	0.01	0.06	1.28	3
Smaller Pitch	1.29504	0.00054	0.01	0.06	1.20	3
Larger Pitch	1.33783	0.00051	0.01	0.06	1.30	3
(Same)	1.34789	0.00049	0.01	0.06	1.36	3
(Same)	1.36045	0.00051	0.01	0.06	1.42	3
(Same)	1.36315	0.00048	0.01	0.06	1.50	3
(Same)	1.35659	0.00048	0.01	0.06	1.60	3
Thicker Gap	1.36358	0.00047	0.015	0.06	1.50	3
(Same)	1.36277	0.00049	0.02	0.06	1.50	3
(Same)	1.36180	0.00050	0.03	0.06	1.50	3

<i>Hex Lattice</i>						
Best Square Lattice Design	1.46975	0.00057	0.015	0.06	1.50	4.95
Smaller Pitch	1.43665	0.00054	0.015	0.06	1.40	4.95
Larger Pitch	1.47658	0.00053	0.015	0.06	1.64	4.95
Optimal Parameters	1.48623	0.00052	0.015	0.06	1.60	4.95

Notes: **Bold** values indicate changes and optimal results after varying one parameter. The fuel pin radius remained at 0.41 cm, as variations in the pin size can be roughly approximated as pitch changes.

Changing the cladding material from natural Zr to *Zircaloy-4* also has minimal effect, so the authors switched to *Zircaloy-4* because of the readily-available thermophysical data.²⁸ Finally, increasing the enrichment always increased the criticality, so the authors decided to use proliferation-resistant 4.95% enriched LEU to ensure the lowest-possible reactor core size.

To determine an initial estimate for the required core size, the authors computed the UO₂ mass required by using the LWR linear burnup model listed in **Equation 8**, where t [days] is the reactor time between refueling, P_{th} [MW] the reactor thermal power, and ϵ_{U-235} [%] the fuel enrichment.

$$m = \frac{tP_{th}}{9000(\epsilon_{U-235}-1)} \quad \text{Equation 8: Linear burnup model for once-through fuel.}^{26}$$

The mass calculated from the model, using the optimal parameters listed in **Table 5**, was 3.04 metric tons. Assuming a cold-temperature density of 10.50 g/cm³ for the fuel, the authors calculated a required volume of 2.90*10⁵ cm³ UO₂. When divided by the area of the fuel in a unit cell, the required volume was converted to a required total fuel rod length of 5.48*10⁵ cm.

To minimize neutron leakage in the core, the authors decided to determine the approximate number of fuel rods required to form a cube, as an initial approximation for a sphere. The number was determined by using **Equation 9**, where L_{Total} [cm] is the total fuel rod length, P [cm] is the pitch of the unit cell, and N [#] is the approximate number of fuel rods required.

$$\left[\frac{\sqrt[3]{L_{Total}P^2}}{P} \right]^2 = N \quad \text{Equation 9: Fuel Rod Requirement Equation.}$$

This equation shows that 5,121 fuel rods of 107 cm in length are required to form a cube with sufficient size to remain critical for three years.

With the optimal unit cell parameters and number of fuel rods required, the authors began to design the 3D reactor core. The authors decided to apply hexagonal symmetry by using hexagonal assemblies for the DREAM reactor core, and hexagonal unit cells to form the assemblies. Because each assembly must not become spontaneously critical when immersed in

water, the authors initially created a hexagonal pattern with 8 fuel rods per side. This arrangement, when simulated with MCNP, had a reactivity of 0.90645 ± 0.00079 . As this arrangement seemed small compared to the 17x17 square assemblies used in the other four explored designs, the authors then simulated a 9-sided hexagonal fuel assembly. This arrangement had a reactivity of 0.96658 ± 0.00075 , which the authors deemed close enough to critical—the 9-sided arrangement is also shown in the central pane of **Figure 18**.

As shown in the right pane of **Figure 18**, the authors then arranged the fuel assembly into a symmetric, spherical pattern until no more than 5,121 fuel rods were placed. To leave space for control rods and supporting material, the authors left space between each fuel assembly. By placing 19 assemblies, the authors arrived at a symmetric pattern with 4,123 fuel rods. Because this number did not reach 5,121 fuel rods, each fuel rod was lengthened to 134 cm in height instead of 107 cm so that the core would contain the same amount of fissile material.

To test this reactor core design, the authors ran an MCNP criticality analysis of the design when placed in a circular flow area of 1 m, as displayed in **Figure 19**. The outside wall of the RPV for this analysis was designed so that the fluid flowing up through the core would flow at the same speed down for natural circulation. The authors also placed 40 cm of water above and below the core to simulate the water flowing through the RPV. For reference, this early MCNP script is listed in **Appendix G**.

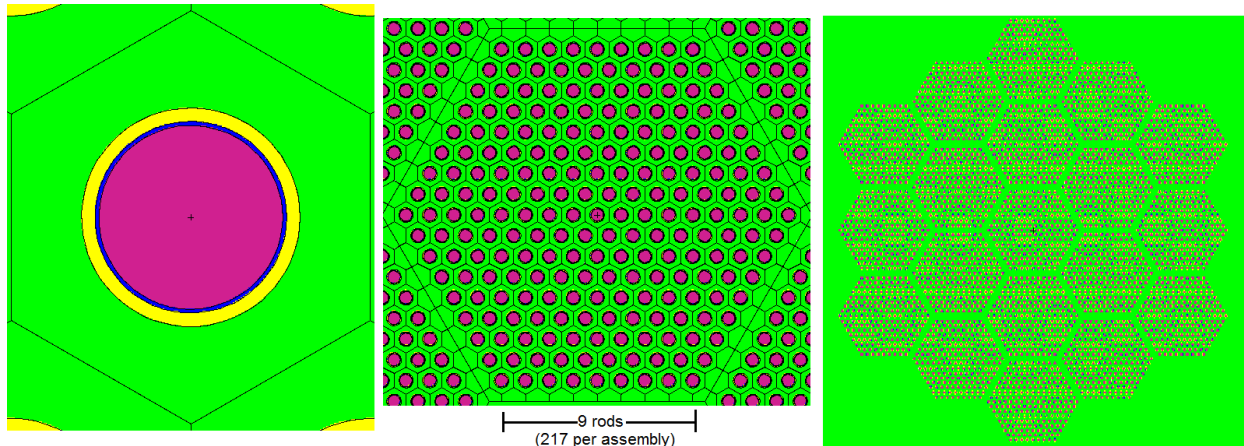


Figure 18: Reactor core in an RPV segment for simulation, top and horizontal side views.

The authors determined the designed reactor core to have a k_{∞} of 1.39142 ± 0.00042 , in comparison to the infinite-lattice k_{∞} of 1.48623 ± 0.00052 . However, as this core does not contain any reflectors or neutron absorbers in the central core area, the authors suspected that this core design would have a high peaking factor. To test this theory, the authors ran a radiographic tally of the core during criticality analysis, which resulted in **Figure 20**.

From the results in **Figure 20**, a clear doubling of neutron flux is visible from the outermost fuel assembly to the innermost fuel assembly, indicating that this initial reactor core design was inadequate for use in the DREAM design.

To improve upon the initial reactor core design, the authors decided to add graphite reflectors above and around the core and control rods. To avoid replacing fuel pins with control rods, the authors decided to design hexagonal control blades which fit in-between the reactor core assemblies. This reactor core, with control blades full-out, is shown in **Figure 21**. With control blades full-out during full-power operation, this core has a MCNP-simulated criticality of

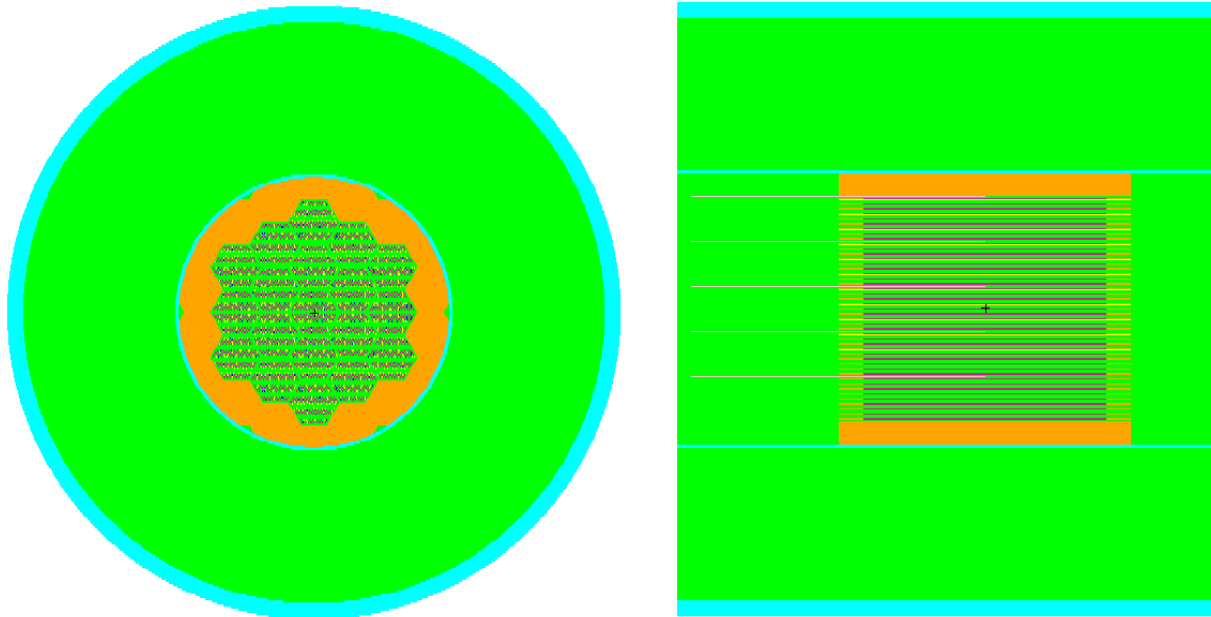


Figure 21: Reactor Core in an RPV segment, top and side views.

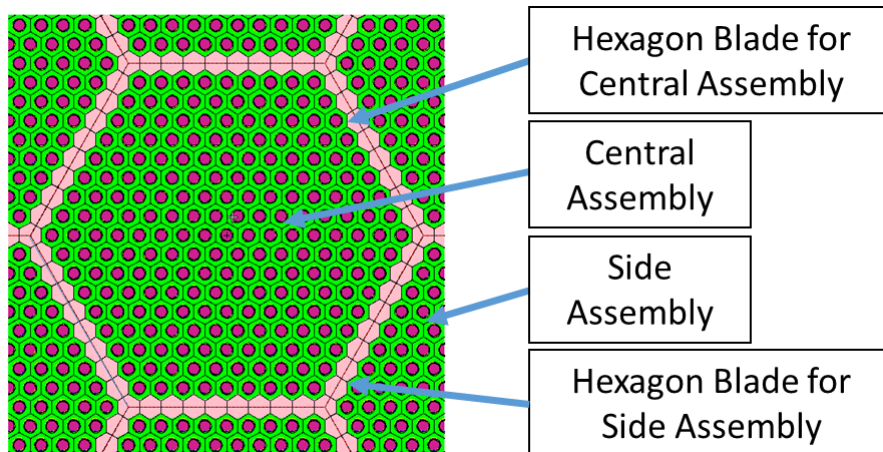


Figure 22: Top close-up view of an assembly with control blade.

Each control rod is as long as the entire core, and is inserted from the top of the core. However, each control rod is supported from underneath the core via a 4 cm diameter passive rod, which exits the RPV from below through the Removable Core Module Structure describe in the *RPV Design* section. This

design, shown in **Figure 23**, minimizes control rod length through the RPV and uses gravity to drop the control rods automatically in the event of a power failure.

The DREAM reactor core is also surrounded by a graphite side reflector extending to 75 cm, and graphite upper and lower reflectors 14.4 cm above and below each fuel rod. These reflectors substantially smooth out the flux distribution in the reactor core itself, as shown in the flux plots in **Figure 24** and flux distributions graphed in **Figure 25**.

From the 1D flux plots shown in **Figure 25**, the authors were able to estimate the nuclear hotspot factors to be 1.42 in the radial direction and 1.33 in the axial direction. The entire core, with control rods full-out, is modeled in **Figure 26**

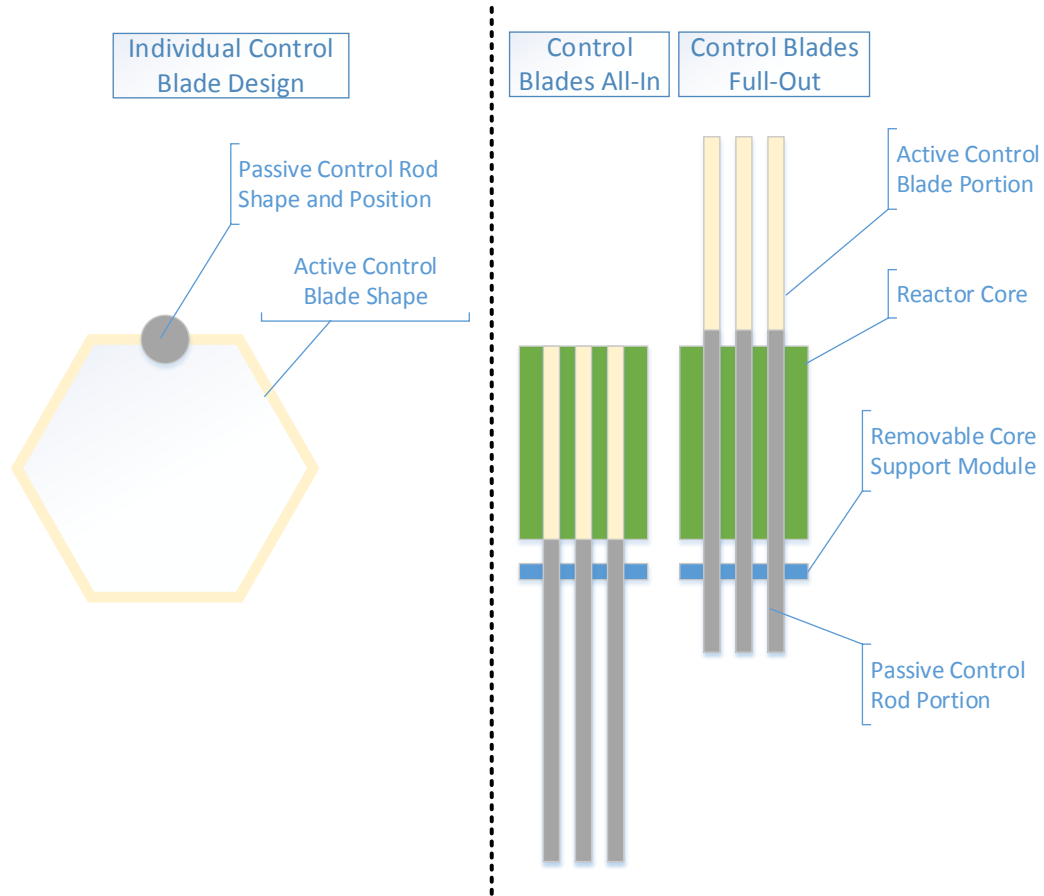


Figure 23: Top-view and Side-view of the control blade schematic.

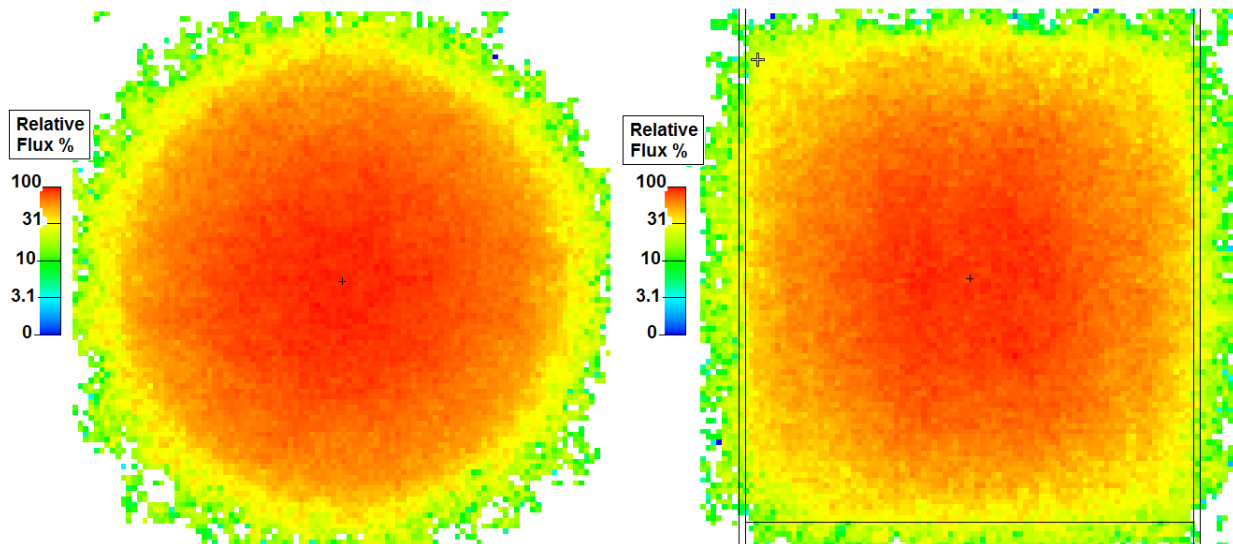


Figure 24: Top and side flux distribution with the addition of the graphite reflectors.

Because the DREAM reactor core is a compact core operating at a low flow rate, close to the saturation temperature of water at 75 atm, the authors ran a critical heat flux calculation to

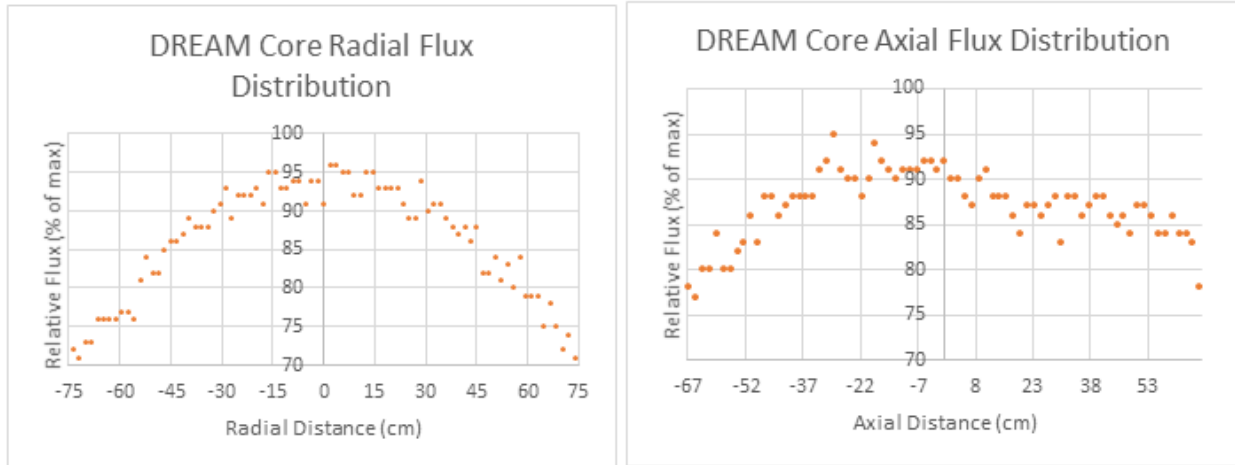


Figure 25: Flux distribution graphs from the reactor core center.

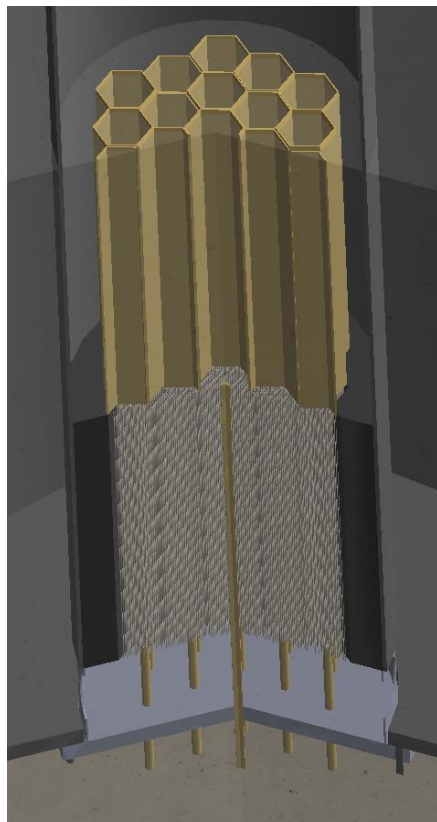


Figure 26: Reactor Core cutaway model, with fuel rods, radial reflector, and control blades.

generated a departure from nucleate boiling ratio (DNBR) graph listed in **Figure 28**. The analyses performed for both figures is listed in the *Reactor Core Analysis* section.

ensure safe operation. From these calculations, listed in the *Reactor Core Analysis* section, the authors determined a critical heat flux of 2.114 MW/m^2 , with a maximum heat flux of 1.992 MW/m^2 . In the *Reactor Core Analysis* section, the authors also determined the average temperatures of a fuel pin, which resulted in a centerline temperature of $1,460 \text{ }^\circ\text{C}$ and maximum cladding temperature of $384 \text{ }^\circ\text{C}$.

Because Zircaloy-4 experiences a *phase change* around $804 \text{ }^\circ\text{C}$,²⁸ the DREAM cladding temperature must remain below this point to prevent excessive mechanical stress. Although the DREAM maximum cladding temperature of $384 \text{ }^\circ\text{C}$ is below this limit, the authors note that Zircaloy-4 melts around $1,816 \text{ }^\circ\text{C}$ and starts oxidizing around $1,038 \text{ }^\circ\text{C}$,²⁸ well below the operating temperature of the DREAM design. In comparison, uranium oxide fuel melts at $2,749 \text{ }^\circ\text{C}$,²⁹ well below the midpoint temperature of the DREAM fuel.

Although there is nearly a $600 \text{ }^\circ\text{C}$ temperature difference across the gap in the fuel pin, the authors note that the fuel centerline temperature remains significantly below the fuel melting point. Because the authors used a thicker-than-normal gap to improve upon the neutron economy, this calculation ensured that the thicker gap will not reduce the safety of the DREAM design.

After analyzing the radial temperature profile of a fuel rod, the authors analyzed the axial temperature profile of a fuel rod and the critical temperatures along the fuel rod, both of which are graphed on **Figure 27**. By dividing the critical temperatures by the fuel rod temperatures, the authors also

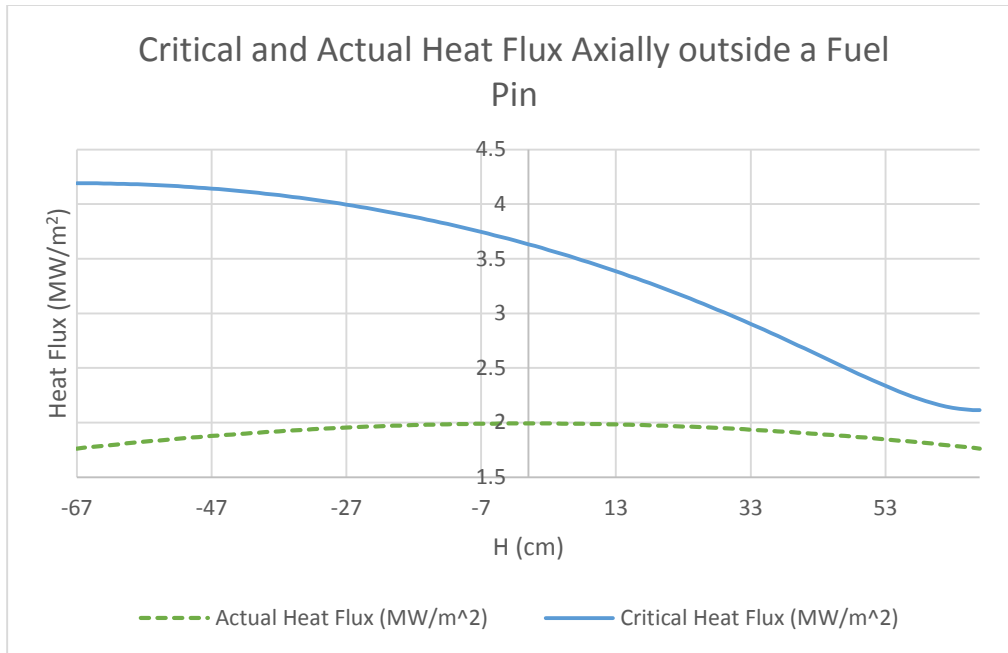


Figure 27: Fuel pin heat flux and critical heat flux along the fuel pin.

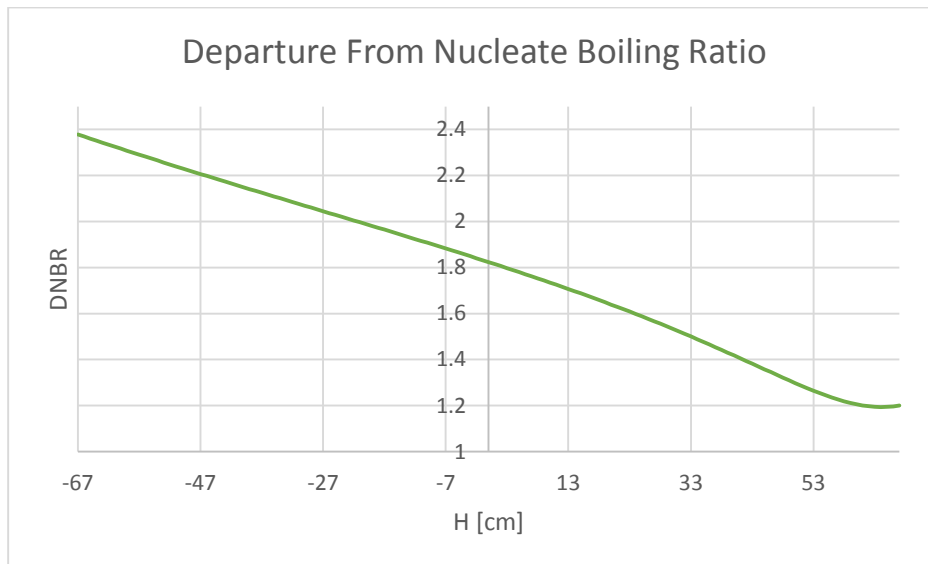


Figure 28: Departure from Nucleate Boiling Ratio along the fuel pin.

Although it has been recommended to keep the DNBR above 1.3 for safe operation,²⁹ the authors also included the hotspot factors when computing the actual heat flux. This inclusion decreased the minimum DNBR to 1.19, but accounts for the thermal fluctuations which necessitate keeping the DNBR above 1.3. Therefore the authors are confident this DNBR provides for safe operation of the DREAM reactor core.

Using the q''' from the *Reactor Core Analysis* section and **Equation 10**, the authors also did a preliminary calculation of the flux in the core.

$$\varphi = \frac{q'''}{G_f \Sigma_f}$$

Equation 10: Neutron flux from volumetric heat flux.²⁹

In this equation G_f is the energy per fission, which was taken to be 180 MeV, and Σ_f is the macroscopic fission cross section, which was calculated to be 0.276 cm^{-1} for the 4.95% enriched fuel. By converting q''' from Btu/hr-ft³ to MeV/sec-cm³ and using **Equation 10**, the average flux was calculated to be $4.31 \cdot 10^{13} \text{ n/cm}^2\text{-sec}$.

In comparison to the flux calculated from the heat flux, beginning-of-life and end-of-life calculations using MCNP resulted in average neutron fluxes of $7.84 \cdot 10^{13} \text{ n/cm}^2\text{-s}$ and $1.07 \cdot 10^{14} \text{ n/cm}^2\text{-s}$, respectively. Because **Equation 10** does not account for neutron leakage from the core or resonance absorption, the authors expected these fluxes to be higher than the initial estimate. The authors also expected the core neutron flux to rise during operation, because of fuel depletion which would decrease the macroscopic fission cross section.

Reactor Pressure Vessel (RPV) Design

By combining the pressurizer, steam generator, and reactor core designs with the natural circulation analysis, the authors generated the inner design of the RPV, shown in **Figure 29** as a *SolidWorks*-generated engineering drawing.

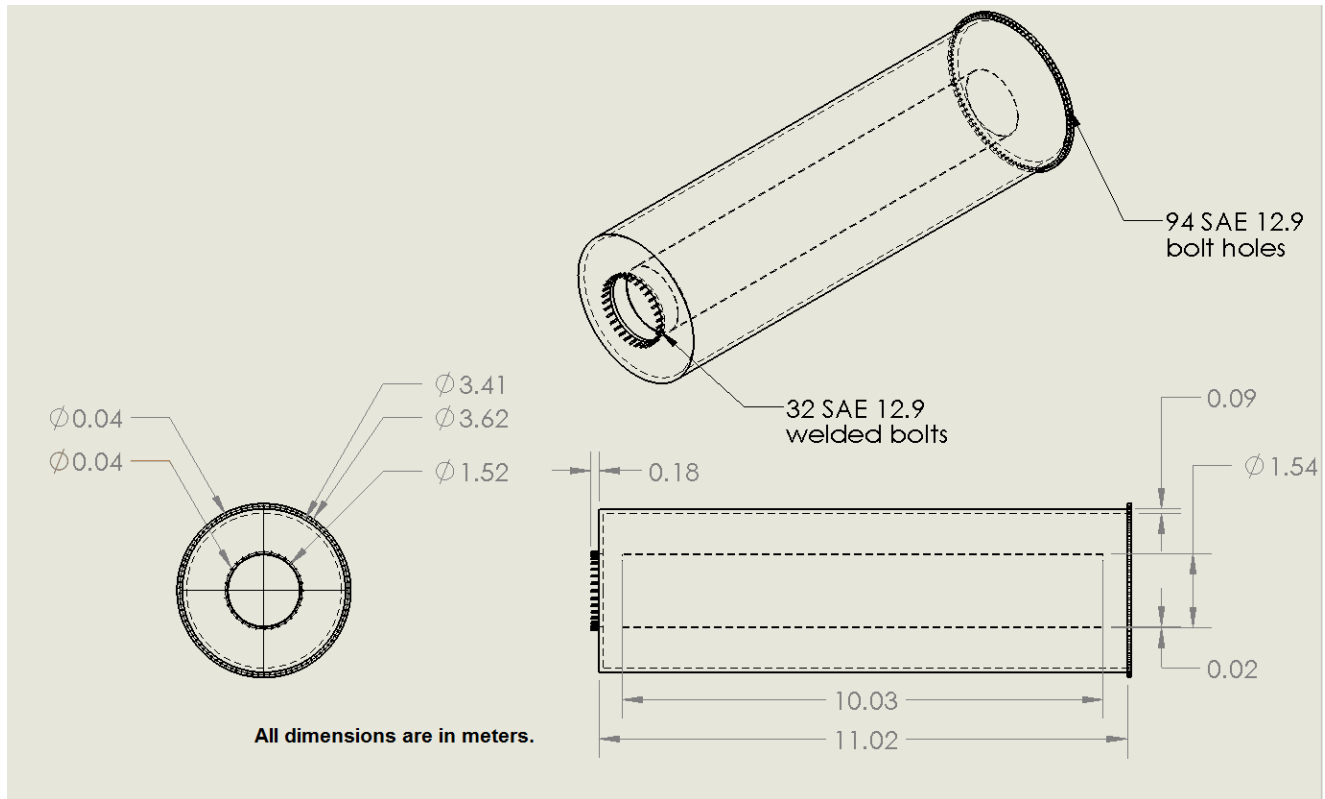


Figure 29: RPV Design and Isometric Drawings.

The DREAM RPV consists of a top lid, outer shell, inner shell, and bottom lid. The bottom and top lids are both bolted to the outer shell of the RPV. The inner shell is held concentric to the outer shell by unspecified support material.

To determine the required outer thickness of the RPV, the authors first researched the material from which to construct the RPV. To save on construction costs, the authors decided to

use a steel for the RPV. This constraint narrowed the choice of material to pearlitic steels, martensitic steels, ferrite steels, and austenitic steels.

The authors rejected pearlitic steels because of their low oxidation resistance in air, even though pearlitic steels are cheaper than austenitic steels.³⁰ The authors also rejected martensitic steels, because of their lower corrosion resistance in water at high temperatures.³⁰ Finally, the authors chose austenitic steels, because of the larger volume of publicly-available information. The authors chose the austenitic stainless steel 316 (SS-316), especially because it offers higher corrosion resistance from alloyed molybdenum in contrast to stainless steel 304.^{30, 31} To reduce cost, the standard grade of 316 was chosen instead of the nuclear grade, because of the low operating temperature and pressure of the DREAM design relative to other LWRs. This austenitic steel grade exhibits excellent creep strength, enabling the DREAM RPV to maintain high-temperature, high-pressure operation for long periods of time without deformation.³¹

Using the physical properties of SS-316, reprinted in **Table 6**, the authors then calculated the required thickness of the RPV to withstand a 74 atm pressure difference. For a cylindrical pressure vessel, the authors used the following stress equations:

$$\sigma_{ends} = \frac{P*r}{2*b} \quad \text{Equation 11: Axial Stress in a Cylindrical Pressure Vessel.}^{32}$$

$$\sigma_{\theta} = \frac{P*r}{b} \quad \text{Equation 12: Circumferential Stress in a Cylindrical Pressure Vessel.}^{32}$$

Table 6: Material Properties of austenitic stainless steel 316.³¹

<i>Tensile Stress (MPa)</i>	<i>Yield Stress (MPa)</i>	<i>Density (g/cm³)</i>	Elastic Modulus (GPa)
515	205	8.0	193

Because the strength of steel is isotropic, the larger result from using **Equation 11** and **Equation 12** must be chosen in the strength analysis. Therefore, by using **Equation 12** and the material properties of SS-316, the authors calculated the minimum thickness b of the pressure vessel to be 5.96 cm. However, accounting for a safety factor of 1.5 for well-known materials under reasonably-constant conditions³³, the minimum thickness is then 8.94 cm. This thickness is roughly half the thickness of the WWER-100 design (19 cm)¹, operating at roughly double the pressure (17.7 MPa), which is consistent with **Equation 12**. In the event of an accident, this pressure limit will be reached before the bulk fluid temperature reaches 1,440 °C,³⁰ the melting point of SS-316.

Because the DREAM design needs to be quickly refueled with a retrievable fuel module, the authors first attached the core to an underlying support structure welded to a removable plate (bottom lid) on the RPV. The support structure contains several holes allowing fluid to flow into the core, which can be partially obstructed if the authors want to reduce the natural circulation flow rate in the DREAM RPV. This component, shown in **Figure 30** as a SolidWorks-generated engineering drawing, is then bolted onto the underside of the RPV.

Because the RCMS must withstand the same maximum pressure as the RPV, the bolts connecting the RCMS to the RPV must withstand that pressure as well. Additionally, because the authors want to keep costs to a minimum, standard SAE 12.9 bolts were used because of their high yield strength.³³

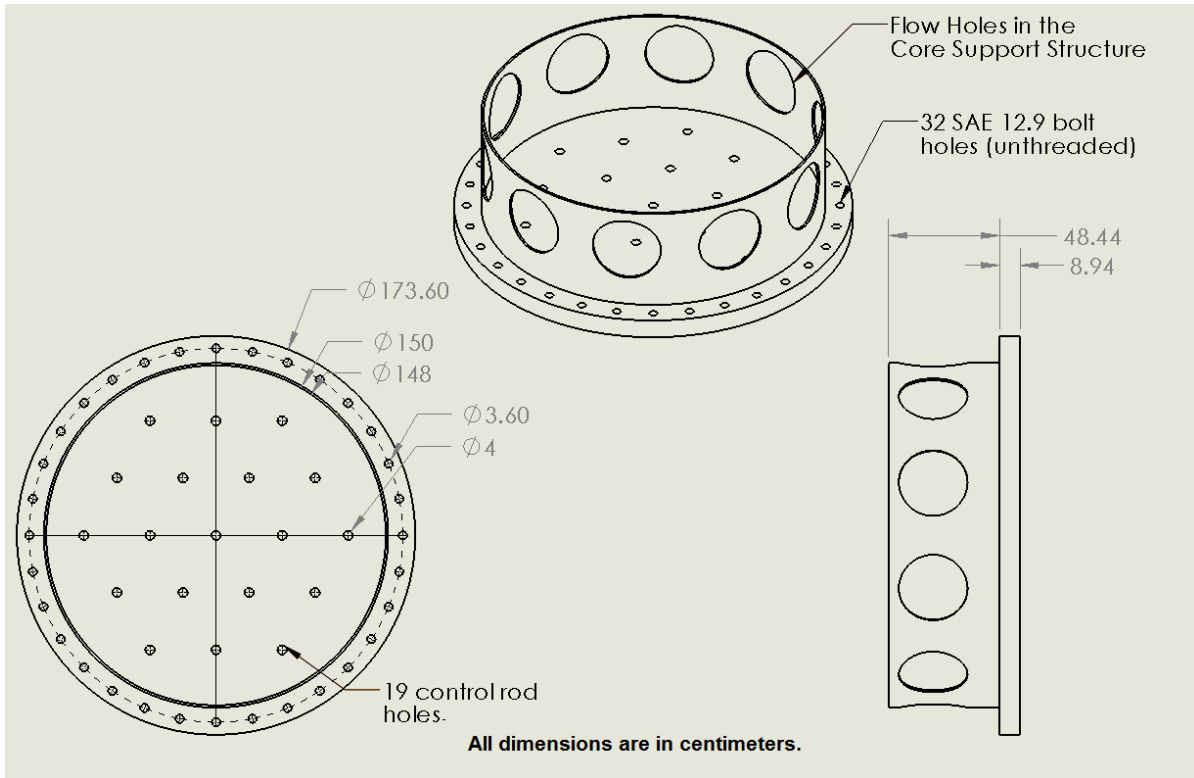


Figure 30: Removable Core Module Structure (RCMS) Drawing.

In designing the Removable Core Module Structure, the authors left 1 cm of radial spacing around the exit area for the core (75 cm in radius), which led to a circular hole 76 cm in radius at the bottom of the RPV. The total downward force on the RCMS bolts is therefore the RPV pressure multiplied by the circular cutout area, plus a small addition from the weight of the water in the RPV. Equating this force to the proof load of an SAE 12.9 bolt results in a total of 32 bolts to affix the RCMS, the calculation parameters of which are summarized in **Table 7**. This calculation procedure was also used to determine the required 94 bolts used to fix the top lid onto the RPV.

Table 7: Calculation Parameters in designing the RCMS bolt pattern.

<i>Parameter</i>	<i>Calculation Result</i>
Circular Cutout Area	1.815 m ²
Maximum RPV Pressure	1.13 * 10 ⁷ Pa
Water Mass	6.70 * 10 ⁴ kg
Total Force	21.25 Mega Newtons (MN)
SAE 12.9 Bolt Maximum Diameter ³³	3.6 cm
SAE 12.9 Bolt Proof Load ³³	970 MPa
Maximum Force per SAE 12.9 Bolt	0.987 MN
Safety Factor ³³	1.5
Total Number of SAE 12.9 Bolts Required	32

To remove the core, the control rods are lowered into the core and then locked in place to the underside of the RCMS. The rods are then cut off, so that the core can fit underneath the RPV. The RCMS is then unbolted from the RPV, lowered until the RPV and containment water levels are in equilibrium, and then completely removed from the RPV. As shown in **Figure 31**, the RCMS completely supports the core and guides it out of the RPV for replacement.

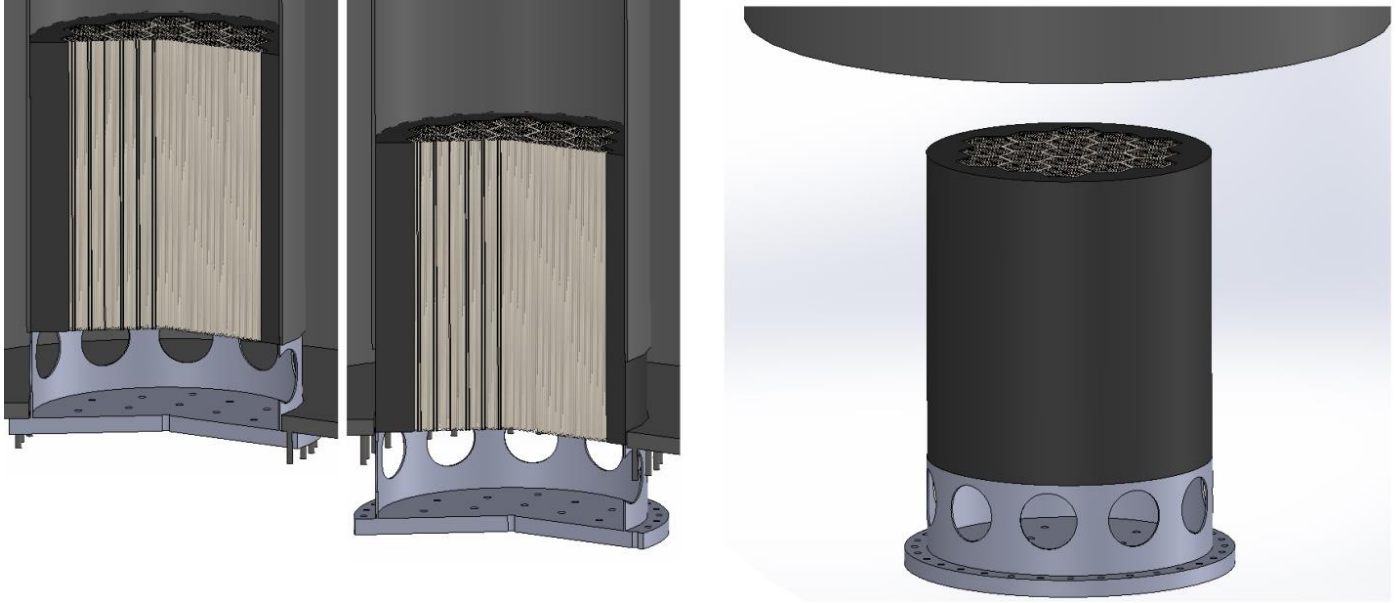


Figure 31: DREAM Reactor Core Removal Procedure (Control blades not shown).

The authors estimate the maximum total time to unthread all 32 bolts and pull out the core to be 4 hours, with roughly 8 minutes allotted to each bolt. Therefore, the entire core replacement time would take 8 hours (1 work-day) of a 1 week (7 work-days) maintenance time.

Because replacing the core and boric acid inventory are the only major actions required in a refueling period, the authors estimate that the additional 6 work-days allocated for every 3-year maintenance period provide more than enough time for preventative maintenance.

Containment Design

Designing the containment requires a complete understanding of all the functions the containment is expected to perform. The DREAM's containment must provide adequate radiation protection around the device, contain radioactive material if the RPV leaks, withstand pressure buildup from an RPV leak, and dissipate decay heat from the RPV under accident scenarios. In addition, DREAM's containment must be reasonably small and inexpensive to meet the transportation and financial goals stated in the previous progress report.

The authors decided to first design the containment based upon the radiation protection required from the containment. Through using the shielding results from the ***Containment Strength and Shielding*** section, the authors determined at least 2.38 m of water was required radially for adequate radiation protection. As such, the authors are designing the containment such that the minimum radius is at least 4.10 m, 2.40 m of which is water, to prevent excessive radiation exposure. Because sufficient shielding was provided from the water inside the containment, the authors set the containment height at 15 m – just enough to hold the RPV and

control blades when fully inserted.

After calculating the minimum radius and desired height of the containment, the authors determined the maximum pressure the containment needed to withstand. The calculations done to determine this pressure, listed below in the *Containment Strength and Shielding* section, resulted in a design pressure of 20 atm, with a maximum pressure of 30 atm using a safety factor of 1.5. Because this pressure resulted in an extraordinarily large amount of concrete, the authors chose SS-316 as the containment material instead of concrete. By using the same pressure calculations as listed in the *RPV Strength and Natural Circulation* section, the authors determined that 6 cm of SS-316 was required for the containment. This containment, along with the enclosed RPV and fill water, is shown in **Figure 32**.

Because the containment must dissipate decay heat in the event of a loss-of-power accident, the authors performed an analysis of the decay heat removal from the containment. This analysis assumed that the water inside the containment would be boiled and vented to the atmosphere, followed by the boiling of the RPV water (which would not be vented to the atmosphere).

To estimate the energy generated from decay heat, the authors used **Equation 13**.

$$E = 7.6 * 10^{-3} P_o [t^{0.8} - (t + T_o)^{0.8} + T_o^{0.8}] \quad \text{Equation 13: Decay energy generated.}^{34}$$

Key: t: Time since shutdown [days] T_o: Uptime before shutdown [days]
 P_o: Operational Power [MWth] E: Decay energy produced [MWth-day]

From thermal analysis, boiling and venting all the containment water requires 5.93*10⁵ MJ of energy. This analysis assumes the containment water boils until 20 atm of pressure is reached, at which the containment water is vented to maintain that pressure.

Using **Equation 13**, the authors generated **Table 8**, which lists the energy generated from the core during shutdown after different increments of time. From **Table 8**, after 28.8 days the containment water can no longer cool the reactor core. At that time, from **Equation 14**, the reactor will be generating 172 kWth of energy.

$$P = 6.48 * 10^{-3} P_o [t^{-0.2} - (t + T_o)^{-0.2}] \quad \text{Equation 14: Decay heat power.}^{34}$$

If the RPV water is then vented to the containment, the DREAM design then can heat up that fluid till it reaches 20 atm of pressure. From similar thermal analysis, heating up the RPV water to this point when vented into the containment requires 6.64*10³ MJ of energy. This lengthens the amount of time to 29.3 days for which the DREAM design can cool the reactor core.

At 29.3 days, the reactor is producing 171 kWth of energy. If the containment is assumed to radiate this heat across the entire surface of 439 m², the heat flux radiated from the containment is then 340. W/m². Because the solar irradiation is the same order of magnitude as this result,³⁵ the authors believe that natural convection and thermal radiation will cool the reactor core at this point.

Table 8: DREAM Reactor Core Decay Heat Generation

<i>Time [days]</i>	1	7	28.8	365
<i>Energy Produced [MJ]</i>	52,700	221,000	593,000	2.78*10 ⁶

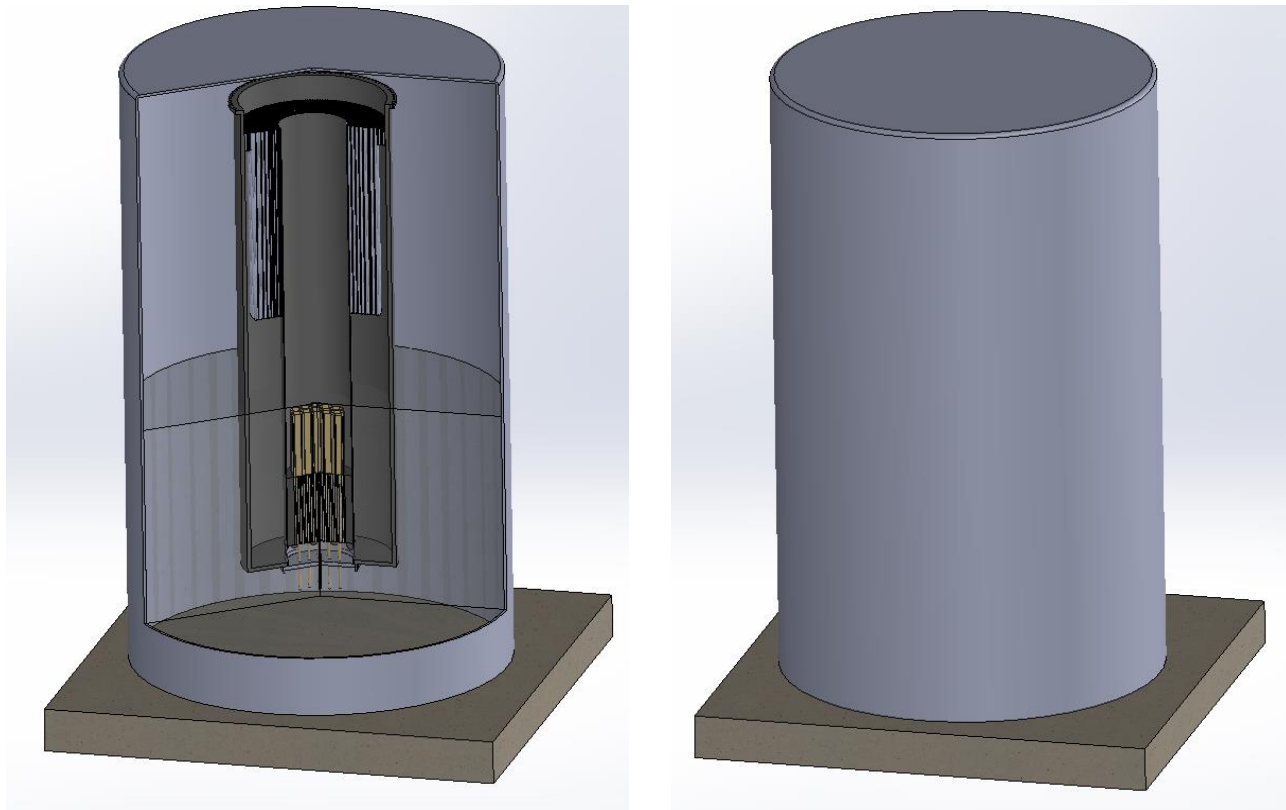


Figure 32: DREAM Containment Design (Cutout and outside view).

Design Safety

Although the authors have not designed additional safety components for the DREAM design, the authors have considered safety when creating the main design. For example, the fill water in the containment serves three purposes: to shield radiation from the reactor core, to remove decay heat in the event of loss-of-power accident, and to prevent the RPV water level from draining past the reactor core in the event of a breach. All these considerations serve to enhance the safety of the device—by reducing the likelihood of releasing radioactive material—even though the containment fill water is required as part of the main design.

In summary, the aspects of the DREAM design which contribute to safety and the resulting effects are:

- Natural circulation in the RPV → No power required for core cooling pumps.
- Gravity-inserted control blades → No power required to insert control blades.
- Containment fill water → No power required for decay heat removal.
- Low heat flux in the core → Safe margin from maximum and critical heat flux.
- Low pressure primary-loop → RPV breaches are less dangerous.
- Higher pressure gap fill gas → Lower temperature rise across the fuel pins.
- No exotic or dangerous materials → Replacing parts is faster and safer.
- Modular design → Maintenance is reduced, limiting radiation dosage.
- Single fuel module → Reactor core can be shipped without disassembly.

In the *Design Safety* section listed under the *Design Analysis* section, the authors

consider potential accident scenarios and how the DREAM design prevents the release of radioactive material in those scenarios.

Non-Electrical Applications

With SMRs, desalination is possible using waste heat; however, with the DREAM design it is more efficient to create electricity and then use the electricity for desalination. Directly using thermal energy directly requires at least 2-3 times more energy than electrical desalination.⁹ Although it provides fresh water, desalination is a costly process, with current methods producing fresh water at costs of \$2-4/kgal.³⁶ This is considerably higher than current costs of about \$1-1.5/kgal for fresh water in the U.S. The energy cost of desalination a gallon of water is equivalent to the cost of pumping a gallon of water from a depth of 6,600 ft.⁹ For these reasons desalination using waste heat is not an economical option with the DREAM design, and using electricity for desalination is only worthwhile in extremely remote locations.

The DREAM design could also perform localized heating and cooling. Steam from the reactor could be piped through radiators to heat buildings or industrial facilities. The important properties to consider with steam radiators are the quality, temperature, and pressure of the steam. The steam needs to be a consistent temperature so that the temperature of the building does not fluctuate. Additionally, the quality and pressure of the steam needs to be within the design parameters of the system so that it operates efficiently. Using hot water is another option for heating using steam from the DREAM. This can be done using hot water radiators, much like steam radiators, or hot water floor heating. These systems use liquid water and would require additional pumps, unlike a steam system.

Cooling using thermal energy can be accomplished using either an absorption or Einstein refrigerator. Both of these systems use a vapor absorption cycle and a water-ammonia cycle. The major problem with these refrigeration cycles is the coefficient of performance, 1/5 that of devices using vapor compression cycle.¹⁷ Therefore, because the electrical efficiency of the DREAM is higher than 20%, using a vapor absorption cycle is not economical unless it is done with waste heat that would otherwise be dumped to the environment.

In general, because the DREAM design separates the thermal energy generation and thermal energy usage in the primary-loop and *secondary-loop*, respectively, the DREAM design can be used for either electrical generation or process heat applications. This flexibility allows for the DREAM designs to be applicable in situations that an electricity-only or heat-only design would not be. In addition, because the DREAM design can only electricity or heat—but not both simultaneously—the user of the DREAM design never needs to waste unused electricity or excess heat if only one is product desired.

3 Design Analysis

After designing the DREAM, the authors performed additional analyses to evaluate the efficiency, safety, and economics of the DREAM design. This section's structure lists the analyses in the same structure as the **Design Methodology** section, while also including additional system-level analyses of the DREAM design.

Thermodynamic Cycle Inefficiencies

To better analyze the DREAM’s thermodynamic cycle, the authors added inefficiencies to the ideal thermodynamic model. The main inefficiencies affecting the performance of the DREAM’s thermodynamic cycle include the turbine and pump efficiencies, terminal temperature differences (TTD) in the condenser and steam generator, and pressure losses in the condenser and steam generator. The authors first attempted to find in-production standard components from global manufacturers to acquire efficiency data. In particular, the authors submitted quotes and specification requests for Arani turbines³⁷, GE turbines³⁸, and Siemens’s turbines^{39, 40}. The authors also submitted a quote and specification request to Weir Specialty pumps⁴¹. However, the authors received very few responses, all of which indicated that the requested quotes and specifications would not be available in time.

Because the DREAM team could not acquire detailed information, the authors instead determined specific thermodynamic components based on publicly-available information, and estimated conservative efficiencies for general thermodynamic components. The authors decided upon the Siemens SST-111 turbine³⁹ for the HP turbine and SST-150 turbine⁴⁰ for the LP turbine because these turbines matched the operating regime required for the DREAM design. These turbines, shown in **Figure 33**, were also chosen as Siemens provided sufficient publicly-available information to choose specific turbine models. Because the technical information provided for each turbine as listed in **Table 9** did not include efficiency information, the authors estimated both turbines to be 92 percent efficient.⁴²



Figure 33: SST-111 and SST-150 steam turbines with generators.^{39, 40}

Table 9: Technical information on the SST-111 and SST-150 turbines.^{39, 40}

<i>Parameter</i>	<i>SST-111</i>	<i>SST-150</i>
Maximum Power Output	12 MW	20 MW
Maximum Inlet Pressure	129 atm	102 atm
Maximum Inlet Temperature	530 °C	505 °C
Dimensions (L x W x H)	8 m x 4.0 m x 4.0 m	12 m x 4.0 m x 5.0 m

After determining the turbine models, the authors chose for the pump a Weir Roto-Jet Model RO D-850, shown in **Figure 34**.⁴¹ The authors decided upon this pump because of the customizable operating range and compact size. Because the D-850 pump is a centrifugal pump, it can operate anywhere within the operating range graphed in **Figure 34**.⁴³ This operating range provides the authors of the DREAM design more design flexibility in the thermodynamic cycle if further changes are required. Because the technical information for the pump, listed in **Table 10**, did not

include efficiency information either, the authors estimated the pump to be 80 percent efficient.⁴²

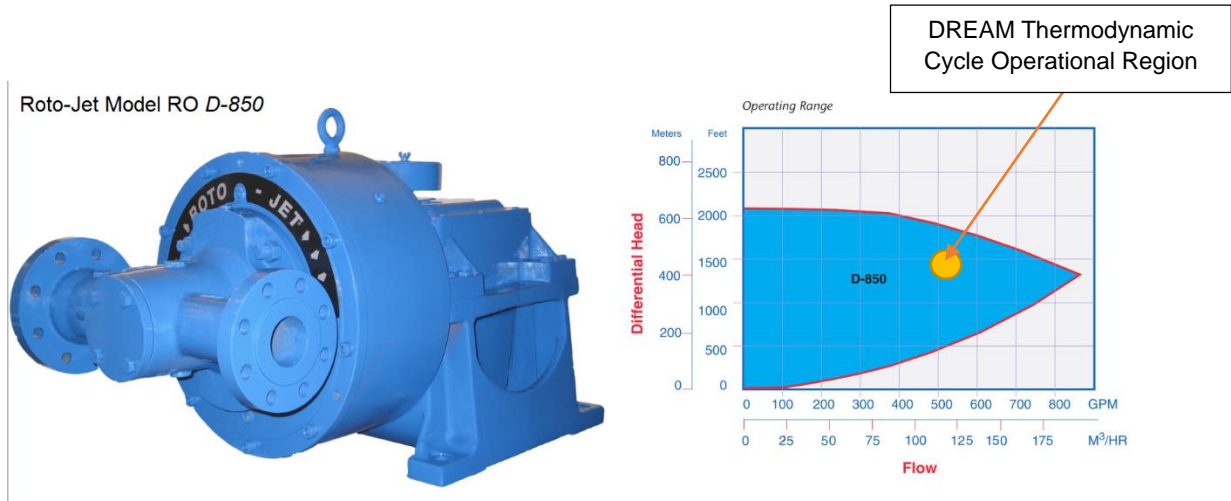


Figure 34: Roto-Jet Model RO D-850 and Operational Range, annotated.⁴¹

Table 10: Technical information on the Roto-Jet Model RO D-850 pump.⁴¹

<i>Parameter</i>	<i>Specification</i>
Maximum Temperature	121°C
Maximum Outlet Pressure (with water from condenser)	61.9 atm
Maximum Flow rate	170 m ³ /hr
Weight	590 kg
Dimensions (L x W x H)	1.20 m x 0.56 m x 0.58 m

Finally, through manual calculations the authors determined the terminal temperature differences and pressure drops of the steam generator and condenser. Because both the steam generator and condenser can be modeled as shell-and-tube heat exchangers, a 10 °C TTD was used between the inlet flows.¹⁷ By using **Equation 15** and **Equation 16**, the authors calculated the pressure losses in the steam generator HP coil, steam generator reheat coil, and condenser to be 105.9, 243.3, and 8.64 kPa, respectively.

$$Re = \frac{D_h v \rho}{\mu}$$

Equation 15: Reynolds's Number definition.

$$\Delta P_{friction} = f_D \frac{L}{D_h} \frac{\rho \bar{v}^2}{2}$$

Equation 16: Darcy Friction formula.²⁹

Key: f_D : Darcy friction factor D_h : Hydraulic diameter ρ : Fluid density
 μ : Fluid viscosity v : Fluid velocity L : Length under consideration

Because acceleration and gravitational losses are negligible for the steam generator coils and condenser, the authors neglected these terms in the pressure loss calculations. Further details on the calculations are provided in the **Steam Generator Sizing and Pressure Loss** and **Condenser Pressure and Energy Loss** sections. After combining all these inefficiencies, the authors

determined the DREAM thermodynamic cycle to be 29.2% efficient, in contrast to the 33.0% efficiency with ideal components.

Steam Generator Sizing and Pressure Loss

To determine the minimum steam generator size, values were then taken from the optimized thermodynamic cycle EES script, values such as pressures for the high and low pressure turbines, inlet and outlet steam generator temperatures, and the mass flow rate through the secondary loop. These parameters are listed in **Table 11**, along with additional important core temperatures that correspond to phase changes on the secondary side.

Table 11: Important primary and secondary thermodynamic data.

<i>Primary</i>		<i>Secondary</i>	
Core inlet - T ₁ [C]	260	LP turbine [kPa]	719.4
T ₂ [C]	268.2	HP turbine [kPa]	4154
T ₃ [C]	280.8	SG inlet [C]	60
T ₄ [C]	284.5	SG outlet [C]	280
T ₅ [C]	287.3	LP Saturation temp [C]	166.1
Core Outlet (T ₆) [C]	290	HP Saturation temp [C]	252.6
Mass flow rate [kg/s]	666.8	Mass flow rate [kg/s]	32.28

Next, the calculations in the steam generator were broken down into 3 separate sections: preheating water from inlet to saturation, heating of water from liquid to steam, and superheating the steam. The energy needed to heat each section, as listed in **Table 12**, was calculated using **Equation 17**, where $Q_{\dot{}}$ is the energy in [kW], $m_{\dot{}}$ is the mass flow rate in [kg/s] and h is enthalpy in [kJ/kg].

$$Q_{\dot{}} = m_{\dot{}}(h_{\text{out}} - h_{\text{in}})$$

Equation 17: Energy change from an Enthalpy change.

Table 12: Energy change for each section of the LP and HP steam generators.

	<i>HP = 4154 kPa</i>			<i>LP = 719.4 kPa</i>	
	Preheat (60°C to 252.6°C)	Heat (0 < x < 1)	Super heat (252.6°C to 280°C)	Heat (0.9016 < x < 1)	Super heat (166.1°C to 280°C)
Energy [kW]	27,325	54,931	3,111	6,550	8,166
Total Energy [kW]	99,993	-	-	-	-

By using the results of **Table 12**, along with the known inlet and outlet core temperatures, the authors calculated the temperatures at which phase changes occurred. Because the DREAM contains a reheat loop, only the HP steam generator contains a liquid-to-steam phase change while the LP steam generator does not. After initially modeling the steam generator as two separate modules, a low-pressure steam generator on top of a high-pressure steam generator, the authors deemed it more efficient to model heating through one combined steam generator for analysis. This assumption has no effect on the end result because the authors later split the combined steam generator into the separate two steam generators.

Finally, sizing calculations were made using **Equation 18**, where U is the heat transfer coefficient in $[\text{kJ}/\text{s}\cdot\text{m}^2\cdot^\circ\text{C}]$, A is the area in $[\text{m}^2]$, and ΔT_{LMTD} is the log-mean temperature difference.

$$Q_{\text{dot}} = UA\Delta T_{\text{LMTD}} \quad \text{Equation 18: Steam generator sizing equation.}^{17}$$

Heat transfer coefficients were calculated by finding Nusselt numbers at the arithmetic mean temperatures of each phase change. In addition, the conductivity of the pipe was taken at the arithmetic mean temperature. By using **Equation 19** provides the calculation used for finding the heat transfer coefficient, h , of the pipes, where D_h is the hydraulic diameter in $[\text{m}]$, and k is the conductivity of water at a given temperature in $[\text{kW}/\text{m}\cdot\text{k}]$.

$$h = \frac{Nu \cdot D_h}{k} \quad \text{Equation 19: Equation for heat transfer coefficient.}^{29}$$

Following the script in **Appendix D**, these values were used to calculate the length of piping needed for each section of the steam generator. Lengths for each section – preheat, heat, and superheat – are listed in **Table 13**.

Table 13: Expected pipe lengths required for the HP and LP steam generators.

	<i>HP = 4154 kPa</i>			<i>LP = 719.4 kPa</i>	
	Preheat (60 °C to 252.6 °C)	Heat (0<x<1)	Super heat (252.6 °C to 280 °C)	Heat (0.901 < x < 1)	Super heat (166.1 °C to 280 °C)
Length [m]	1,774	5,356	778.9	135.4	463.1
Total [m]	8,507	-	-	-	-

The authors assigned values for the diameter and thickness of the pipes to prevent implosion of the steam generator tubes from the 34 atm pressure difference between the primary loop and secondary loop. Because the minimum proof strength of Sanicro 69 at 300 °C is 187 MPa,¹⁸ a steam generator tube with a 1 cm radius and 0.25 cm wall thickness will withstand up to 453 atm in pressure. Although this pressure is much larger than the 34 atm pressure difference expected in normal operation, the authors note that in a secondary-side pressure failure accident the steam generator is exposed to a 75 atm pressure difference. Because the authors did not complete radiation damage estimates for the steam generator, nor analyze the steam generator durability when exposed to thermal shock, the authors did not reduce the thickness of the steam generator tubes.

With those inputs, in combination with the total lengths of pipes, the area and the height of the steam generator were calculated, along with the initial radius of the RPV required to house the steam generator. These dimensions are listed below in **Table 14**.

Table 14: Piping and overall dimensions for the steam generator.

Parameter	SG Dimensions
Pipe Diameter [m]	0.02
Pipe Thickness [m]	0.0025
Area SG [m ²]	2.454
Total area SG [m ²]	4.811
Height [m]	1.701
R_RPV (Initial) [m]	1.744
# of Pipes	5,000

Once the sizing of the steam generator was completed, the secondary-side frictional pressure loss was calculated. The authors used the Darcy-Weisbach equation written in **Equation 16** and found the Darcy friction factor, f_D , to calculate this pressure loss. The density and velocity values were taken as average values through the steam generator for this manual calculation.

Originally the number of pipes was set to 3,000, but the Darcy-Weisbach equation yielded too large of a pressure loss. An exponential correlation, shown in **Figure 35**, results from **Equations 16 and 15** between the number of pipes and the reduction of pressure losses.

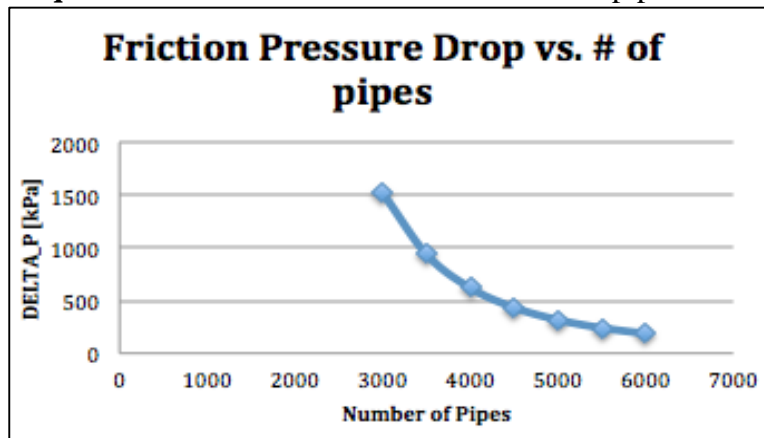


Figure 35: Correlation between pressure loss and steam generator pipes.

The increase in pipes, however, leads to an increase in RPV sizing which *increases* the primary-side pressure loss. After looking at several situations, the authors decided that having 5,000 pipes would be optimal to minimize both the frictional pressure loss and steam generator size. The pipe-to-pressure-loss correlation for different pipe numbers is listed in **Table 15**, below.

Table 15: Pipe number and pressure loss relation for the steam generator.

Number of Pipes	ΔP [kPa]	R_RPV [m]	H_SG [m]
3000	1536	1.492	2.616
3500	940.4	1.559	2.288
4000	621.1	1.623	2.043
4500	434.2	1.684	1.853
5000	317.4	1.744	1.701
5500	240.3	1.802	1.578
6000	187.3	1.857	1.476

After designing the reactor core, the inner core radius was decreased to 75 cm from 100 cm. Because the inner core radius was reduced, the outer RPV radius was decreased to 1.614 m. This change maintained a 1 cm spacing between all of the steam generator tubes in the primary loop, while also minimizing the volume of the DREAM RPV.

To more accurately analyze friction pressure losses from the steam generator, both primary and secondary, the fraction of main and reheat pipes had to be set. A parametric table was created in EES from the script listed in **Appendix D**, to optimize the steam generator height and pressure losses associated with main and reheat circulation. These values were calculated with varying tube fractions, f , where f is the fraction of the 5,000 tubes determined from the sizing analysis. These parametric calculations showed that reheat pressure losses on the secondary side could grow extremely large, near 200 atm, drastically decreasing system efficiency. Minimizing the secondary-side pressure loss resulted in a steam generator piping pressure loss of 301.1 kPa, with $f = 0.515$.

However, this value for f resulted in a steam generator height of 5.47 m. Because the DREAM design utilizes natural circulation, the authors couldn't fit in that large a steam generator without making the RPV unreasonably tall. Therefore, the authors included the steam generator height in the optimization to keep the RPV reasonably small. The authors decided to trade 0.5% of system efficiency for a reduced steam generator height of 4.5 m and a pipe fraction of $f = 0.626$. This change only slightly increased the combined steam generator secondary-side pressure losses to 349.2 kPa.

Condenser Pressure and Energy Loss

After determining the total number of condenser modules required for the DREAM design, the authors then created an EES code to estimate the pressure loss throughout the condenser. This script, listed in **Appendix I**, uses **Equation 15** and **Equation 16** to determine an estimated frictional pressure loss of 8.64 kPa through the condenser. Because the dry condenser system did not list specific component sizes for the tubes in the condenser, the authors used the following estimations listed in **Table 16**.

Table 16: Estimated specifications for DREAM's dry condenser

<i>Component</i>	<i>Specification</i>
Dry Condenser Assemblies	36
Flow Tubes per Dry Condenser	50
Flow Tube Diameter	2.0 cm
Flow Tube Thickness	0.25 cm
Flow Tube Length	2.0 m
Flow Tube Material	SS-316

Because the ModuleAir™ system uses forced-convection fans, the authors also estimated the expected power required to run the fans. This calculation was performed with an energy balance to determine the mass flow rate of air, followed by another energy balance to determine the required velocity of the air exiting the fans. The fan efficiency was estimated to be 40%, because the authors did not

know precise details of the ModuleAir™ design. From this calculation, listed in **Appendix J**, the authors calculated a power of 8.92 kWe to operate the forced condenser.

Reactor Core Analysis

Although the Westinghouse correlation is more precise in computing the critical heat flux, the authors used the Argonne National Lab (ANL) correlation as the ANL correlation is a more conservative estimate for low amounts of subcooling.²⁹ Given the input parameters listed in **Table 17**, and the correlation in **Equation 20**, the critical heat flux (q''_c) was determined to be 2.114 MW/m² through the EES code listed in **Appendix K**.

$$q''_c = C \left(\frac{G}{10^6} \right)^m (T_{sat} - T_b)^{0.22} \quad \text{Equation 20: ANL correlation for critical heat flux.}^{29}$$

For **Equation 20**, C and m are determined from the pressure using the table in Nuclear Heat Transport, p. 311, G is the mass flow rate in lb_m/ft²-hr, and both temperatures T are in °F.

Table 17: DREAM Core parameters used for critical heat flux analysis.

Parameter	Specification
Active Fuel Area of the Core	7,158 cm ²
Primary Loop Flow rate	666.8 kg/s
Fuel Rod Count	4,123
Fuel Rod Active Height	134 cm
Fuel Rod Radius (UO ₂)	0.41 cm
Fluid Bulk Temperature	290 °C
Fluid Saturation Temperature (at 75 atm)	291.4 °C

Computing a uniform heat flux through the DREAM core at maximum operational temperature results in an actual heat flux of 0.703 MW/m². As the DREAM core does not contain a completely uniform heat flux, the authors estimated a conservative engineering hotspot factor of 1.5.²⁹ By combining the nuclear and engineering hotspot factors, the authors computed a combined hotspot factor of 2.83. When multiplied with the uniform heat flux in the DREAM core the resulting maximum heat flux, 1.992 MW/m², is still under the critical heat flux for the DREAM design, ensuring safe operation.

To further assess the safety of the DREAM design, the authors calculated the average temperatures of the fuel rods to ensure no part of the fuel approached the material melting temperature. This was done by applying the parameters in **Table 18** to **Equations 21, 22, 23 and 24**, converted from Imperial to SI units.

Table 18: Core Parameters for Temperature Profile Calculations

q''' [MW/m ³]	s [m]	g [m]	c [m]	k_f [W/m-K]	k_g [W/m-K] ⁷⁸	k_c [W/m-K]	h [W/m ² -K]
342.7	0.0041	0.00015	0.0006	6.06	0.3554	19.0	28,390

To compute a conservative estimate for the fuel pin temperature, the authors used a low estimate for the heat transfer coefficient by assuming minimal nucleate boiling. Unless otherwise noted, all thermophysical properties and equations are taken from Nuclear Heat Transport by M. M. El-Wakil.

$$t_c = t_b + \frac{q'''s}{h} \quad \text{Equation 21: Temperature at Cladding/Fluid Boundary.}$$

$$t_g = t_c + \frac{q'''sc}{k_c}$$

Equation 22: Temperature at Cladding/Gap Boundary.

$$t_s = t_g + \frac{q'''sg}{k_g}$$

Equation 23: Temperature at Gap/Fuel Boundary.

$$t_m = t_s + \frac{q'''s^2}{2k_f}$$

Equation 24: Temperature at Fuel Center.

Key:
 k#: Thermal conductivity for substance # s: Fuel radius
 h: Heat transfer coefficient h: Heat transfer coefficient g: Gap thickness
 t_b: Fluid bulk temperature q''': Volumetric thermal energy rate c: Cladding thickness

By starting with a maximum bulk fluid temperature of 290 °C, the authors calculated the maximum temperature throughout the core during normal operation and listed these temperatures in **Table 19**.

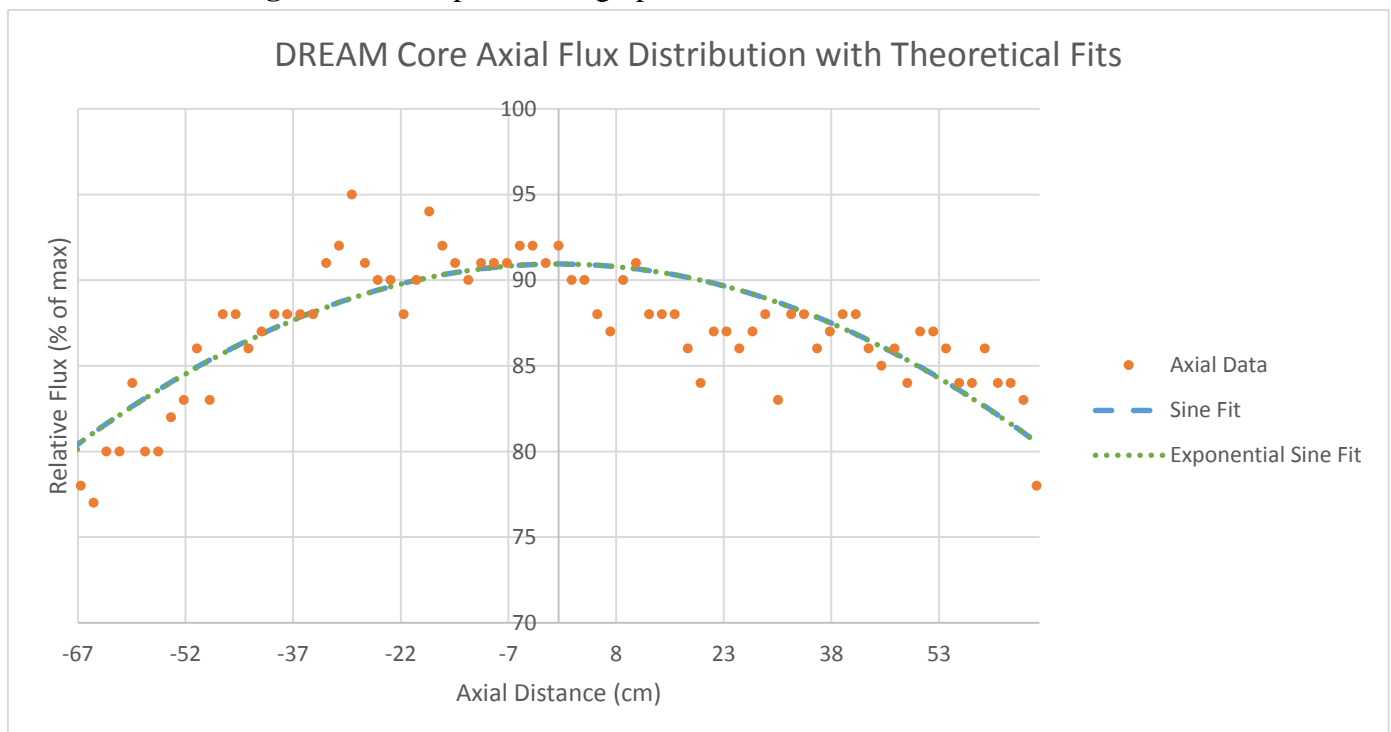
Table 19: Temperatures of a Fuel Rod.

	t _{fluid}	t _{cladding}	t _{gap}	t _{fuel}	t _{midpoint}
°F	554	643	723	1,790	2,650
°C	290	340	384	977	1,460

After analyzing the radial temperature profile of a fuel rod, the authors analyzed the axial temperature profile of a fuel rod and the critical temperatures along the fuel rod. By dividing the critical temperatures by the fuel rod temperatures, the authors also generated a departure from nucleate boiling chart.

Although the authors expected the axial profile to vary with an exponential sinusoidal fit, the authors instead found that a sinusoidal fit worked nearly as well when fit via least-squares regression, both of which are plotted in **Figure 36**.

Figure 36: Flux profile fits graphed on the actual axial flux distribution.



Therefore to simplify the analysis, the authors assumed a sinusoidal heating flux throughout the reactor core. If the heat capacity of water is approximated to be constant throughout the reactor core, the temperature at an axial position is then given by **Equation 25**, with $z = 0$ at the entrance to the reactor core.

$$T(z) = T_i + \frac{(T_f - T_i)}{2} \int_0^z \sin \frac{\pi z'}{H} dz' \quad \text{Equation 25: Axial Fuel Pin Temperature.}^{29}$$

By integrating this equation, the authors formed **Equation 26**.

$$T(z) = T_i + \frac{(T_f - T_i)}{2} \left(1 - \cos \frac{\pi z}{H}\right) \quad \text{Equation 26: Integrated Axial Temperature.}$$

By using **Equation 26**, along with the sinusoidal heat flux and **Equation 18** for the critical heat flux, the authors generated the plots listed in the *Reactor Core Design* section.

After analyzing the thermal hydraulics of the DREAM reactor core, the authors carefully analyzed the reactor neutron economy by running multiple tests with MCNP. The core was initially designed with no *burnable poison*, which resulted in a k_{eff} of 1.4234 and an excess reactivity, ρ_{ex} , of 0.297. This large amount of excess reactivity was deemed unsafe by the authors, so 600 ppm of burnable boron poison was inserted into the core to reduce the excess reactivity and to stabilize the reactivity throughout the life of the core.

With the concentration of the burnable poison set and all other key parameters for the core finalized, an in depth analysis of the core was begun. The authors began with the gradual insertion of the control rods into the core in order to establish at which bank height the core would become critical. After multiple MCNP runs the authors concluded that the core went critical at a bank height of 43.5 cm. The reactivity of the core at various bank heights can be seen below in **Figure 37**.

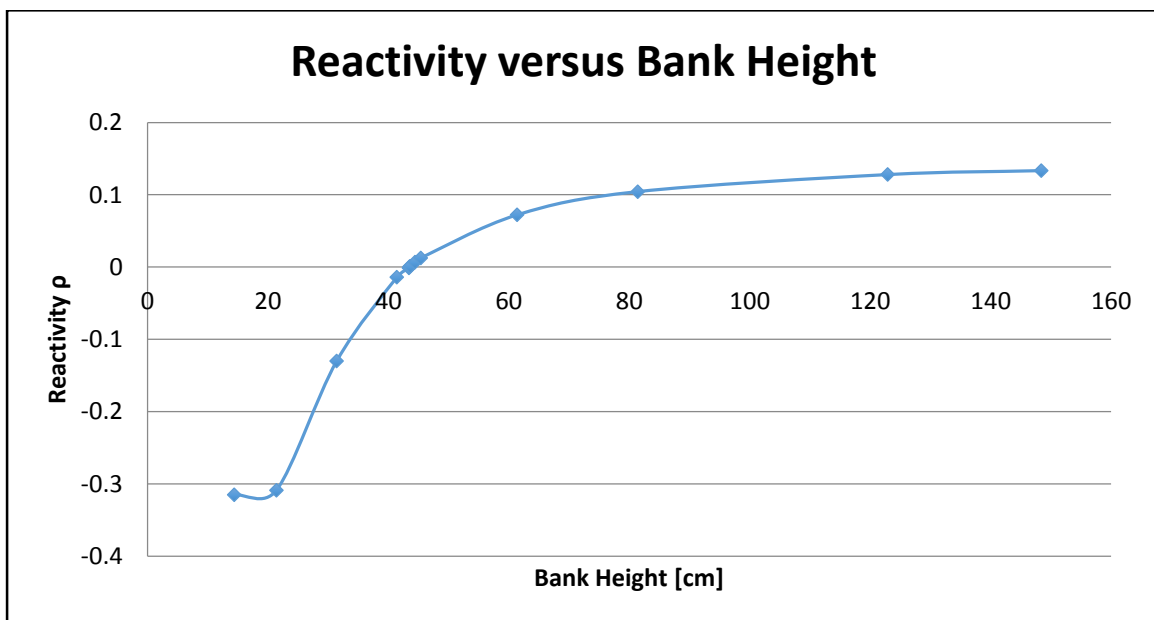


Figure 37: Beginning-of-life reactivity for the reactor core at various control rod bank heights.

To further analyze the DREAM core throughout its lifetime, a burnup calculation was run using MCNP, in which an assumption was made that the burnable poison would be removed from the core linearly. The MCNP code listed in **Appendix H** was setup to produce burnup outputs every 100 days and to track all of the isotopes created inside of the fuel. Once the calculation was completed it was found that the DREAM core would only last for about 1,000 days (approximately 2 years and 9 months) with an accumulated burnup of 37.04 GWd/MTU, only 91.7% of the desired 3 year operational range. Because this time period is very close to the desired 3 year operational range, the authors are confident that additional analysis and optimization would permit operation of the DREAM core for the desired 3-year time frame. The computed burnup over the life of the core is shown below in **Figure 38**, with and without the 600-ppm burnable poison to emphasize the impact of the poison. Each data point corresponds to 100 days of core life.

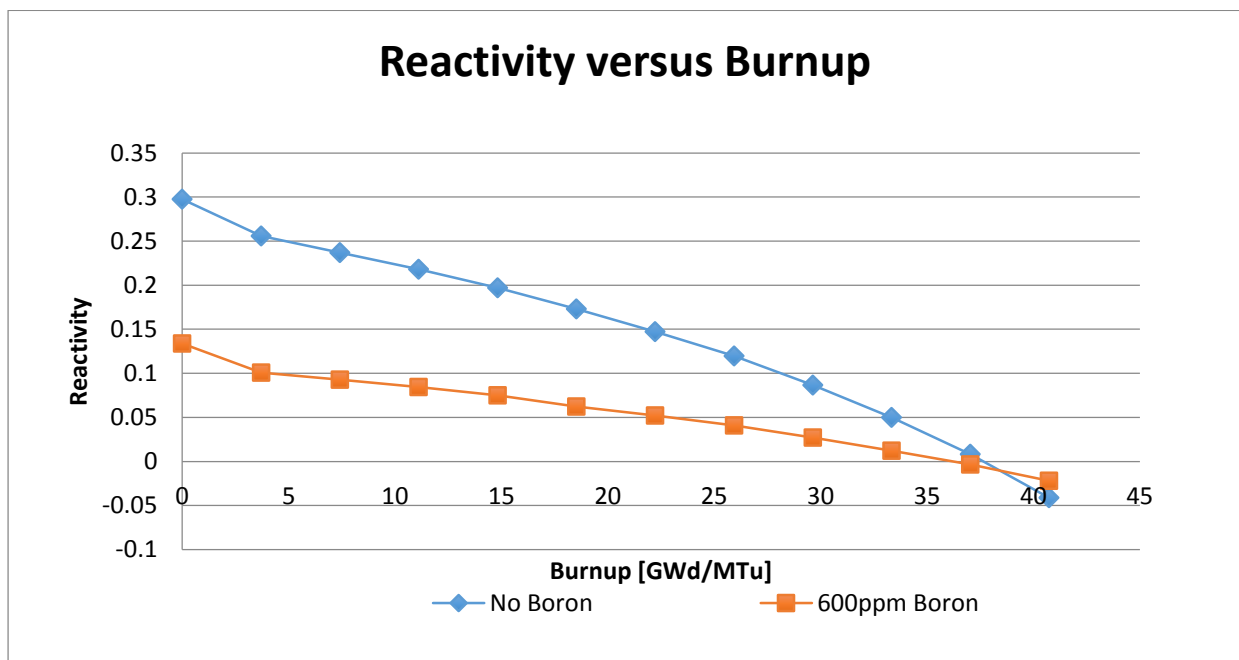


Figure 38: Reactivity versus Reactor Core Burnup.

In addition to tracking the reactivity and burnup of the core throughout its lifetime, the authors also wished to track the fissile isotopes in order to ensure proper reactor behavior. The authors expected a steadily decreasing supply of ^{235}U , with a gradual increase in both ^{239}Pu and ^{241}Pu ending with a near 50/50 split between plutonium and uranium energy production at the end of core life. After tracking the fissile isotopes through the 1,100-day burn up, the authors determined and listed in **Figure 39** that only about 26% of the fissile material was made up of ^{239}Pu and ^{241}Pu , likely due to the lower-than-average flux in the DREAM core. Because of the less-pronounced plutonium breeding, this effect may be the reason for the DREAM core lasting for a slightly-shorter time frame than what was expected.

Lastly, the authors looked at several safety coefficients—boron worth, moderator void coefficient and fuel temperature coefficient—to ensure that the reactor would operate safely under off-normal situations. The core was analyzed under transient conditions for each coefficient, with the results listed below in **Table 20** and **Table 21** along with the corresponding transient perturbation. In order to obtain these values, **Equation 27** was used.

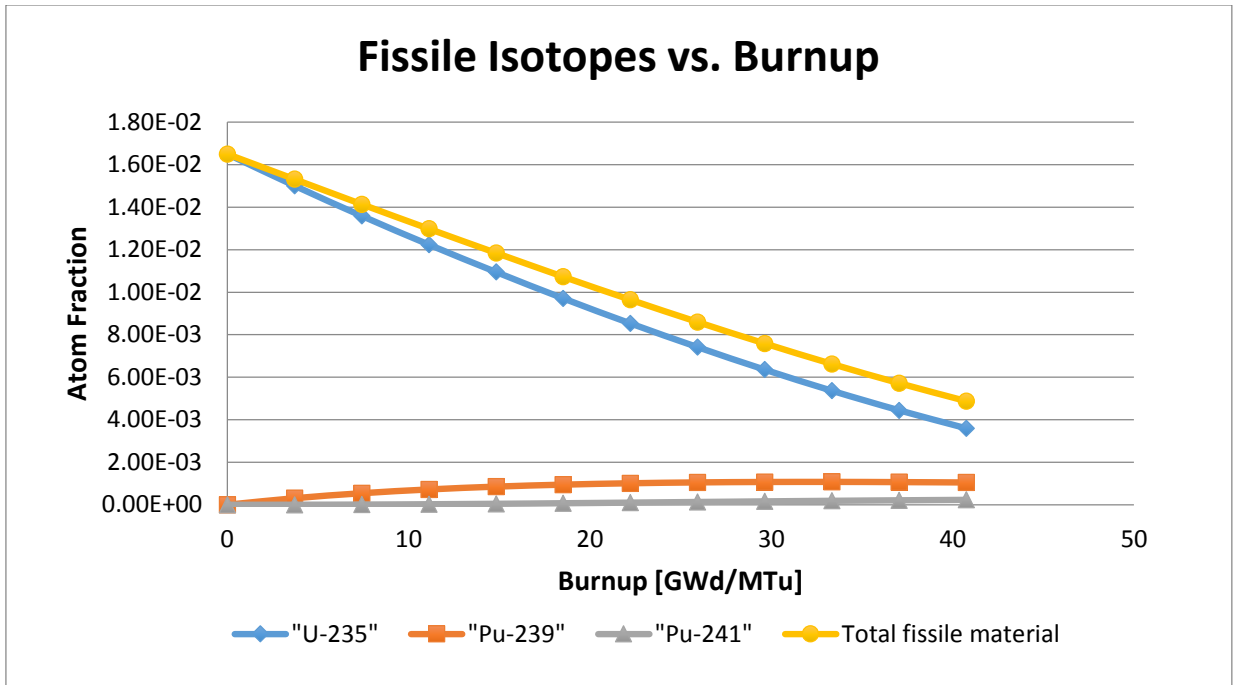


Figure 19: Tracking of fissile material throughout the lifetime of the Dream Core

$$\frac{\partial \rho}{\partial X} = \frac{\Delta \rho}{\Delta X} \quad \text{Equation 27: Differential reactivity from perturbations with discrete steps.}$$

In this equation, $\Delta \rho$ was the change in reactivity as a result of the perturbation and ΔX was the perturbation. As listed in **Table 21**, the DREAM core has a negative reactivity effect near the end-of-life. However, at the beginning-of-life the moderator density depicts a positive void coefficient, as also listed in **Table 20**.

Table 20: DREAM reactor core perturbation analysis results (beginning-of-life)

	<i>Perturbation</i>	<i>Reactivity Change [pcm]</i>
Moderator Density	-1%	87.79
Fuel Temperature	+200 K	-0.4285 ^a
Boron Worth	+33 ppm	-2.557 ^b

- a. Normalized to a 1 K increase.
- b. Normalized to a 1 ppm increase.

Table 21: DREAM reactor core perturbation analysis results (near end-of-life, 900 days)

	<i>Perturbation</i>	<i>Reactivity Change [pcm]</i>
Moderator Density	-1%	-53.22
Fuel Temperature	+200 K	-1.053 ^a
Boron Worth	+33 ppm	-38.97 ^b

- a. Normalized to a 1 K increase.
- b. Normalized to a 1 ppm increase.

Although having a positive void coefficient indicates a reactor unstable to pressure

variations, the authors would like to note that temperature increases from a reactivity incursion will quickly swamp the positive void coefficient. Additionally, adding extra boron will also counteract this increase. Finally, the authors recommend additional analysis be done to verify the perturbation analysis, because of the large variations in changes of reactivity between the end-of-life and beginning-of-life.

Spent Fuel

The DREAM team analyzed 3 different methods of transporting spent fuel. After noting that most reactor designs ship spent fuel in a shielding cask with multiple fuel assemblies, the authors decided to ship the DREAM reactor with all 19 fuel assemblies in a HT9 Stainless Steel cask. The DREAM team analyzed 1 fuel assembly stored in a 50 cm radius steel shielding cask to first assure a criticality value of less than one. By adding the next layer of fuel assemblies, the authors analyzed 7 fuel assemblies stored in an 85 cm radius concrete shielding cask to assure a criticality value of less than 1. Finally, 19 fuel assemblies were analyzed with a 110 cm radius concrete cask. For all of these analyzed situations, the 50 cm, 85 cm, and 110 cm radii included the fuel assemblies along with the concrete, with the graphite radial reflector removed from around the fuel assemblies. A summary of this reactivity analysis is listed in **Table 22** and plotted in **Figure 40**.

Table 22: Reactivity Analysis for the DREAM spent fuel casks.

# of fuel assemblies	Radius (cm)	K
1	50	.33
7	85	.51
19	110	.58

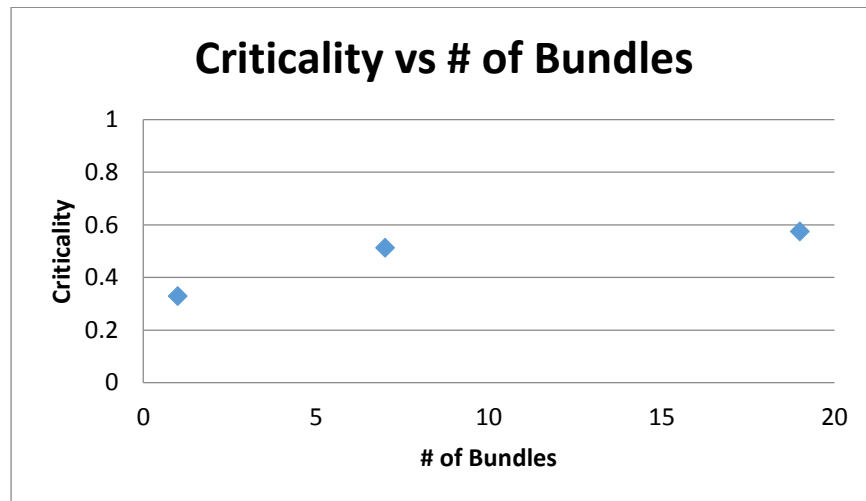


Figure 40: Criticality of the spent fuel casks versus number of assemblies per cask.

All of these analyses were performed using MCNP version 5 (MCNP5) and MCNP version 6 (MCNP6). From the results, the authors decided to ship the DREAM reactor spent fuel in one concrete cask with all 19 fuel assemblies, the MCNP code of which is listed in **Appendix N**.

The DREAM team also used MCNP5 to analyze the flux and dose equivalent. The dose was measured 1 meter away from the spent fuel cask to determine the approximate dose to an individual at that position. The shielding analysis was done using combined neutron and gamma tallies in MCNP5. The DREAM team used tally type 4 (Flux averaged over a cell) to approximate the flux and to approximate the dose. To simplify the analysis, the radiation from the fuel was approximated as a point source at the center of the fuel from typical LWR spent fuel.⁴⁵ The intensity of the source was pulled from a similar reactor type to finish the MCNP5 energy card. Using all these parameters, the flux maps shown in **Figure 41** were generated, along with the neutron flux plotted in **Figure 42** and listed in **Table 23**. However, the gamma tallies displayed as 0 mRem/hr, indicating no gamma dose or flux. For future work the DREAM team will use variance reduction to determine the gamma flux and dose.

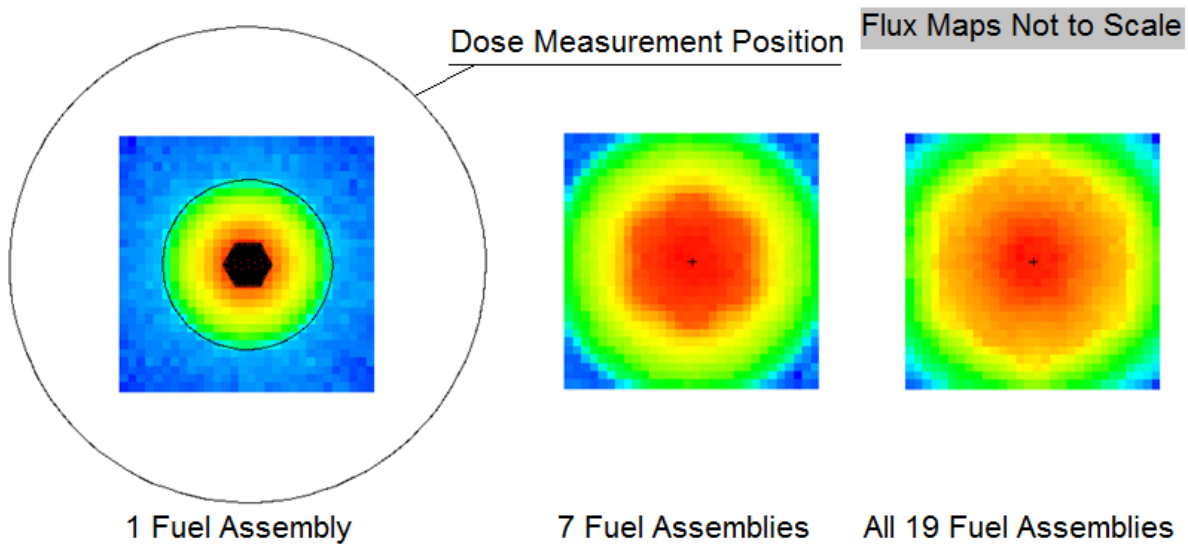


Figure 41: Flux Maps from all analyzed spent fuel shipping casks.

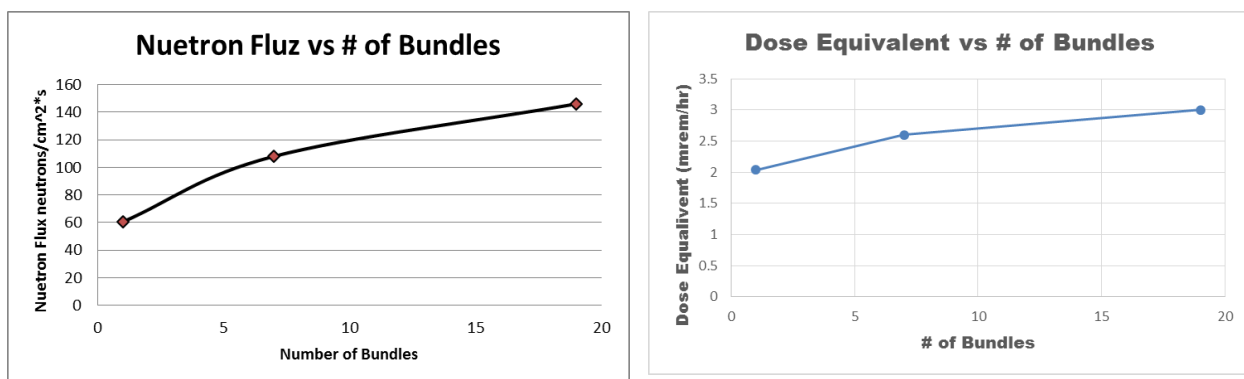


Figure 41: Neutron Flux and Dose versus Bundle Count for the spent fuel casks.

Because the dose-equivalent is less than 5 mRem/hr at the contact point where the spent fuel canister would be handled,⁴⁶ the spent fuel assemblies do not need to be separated for shipping. Therefore according to **Table 22** and **Table 23**, the DREAM spent fuel can be shipped with 19 fuel assemblies together without accidental criticality occurring or exposing the surrounding area to excessive radiation dosages.

Table 23: Neutron Flux and Dose for the spent fuel casks calculated from MCNP5.

# of Fuel Bundles	Flux (n/cm ² -s)	Dose Equivalent (mRem/hr)
1	60.5	2.04
7	108	2.6
19	146	3

RPV Strength and Natural Circulation

Designing the DREAM core to support natural circulation removes the need for primary-loop coolant pumps, reducing system weight and cost. Natural circulation also increases system safety through passive decay heat removal from the core under accident scenarios.¹

Because the DREAM designers wanted the benefits of natural circulation, manual calculations were done to determine the required RPV chimney height at which natural circulation would occur. These calculations also allowed for the integrated pressurizer to be designed. Finally, both of these parameters allowed for the RPV inner structure to be designed, as shown earlier in **Figure 5**.

The authors conducted a manual natural circulation analysis by comparing the pressure drops from acceleration, friction, and constrictions to the pressure rises from expansions and gravitational buoyancy. Through equating the drops to the losses, the authors determined the minimal RPV height for natural circulation. The authors used the following equations²⁹, generalized to SI units from the Imperial standard, to determine the pressure drops and rises:

$$\Delta P_{acceleration} = G^2(v_f - v_i) \quad \text{Equation 27: 1-Phase Acceleration } \Delta P \text{ loss.}$$

$$\Delta P_{area\ change} = \rho(A_{out}v_{out})^2 \left(\frac{1}{A_{in}A_{out}} - \frac{1}{A_{out}^2} \right) \quad \text{Equation 28: Flow area } \Delta P \text{ changes.}$$

$$\Delta P_{buoyancy} = g(\rho_{core}H_{core} + \rho_{hot}H_{chim} - \rho_{SG}H_{SG} - \rho_{cold} * (H_{core} + H_{chim} - H_{SG})) * g$$

Equation 29: Gravitational Buoyancy ΔP driving force for all core components.

Key: G: Mass velocity A: Flow area μ : Liquid viscosity
 ρ : Liquid density v: Fluid velocity g: Gravitational constant
 H#: Height of the specified component #

For an initial approximation of the core height, the authors took the densities and velocities to be constant in the reactor core, steam generator, riser, and downcomer. The fluid turnaround points, where the flow transitions from the riser to the steam generator and the downcomer to the reactor core, were also designed so that no pressure losses occurred at those points. Because the DREAM core operates in the single-phase regime of liquid water, the authors consider this approximation reasonable. With the EES calculation code in **Appendix L**, the authors determined the required natural circulation chimney height to be 8.4 m.

With the natural circulation height, the authors were able to complete the design of the pressurizer in the RPV. Similar to NuScale's and MODULUS's designs, the DREAM design integrates the pressurizer into the RPV to both decrease system size and penetrations through the RPV.^{12, 13} In these designs, the pressurizer consists of an electric heater at the top of the RPV

which increases the system pressure by forming water vapor. To prevent excessive mixing of the flowing liquid water with the water vapor in the pressurizer, a flow barrier is used below the pressurizer in NuScale's design.¹³

To determine the pressurizer height, the authors first used the natural circulation EES code to determine the maximum fluid velocity occurring in the RPV. This velocity, 1.23 m/s, could cause the fluid to rise at most 7.7 cm above the turnaround height if, as indicated with **Equation 30**, all the kinetic energy were converted to gravitational energy. Therefore, the authors set the pressurizer height to 20 cm, with 12 cm of leeway to prevent the fluid from hitting the heater coils at the top of the pressurizer.

$$h = \frac{v^2}{2g} \quad \text{Equation 30: Energy Balance between gravity and velocity.}$$

Additionally, due to the slow flow speed present in the DREAM design and large spacing between the fluid surface and top of the RPV, the authors decided that no flow separator would be required in the DREAM pressurizer.

Combining all these parameters gives a total RPV height of 11.02 m. In comparison, NuScale's RPV is designed with a total height of about 45 feet (13.7 m) to permit natural circulation.¹³ However, because NuScale's design operates at a higher pressure and higher thermal power than the DREAM design, NuScale's RPV design is expected to be taller than the DREAM design. While MODULUS was unable to achieve natural circulation because of a lower core temperature difference (~20 °C)¹², both the DREAM and NuScale reactor cores feature higher core temperature differences (~30 °C)²³ which makes natural circulation easier to achieve.

Removable Core Module Structure (RCMS)

The authors estimated that the core would be supported in the RPV if the circular cutout area was 1 cm in thickness. In order to analyze these structural supports, the authors determined the estimated core mass, 5.89 metric tons, by using the specified reactor core parameters. This mass was then converted to a gravitational force on the circular cutout support structure of 56.8 kilo-Newton (kN).

Due to the complicated design of the RCMS, manual calculations are not able to verify the fitness of the RCMS for the DREAM design. Therefore, the authors ran a numerical, static-structural ANSYS simulation of the RCMS taking into account the gravitational force from the core, maximum design pressure of the RPV, and component fixture from the SAE 12.9 bolts.

The input mesh to ANSYS and the resulting scaled deflection map of the RCMS are displayed in **Figure 42**. From this simulation, the maximum deflection of the RCMS was computed to be 4.8 mm, with negligible deflection on the circular cutout core support structure.

Containment Strength and Shielding

The authors first analyzed the radiation protection required for the containment by estimating the radiation emitted from the reactor core. The amount of radiation was initially estimated as 1.52×10^{13} n/cm²-s from the reactor core and 4.22×10^{11} γ/cm²-s by assuming approximately 5 MeV of the 180 MeV fission energy produces gamma radiation⁴⁷. However, as listed in the **Reactor Core Updates** section, at full power the average core neutron flux is

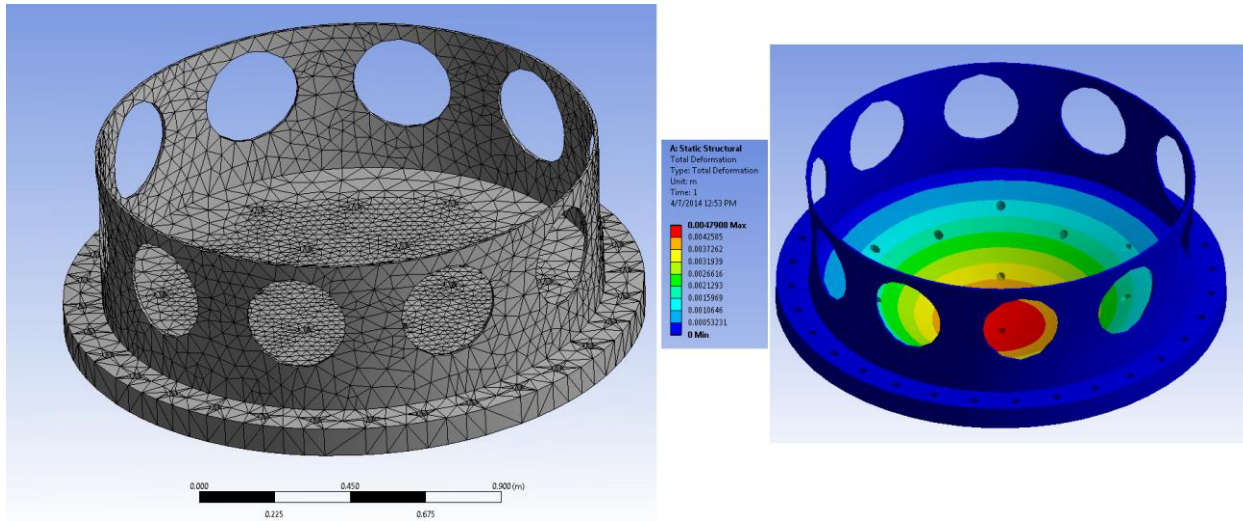


Figure 42: RCMS Mesh and 53x scale⁺ Deflection Map.

+Actual deflections are unnoticeable with an unscaled deflection map.

The mesh quality is limited by the ANSYS Academic Teaching license to 32,000 nodes and elements.

$4.31 \cdot 10^{13}$ n/cm²-s with an estimated gamma flux of $1.20 \cdot 10^{12}$ γ/cm²-s. Additionally, at the end-of-life of the reactor core, the neutron flux is $1.07 \cdot 10^{14}$ n/cm²-s with a gamma flux of $2.97 \cdot 10^{12}$ γ/cm²-s – higher than both the estimates! Therefore, the authors designed the containment using the lower radiation estimate but also verified the containment would provide sufficient radiation protection by using the higher radiation estimate.

In addition, none of these flux measurements list the average neutron-particle or gamma-ray energy. For the neutrons, the authors assumed a thermal distribution because of the large volume of water in the RPV. For the gamma rays, the authors did not assume any average energy but instead chose energies for an average gamma buildup of 1.1. Because a gamma buildup increases the estimated radiation dose, this assumption results in a conservative radiation shielding estimate.

To estimate the maximum flux outside of the RPV, the authors approximated the flux to fall off linearly throughout the RPV. The authors also applied **Equation 31** for neutron attenuation, and **Equation 32** for gamma attenuation.

$$I_n = I_{o,n} e^{-\Sigma_r x} \quad \text{Equation 31: Neutron attenuation for thermal neutrons.}^{47}$$

$$I_\gamma = B I_{o,\gamma} e^{-\mu x} \quad \text{Equation 32: Gamma attenuation with buildup.}^{47}$$

In these equations, I_o is the initial flux, x is the material thickness, B is the buildup from lower-energy gamma rays, Σ_r is the neutron attenuation coefficient, and μ is the gamma attenuation coefficient. The results from the flux attenuation calculations are listed in **Table 24**.

After determining the flux exiting from the RPV, the authors determined the required thickness of water around the RPV to reduce the radiation dose below 2.5 mR/hr. For the gamma rays, the authors applied **Equation 33** to determine the dose, setting the average gamma energy to a conservative value of 5 MeV. This equation results in a maximum gamma flux of $3.56 \cdot 10^7$ γ/cm²-s.

Table 24: Neutron flux and gamma flux attenuation through the RPV.

<i>Material</i>	<i>Start Radius (cm) / Thickness (cm)</i>	$1/\Sigma_r$ (cm) / $1/\mu$ (cm)	<i>Neutron Flux (n/cm²-s)</i>	<i>Gamma Flux (γ/cm²-s)</i>
SS-316	75 / 2	6.34 / 5.56	1.08*10 ¹³	3.16*10 ¹¹
H ₂ O	77 / 84.4	9.70 / 50.0	8.57*10 ⁸	4.18*10 ¹⁰
SS-316	161.4 / 8.94	6.34 / 5.56	1.98*10 ⁸	1.19*10 ¹⁰

$$Dose \left(\frac{mR}{hr} \right) = 519.4 * I_o \left(\frac{\gamma}{cm^2s} \right) * E (MeV) / 3.7 * 10^{10} \quad \text{Equation 33: Gamma dose.}^{47}$$

For the neutrons, because the neutrons are all thermalized after passing out of the RPV, the authors limited the flux to 680 n/cm²-s which reaches the dose limit of 2.5 mR/hr.⁴⁷ For both forms of radiation, the authors assumed quadratic distance attenuation away from the RPV.

By backtracking the attenuation distance in water using **Equation 31** and **Equation 32**, the authors initially determined that 1.12 m of water was needed to reduce the neutron dose, and 2.38 m of water was needed to reduce the gamma dose.

However, after performing the radiation estimates again with the end-of-life radiation estimates, the authors found a gamma flux of 7.02*10⁷ γ/cm²-s past the water shield, well above the limit listed above. Therefore, the authors performed an additional radiation attenuation calculation including the 6 cm of SS-316 comprising the containment. This material had not been included in the initial estimate because the containment design had not been finalized. This extra analysis resulted in a gamma flux of 2.55*10⁷ γ/cm²-s outside of the SS-316 containment wall, which is under the maximum permissible gamma flux.

The authors decided to use stainless steel 316 for the containment for its high corrosion resistance and compactness in comparison to concrete. After deciding on SS-316 the thickness of the containment was determined from the pressure which the containment would be designed to withstand. Using the ideal gas law it was determined that if a breach in the RPV occurred the pressure in the containment would rise from 1 atm to 13 atm. For additional safety it was determined that the containment would be designed to withstand 20 atm of pressure. The authors are confident that with a containment spray system, and the fact that this pressure is nearly twice that of the containments of PWRs, the containment will not experience a pressure difference greater than 20 atm.

Using the physical properties of SS-316 the authors calculated the required thickness of the containment to withstand a 20 atm pressure difference. For a cylindrical pressure vessel, the authors used **Equation 12** as done for the RPV. By using this equation and the material properties of SS-316, the authors calculated the minimum thickness *b* of the pressure vessel to be 3.99 cm. However, accounting for a safety factor of 1.5, the minimum thickness is then 5.98 cm. At this thickness the containment can withstand a maximum pressure difference of 30 atm.

Design Safety

Although the authors were not able to perform a safety assessment to determine an approximate core damage frequency, the authors instead considered several different accident scenarios and how the DREAM design would react to those scenarios.

For the first scenario, the authors considered a loss-of-power accident. In this scenario, no power is available to run the secondary-loop, instrumentation, or control rod drives. Because the

DREAM design has gravity-inserted control blades, this design will automatically SCRAM if a loss-of-power occurs. As discussed in the *Containment Design* section, the containment fill water will then boil and be vented through a pressure-operated valve upon reaching 20 atm in pressure. Although this process will remove the containment fill water acting as a radiation barrier in the DREAM design, the authors expect the neutron and gamma dose to be adequately shielded by the RPV and containment because the reactor is not actively operating. If power has not been restored by 28 days, the authors expect that natural convection with the outside air or thermal radiation will adequately cool the core. However, for future analysis a more in-depth consideration of the heat transfer in this accident scenario should be considered.

For the second scenario, the authors considered a breach in the RPV. Because the DREAM RPV operates at nearly half the pressure of a typical PWR, the authors expect that flying debris from the breach to be of minimal concern. This lower pressure also allows for the containment to easily prevent the potentially-radioactive RPV water from escaping to the environment, as discussed in the *Containment Strength and Shielding* section. Finally, because the DREAM design contains fill water past the height of the reactor core, the reactor core can never become exposed to air without the containment itself leaking.

For the third scenario, the authors considered a breach in the thermodynamic cycle, also known as a loss-of-heat-sink accident. Because the secondary-loop is isolated from the primary-loop, the authors do not anticipate any removal of radioactive material in this event. If the secondary-loop becomes completely inoperable, the DREAM design would have to be cooled using the containment water, similar to the situation analyzed in the loss-of-power accident.

Finally for the fourth scenario, the authors considered a plethora of system malfunctions. If the DREAM reactor SCRAMs with the most worth control blade stuck at full out, the DREAM core will become subcritical, allowing for a safe system shutdown. If the RCMS becomes disconnected from the RPV, the control blades will SCRAM the reactor and the control blades will physical prevent the reactor core from falling into the containment. Finally if a fuel pin fails, the primary-loop water remains separate from the secondary-loop water, which prevents the release of radioactive material.

Design Economics

Because the design requirements for the DREAM specified that the design must be economically competitive with other energy options⁶, the authors began computing the costs required to construct, operate, and retire the DREAM design. This analysis was started by estimating the material costs for the current DREAM design and the manufacturing costs for the components of the DREAM design.

The material costs for the DREAM design were determined by finding the mass of each custom component and the per-mass material costs for the material for each component. These per-mass costs were analyzed as after-manufacturing costs, including the cost for machining tails. All per-mass costs were normalized to 2013 dollars, which are listed in **Table 11**. This table does not list the cost for the uranium fuel, because of the additional calculation steps required in the economic analysis.

The authors then determined the masses of all non-fuel components of the current DREAM design and multiplied these masses by the per-mass material costs listed in **Table 25**, resulting in the custom-made material component prices listed in **Table 26**.

Table 25: Per-Mass Material costs used in the DREAM design (excluding reactor fuel).

<i>Material</i>	<i>Year</i>	<i>Non-normalized Cost (\$/kg)</i>	<i>Cost (2013 USD, \$/kg)</i>
Stainless Steel Alloy 316 ⁴⁸	2009	4.40	4.77
Nickel-based Alloys ⁴⁸	2009	29.00	31.42
Zirconium ⁴⁹	2013	64.00	64.00
Helium ⁵⁰	2011	34.69	35.95
Water ⁵¹	2004	0.00053	0.00065
Concrete ⁴⁸	2010	0.04	0.044
Graphite (non-powder) ⁴⁸	2011	15.00	15.54
Boron Carbide ⁵²	2011	200	207.26
Boric Acid ⁵³	2013	23.34	23.34

Table 26: Material costs for the custom-made components in the current DREAM design.

<i>Component</i>	<i>Material</i>	<i>Mass (metric tons)</i>	<i>Material Cost (\$)</i>
RPV outer shell	SS-316	87.88	419,200
RPV inner shell	SS-316	7.59	36,200
RPV lid	SS-316	6.74	32,124
RCMS	SS-316	1.76	8,400
Steam Generator Tubes	Sanicro 69 (Nickel-based Alloy)	21.30	669,200
Condenser Tubes	SS-316	5.04	24,034
Radial Reflector	Graphite	2.53	39,400
Axial Reflectors	Graphite	0.37	5,800
Fuel Cladding	Zircally-4 (Zirconium-based Alloy)	0.62	39,900
Fuel Gap	Helium	< 0.01	< 100
Control Rods	Boron Carbide	0.49	101,600
RPV fill material	Water	6.70	< 100
Containment fill ⁺	Water	218.27	200
Containment	SS-316	492.86	2,055,300

+ Includes water surrounding the RPV in the containment to a height of 5 m.

After determining the material costs for components in the DREAM design, the authors estimated the manufacturing costs to convert the raw materials into finished products. Until more accurate machining information can be acquired, the authors have estimated machining costs as equivalent to the material costs of each component, which doubles the price of each part. Although this scaling will tend to underestimate the low-material cost components of the DREAM design, such as the graphite reflectors, this scaling will overestimate the machining cost of high-material cost components. Because the DREAM design consists of large volumes of expensive steels, the authors consider the machining estimate a reasonable approximation.

Because enrichment and spent fuel disposal should be considered in the cost of uranium fuel, the authors conducted a more detailed economic analysis. First, the authors determined that the DREAM reactor core contains 291,767 cm³ (3.06 metric tons) of 4.95% enriched UO₂ fuel. This mass is equivalent to 2.70 metric tons of heavy metal after converted from oxide form. The authors then ran an economic optimization using **Equation 34**, **Equation 35**, and **Equation 36**; a 0.711 weight % ²³⁵U feed concentration; and the step costs listed in **Table 27** to determine an optimal tails ²³⁵U weight percent of 0.369 %. This economic analysis used a discount factor of 10%, which was provided in a sample problem in NE 571. With the optimal tails concentration, the authors determined the mass flow rates for each step and listed these rates in **Table 27**. The optimization and mass flow rate EES code is listed in **Appendix M**.

$$\frac{F}{P} = \frac{x_p - x_w}{x_F - x_w} \quad \text{Equation 34: Feed and Product Mass Flow Rate Ratio.}^{54}$$

$$\frac{W}{P} = \frac{x_p - x_F}{x_F - x_w} \quad \text{Equation 35: Waste and Product Mass Flow Rate Ratio.}^{54}$$

$$\frac{S}{P} = V_p + \frac{W}{P} V_w - \frac{F}{P} V_F \quad \text{where } V_i = (2x_i - 1) \ln \left(\frac{x_i}{1-x_i} \right)$$

Equation 36: Separative Work and Product Mass Flow Rate Ratio.⁵⁴

Key: P: Product mass flow rate W: Waste (tails) mass flow rate x_i: ²³⁵U fraction for each flow i
 F: Feed mass flow rate S: Separative work mass flow rate

To determine the step costs listed in **Table 27**, the authors took a similar table listed in the “Nuclear Power: Nuclear Fuel Cycle – Mining-Milling” handout provided in NEEP 571, copied over the relative times and costs, and converted the costs from year 2000 USD to year 2013 USD. The mass flow rates were also changed to reflect the mass flow rates in the DREAM design.

Table 27: Mass Flow Rates and Unit Costs for each Manufacturing Step.⁵⁵

Step	Mass Flow Rate	Cost/Step (2013 USD)	Relative Time (year)
Mining & Milling	42,646 kg U ₃ O ₈	\$35.36 / kg U ₃ O ₈	0
UF ₆ Conversion	36,166 kg U	\$4.68 / kg U	0.5
Enrichment	17,080 SWU	\$180.43 / SWU	0.7
Waste (Tails)	33,470 kg U	Assumed Negligible	0.7
Fabrication	2,700 kg HM	\$126.97 / kg HM	1.2
Spent Fuel Transport ⁺	2,700 kg HM	\$20.05 / kg HM	6
Spent Fuel Storage	2,700 kg HM	\$6.68 / kg HM	7-11
Spent Fuel Disposal	2,700 kg HM	\$133.65 / kg HM	11

⁺ Only includes additional safety costs in transporting spent fuel, not the transportation costs to and from the remote operational site of the DREAM reactor.

To determine the total cost for refueling, the authors summed all the costs listed in **Table 27** after converting these costs to be all relative to the start of irradiation time at year 2. The authors also added the estimated total costs for the control rods, graphite reflectors, zirconium cladding, fill gas, and RCMS to the total fuel cost, because these components are removed from

the reactor as a module, as shown in **Figure 31**. The resulting costs for refueling, excluding transportation, are listed in **Table 28**.

Table 28: DREAM reactor refueling costs.

<i>Component</i>	<i>Cost (2013 USD)</i>
Control Rods	203,200
Axial and Radial Graphite Reflectors	90,400
Zirconium Cladding	79,800
Fill Gas	< 200
RCMS	18,800
Total Non-Fuel Cost	390,400
Fuel Cost	5,744,000
Estimated Replacement Operation Cost ⁺	80,000
Total Refueling Cost	6,214,400

+ Team of 100 working at \$50/hour for one work-day (8 hours)

for Brayton and Stirling systems, the estimate closely matches a 833 \$/kWe estimate for the entire Rankine cycle of a solar power plant.⁵⁷ Therefore, the authors decided it was appropriate to use in the DREAM design.

Even though the authors did not finalize the design of systems necessary for a PWR, such as the boric acid chemical control system, the authors were able to estimate the cost of including such systems in the design. The resulting construction cost, including these systems, is listed in **Table 29**.

Table 29: DREAM design construction costs.⁺

<i>Item</i>	<i>Parameter</i>
Raw Materials for Custom Components	\$3,236,100
Manufacturing Factor	2x
Custom Components	\$6,472,200
Thermodynamic Components	\$80,000,000
Accident Prevention and Limitation Systems ⁴⁸	\$5,508,100
Water Filtration System ⁴⁸	\$6,196,600
Subtotal	\$98,176,900
Prototyping Factor	2x
Total	\$196,353,700

+ Excludes the first fuel and operational material load, such as boric acid.

and RPV fill water, along with 1,600 kg/yr of boric acid. The boric acid amount required was determined by linearly scaling the amount of boric acid consumed by a 600 MWth PWR.⁵⁶ Because the DREAM design mixes the RPV and containment water upon refueling, the authors decided to include the water material cost as an operational cost if extra filtration is required.

Because the DREAM design will be operating in remote locations, the authors did not want to heavily-staff the reactor. However, sufficient staff must be at the plant to protect against external threats, provide regular maintenance, and handle unexpected scenarios. Therefore, the authors estimated the number of employees and their salaries by linearly-scaling the number of employees at Point Beach to the thermal power output of Point Beach (1026 MWth)⁵⁸ and the

To determine the total construction cost for the DREAM design, the authors estimated manufacturing and prototyping scale factors of 2. Because the authors did not receive any quotes for the thermodynamic components used, the authors estimated a cost of 800 \$/kWe for both turbines and the pump.⁵⁶

Although this thermodynamic estimate was

To determine the total operational cost for the DREAM design, the authors included the refueling costs listed in **Table 29** along with additional costs for operational materials. These materials included the containment

costs as used for the DREAM design except without the fuel cost, the same fixed charge rate, and an estimated construction cost of \$80 million per 4S reactor.¹¹ With these parameters, the author calculated a levelized cost of electricity of 29.98 mills/kWh for the 4S reactors. As analyzed before, if the total number of employees is instead 280, the levelized cost of electricity is 100.80 mills/kWh for the 4S reactors.

Finally, the authors computed the cost for operating the DREAM design during a 3-year period plus the levelized construction costs during that period. This total cost was then compared to the total cost for several other portable power supplies all producing the same power as the DREAM design. The total volume for the compared power supplies is listed in **Table 32** and the total prices for the compared power supplies is listed in **Table 33**.

Table 32: Total volumes for each portable power supply.

<i>Technology</i>	<i>Non-Fuel Volume (m³)</i>	<i>Combined Volume (m³)</i>
NiMH ^a	N/A	2,115,000
Ultracapacitor ^a	N/A	114,100,000
Lithium ^a	N/A	675,600
Diesel Gen	707.7	255,600
CCGT	1,894	810,100
Solar PV ^b	16,730 ^c	18,660
4S SMR	3,425	3,429
DREAM SMR	2,716	2,717
Antimatter	2,716	3,031

a. System terminals and case included as “fuel”.

b. 18.5% efficient with 4.5 kWh/m²-day.^{61, 10, 35}

c. Including NiMH battery backup system for uninterrupted operation.

Although the DREAM design has a larger system volume than the fossil-fuel based systems, the authors note that fuel volumes dwarf the combined volumes for these power supplies.

Table 33: Non-fuel prices and total prices.

<i>Technology</i>	<i>Non-Fuel Price</i>	<i>Total Price (2013 USD)</i>
NiMH ^a	N/A	607,500,000,000
Ultracapacitor ^{a,b}	N/A	13,550,000,000,000
Lithium ^a	N/A	400,500,000,000
Diesel Gen	128,600	266,100,000
CCGT	432,700	30,110,000
Solar PV	4,175,000	558,900,000
4S SMR	17,400,000	17,400,000
DREAM SMR	15,110,000	21,330,000
Antimatter	150,110,000	262,700,000

a. Neglecting support circuitry.

b. Neglecting electricity costs for charging.

From this analysis, the authors would like to note that the DREAM design is economically competitive to both fossil-fuel and renewable power supplies in providing large amounts of power for long periods of time. As listed in **Table 33**, this design is also economically

comparable to other SMRs, such as Toshiba’s 4S SMR. Finally for brevity’s sake, the detailed calculations and citations for all other portable power supplies are listed in **Appendix A**.

Design Transportation

To determine how to transport the DREAM design, the authors first determined the total system volume and mass. A summary of this analysis is provided in **Table 34**. Although the authors were unable to determine the exact masses of the thermodynamic components, the total mass was estimated from the dimensions of each component and the density of stainless steel.

Table 34: DREAM component volumes and masses.

<i>Component</i>	<i>Volume (m³)</i>	<i>Total Mass (metric tons)</i>
Containment w/ RPV inside	822	889
Condenser	1,525	5.04
Thermodynamic Components	369	462
Total	2,716	1,356

After determining the total volume and mass of the DREAM design, the authors estimated the number of semi-trailers it would take to ship the DREAM design. To simplify the analysis, the authors assumed all components could be split into separate parts which would be attached or welded together on-site. Because this number depends upon how efficiently each component can be packed into the semi-trailers, the authors generated **Figure 43**. This figure details the number of required semi-trailers by volume and by mass, when each semi-trailer is assumed to hold at most 114.7 m³ and 18.37 metric tons of material.^{62, 63}

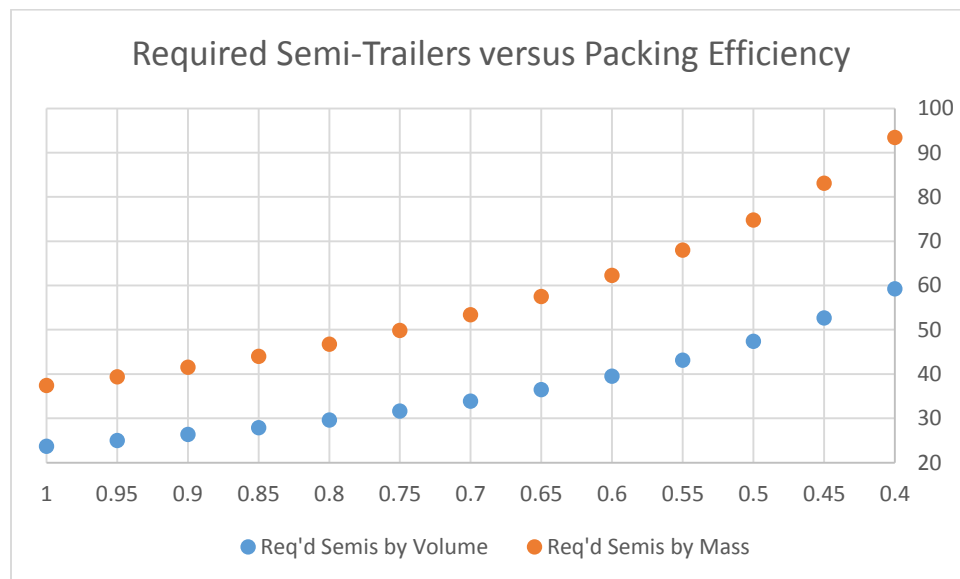


Figure 43: Semi-Trailer Transportation Requirement

To avoid using more than 50 semi-trailers, which the authors have arbitrarily-set as a limit for which using standard semi-trailers seems impractical, the DREAM design will need to pack with an efficiency of at least 75%. From geometrical analysis, because a circular shape can fit into a

square cutout with a packing efficiency of 78.54%, the authors are confident that the DREAM design can ship via semi-trailers, needing at most 50 semi-trailers and ideally 38.

Unfortunately, because of the heavy containment vessel used in the DREAM design, this design cannot fit into a single airplane for deployment. With a packing efficiency of 75%, this design fits into 6 Boeing 747-8F aircrafts by volume (857.7 m^3 cargo capacity/aircraft)⁶⁴ or 11 by weight (134 metric tons cargo weight/aircraft)⁶⁴.

4 Conclusion

The DREAM design holds a thermal efficiency competitive to the four other existing designs compared. However, the DREAM design varies substantially from other small modular reactor designs. In addition, while this design has been heavily-analyzed, more design work and analysis work must be done to actually build a DREAM.

Proposed Design Comparisons

The DREAM design's 29.2% thermal efficiency is competitive with the four other existing designs described in the previous progress report. While the DREAM does contain two steam generators, each steam generator serves a different part of the thermodynamic cycle. This design is similar to NuScale's design, except that NuScale's steam generators both serve the same part of NuScale's thermodynamic cycle. The dry condenser used in the DREAM design allows for operation in dry climates, unlike the other four designs.

By using a lower-pressure primary-loop cycle, the DREAM design will remain reasonably portable, and safer, than other existing designs. Like the other designs, the DREAM uses 4.95% fuel, with a once-through easily-removable reactor core module. This module is removed in a manner similar to NuScale's design, through the bottom of the RPV. However unlike NuScale's design, this removable structure also carries the control rods to facilitate replacement of the control rods with the core.

Unlike the other researched designs, the DREAM uses slightly-smaller, hexagonal fuel assemblies. The DREAM reactor core is also controlled using hollow hexagonal control blades, versus the standard control rods used in the other researched designs. Finally, the DREAM reactor core contains a graphite reflector around the core, which is similar to the SP-100 design, but the DREAM's reflector is used only for flux smoothing.

While both the DREAM design and the NuScale design refuel by pulling the reactor core out the bottom of the RPV, the method in which this is performed varies substantially with these two designs. With NuScale's design, the lower half of the reactor pressure vessel is removed completely.¹³ However with the DREAM design only a small part of the reactor pressure vessel is removed, the part of which also holds onto the reactor core.

Finally, the DREAM design is very comparable to other designs in terms of portability and economics. In particular, 2.9 Toshiba 4S reactors capable of supplying 29 MWe in total would cost \$232 million,¹¹ in comparison to the \$197 million required for the DREAM design. However, over a 39 year operating period the 4S design is economically-competitive, because of the higher refueling costs for the DREAM design. Both designs are much more economically competitive than fossil fuel or renewable sources of electricity when providing large amounts of electricity for extended periods of time.

Future Work

Although the authors have successfully designed the DREAM device to meet the requirements for their senior design course, there are several facets of the design which could be improved. These facets include analyses which were not possible to complete in the limited time the authors had available and design work which builds upon the current DREAM design. This section provides a non-comprehensive list of features the authors would improve upon the DREAM design if this design is considered for future analysis.

For future work on the thermodynamic cycle, the authors would acquire manufacturing and transportation quotes for the thermodynamic components. The authors would also design the complete valve system for the thermodynamic cycle and estimate the economics of this system. Finally, the authors would design the steam generator feed tubes, which connect the thermodynamic cycle outside of containment to the steam generator inside of the RPV.

For future work on the reactor core, the authors would perform a radiation damage estimate of the Zircaloy-4 fuel cladding. Because the DREAM design operates at a lower flux level than a typical LWR, the authors do not anticipate any structural damage to the fuel cladding from the radiation damage. However, completing this analysis would verify the integrity of the cladding and further clarify the safety in the DREAM design. The authors would also complete the spent fuel analysis to acquire the flux and dose for gamma rays, instead of just neutrons.

For future work on the reactor pressure vessel, the authors would analyze changing the cylindrical shape to a cylinder with spherical ends. Although the ends may be harder and more costly to manufacture, this shape may prevent flow stagnation in the corners of the vessel. The authors would also perform a computational fluid dynamic (CFD) simulation of the RPV, determine the maximum lifetime of the RPV from radiation damage estimations, and design the mounting structure to connect the RPV to the containment.

For future work on the containment, the authors would determine what foundation would be necessary to mount the DREAM design upon. The authors would also analyze a spherical end for the roof of the containment, similar to the end design for the reactor pressure vessel. Finally, the authors would verify through flow calculations that natural convection can sufficiently cool the reactor core after 29 days in the event of a loss-of-power accident.

For future work on the entire DREAM design, the authors would acquire accurate quotes for all manufacturing processes required in constructing the DREAM design. The authors would also determine how long each manufacturing process would take and how long constructing the DREAM design would take. Based upon the construction time estimates, the authors would be able to verify the 7 work-day maintenance estimate in the event a major non-fuel component needed replacement. The authors would also completely 3D model the thermodynamic side of the DREAM design, so that the transportation packing factor of the design could be computed. Finally, because standard electrical components—such as transmission wires and transformers—have not been included in this design, the authors would determine which components are necessary and add them to the DREAM design.

5 References

1. “Current Status, Technical Feasibility, and Economics of Small Modular Reactors,” Organization of Economic Cooperation and Development, Nuclear Energy Agency (2011). Retrieved February 2, 2014 from <http://www.oecdnea.org/ndd/reports/2011/current-status-small-reactors.pdf>.
2. “Nuclear Reactors,” Information Digest 2013-2014, Nuclear Regulatory Commission (2014). Retrieved February 10, 2014 from <http://www.nrc.gov/reading-rm/doc-collections/nuregs/staff/sr1350/v25/sr1350v25-sec-3.pdf>.
3. “KLT-40S System Overview,” International Atomic Energy Agency (2013). Retrieved January 28, 2014 from <http://www.iaea.org/NuclearPower/Downloadable/aris/2013/25.KLT-40S.pdf>.
4. J. F. Aherne, et. al, “The Future of Nuclear Power in the United States,” Federation of American Scientists, Washington and Lee University (2012). Retrieved January 29, 2014 from http://www.fas.org/pubs/_docs/Nuclear_Energy_Report-lowres.pdf.
5. G. A. Coles, et. al, “Trial Application of the Facility Safeguardability Assessment Process to the NuScale SMR Design,” Pacific Northwest National Laboratory (2012).
6. “Small Modular Reactor (SMR) Design Requirements,” NEEP 412 Senior Design (2014).
7. “Generation mPower Snapshot,” The Babcock & Wilcox Company (2013). Retrieved February 16, 2014 from <http://www.babcock.com/library/Documents/SP201-100.pdf>.
8. “737 Airplane Characteristics for Airport Planning: Airplane Description,” Boeing (2013). Retrieved February 16, 2014 from <http://www.boeing.com/assets/pdf/commercial/airports/acaps/737sec2.pdf>.
9. Y. Zhou, R. SJ. Tol, “Evaluating the Cost of Desalination and Water Transport, “Sustainability and Global Change Research Unit, Hamberg University and Centre for Marine and Atmospheric Science (2004). Retrieved February 15, 2014 from http://web.archive.org/web/20090325031333/http://www.uni-hamburg.de/Wiss/FB/15/Sustainability/DesalinationFNU41_revised.pdf.
10. “Levelized Cost of New Generation Resources in the Annual Energy Outlook 2013,” U. S. Energy Information Administration, Annual Energy Outlook (2013). Retrieved May 2, 2014 from http://www.eia.gov/forecasts/aeo/er/electricity_generation.cfm.

11. G. Fay and T. Schwörer, “Potential Economies of Nuclear Small Modular Reactor Technology For Alaska,” SMR Workshop, University of Alaska – Anchorage Institute of Social and Economic Research (2010). Retrieved May 2, 2014 from <http://www.uaf.edu/files/acep/Ginny-Fay---Potential-Economics-of-Nuclear-Small-Modular-Reactor-Technology-for-Alaska.pdf>.
12. Z. Bundies, L. Loehrke, B. Semerau, “MODULUS Design,” NEEP 412 Senior Design (2011).
13. “NuScale Plant Design Overview,” NuScale Power, LLC (2012).
14. M. D. Carelli, “IRIS: A Global Approach to Nuclear Power Renaissance,” Nuclear News (2003).
15. S. F. Demuth, “SP100 Space Reactor Design,” Los Alamos National Laboratory (1970).
16. N. Berrahmouni, N. Burgess, “Northern Africa,” World Wildlife Foundation (2014). Retrieved February 15, 2014 from <http://worldwildlife.org/ecoregions/pa1327>.
17. G. F. Nellis, S. A. Klein, Thermodynamics, 1st ed., p. 396, 405, Cambridge University Press, New York (2012).
18. "Sanicro 69 (Tube and pipe, seamless)," Sandvik Materials Technology (2014). Retrieved April 3, 2014 from <http://www.smt.sandvik.com/en/materials-center/material-datasheets/tube-and-pipe-seamless/sanicro-69/>.
19. G. G. Eichholz, Environmental Aspects of Nuclear Power, 4th ed., Ann Arbor Science Publishers, Inc (1982).
20. “Dry Cooling Systems,” SPX Power+Energy (2014). Retrieved March 11, 2014 from <http://spxcooling.com/pdf/drycooling-13A>.
21. “Bing Maps (Cartographer),” Microsoft Corporation (2014). Retrieved March 24, 2014 from <http://binged.it/1dECrkR>.
22. “ModuleAir™ Air Cooled Condenser,” SPX Power+Energy, Dry Cooling Insight (2014). Retrieved March 12, 2014 from <http://spxcooling.com/pdf/IN-DryMA-13.pdf>.

23. "Rule 1: The Field," National Football League (2013). Retrieved March 26, 2014 from http://static.nfl.com/static/content/public/image/rulebook/pdfs/4_2013_Field.pdf.
24. D. Olander, Fundamental Aspects of Nuclear Reactor Fuel Elements, 1st ed, Ch. 10, p. 136, U. S. Department of Energy (1976).
25. "Evaluated Nuclear Data File (ENDF) Retrieval and Plotting," ENDF/B-VII.1, National Nuclear Data Center (2011). Retrieved February 14, 2014 from <http://www.nndc.bnl.gov/sigma/>.
26. J. J. Duderstadt, L. J. Hamilton, Nuclear Reactor Analysis, 1st ed., p. 68, 81, John Wiley & Sons, Inc (1976).
27. T. Goorley, et. al, "Initial MCNP 6 Release Overview", LA-UR-11-07082, Los Alamos National Laboratory, also Nuclear Technology, 180, p. 298-315 (Dec 2012).
28. C. L. Whitmarsh, "Review of Zircaloy-2 and Zircaloy-4 Properties relevant to N. S. Savannah Reactor Design," Oak Ridge National Laboratory (1962). Retrieved April 11, 2014 from <http://www.ornl.gov/info/reports/1962/3445605716311.pdf>.
29. M. M. El-Wakil, Nuclear Heat Transport, 3rd ed., p.105, 233, 336-352, 368-399, International Textbook Company (1981).
30. "Thermophysical Properties of Materials for Nuclear Engineering: A Tutorial and Collection of Data," International Atomic Energy Agency (2008). Retrieved March 28, 2014 from http://www-pub.iaea.org/MTCD/Publications/PDF/IAEA-THPH_web.pdf.
31. "The Atlas Steels Technical Handbook of Stainless Steels," Atlas Steels (2013). Retrieved March 29, 2014 from <http://www.atlassteels.com.au/documents/Atlas%20Technical%20Handbook%20rev%20Aug%202013.pdf>.
32. Roylance, Pressure Vessels, Massachusetts Institute of Technology (2001). Retrieved March 27, 2014 from <http://web.mit.edu/course/3/3.11/www/modules/pv.pdf>.
33. R. C. Juvinall, K. M. Marshek, Fundamentals of Machine Component Design, 5th ed., p. 276, 444, John Wiley & Sons, Inc (2012).
34. M. Ragheb, Nuclear, Plasma, and Radiation Science. Inventing the Future, Ch. 8, Sec. 6 (2011). Retrieved May 9, 2014 from <http://www.ewp.rpi.edu/hartford/~ernesto/F2011/EP/MaterialsforStudents/Petty/Ragheb-Ch8-2011.PDF>.

35. "Average Daily Solar Radiation, Annual Average," National Renewable Energy Laboratory Resource Assessment Program (1990). Retrieved April 30, 2014 from http://rredc.nrel.gov/solar/old_data/nsrdb/1961-1990/redbook/atlas/colorpdfs/208.PDF.
36. "Energy Requirements for Desalination Processes," "Encyclopedia of Desalination and Water Resources (2014). Retrieved February 15, 2014 from <http://www.desware.net/desa4.aspx>.
37. "Steam Turbines, Balance of Plant, & Services," Arani Power Systems Limited (2014). Retrieved March 22, 2014 from http://aranipower.com/images/pdfs/Arani_Products_Online.pdf.
38. "GE Oil & Gas: Industrial Steam Turbines," GE Oil & Gas (2014). Retrieved March 22, 2014 from http://site.ge-energy.com/businesses/ge_oilandgas/en/downloads/st_tur_cat.pdf.
39. "Pre-designed Steam Turbines: The comprehensive product range up to 12 megawatts," Siemens (2014). Retrieved March 22, 2014 from http://www.energy.siemens.com/us/pool/hq/power-generation/steam-turbines/Pre-Designed_Steam_Turbines_en.pdf.
40. "Industrial Steam Turbines: The comprehensive product range from 2 to 250 megawatts," Siemens (2014). Retrieved March 22, 2014 from http://www.energy.siemens.com/hq/pool/hq/power-generation/steam-turbines/Industrial_Steam_Turbines_en.pdf.
41. "Roto-Jet[®] High Pressure Pitot Tube Pumps: Model RO D--850," Weir Specialty Pumps (2012). Retrieved March 20, 2014 from <http://www.weirpowerindustrial.com/pdf/Roto-Jet%20Model%20RO%20D-850.pdf>.
42. K. C. Weston, *Energy Conversion – The Ebook*, 1st ed, p. 45, 47 (1992). Retrieved March 20, 2014 from <http://www.personal.utulsa.edu/~kenneth-weston/chapter2.pdf>.
43. "Water Products Technical Data and Pump Fundamentals," ITT Manufacturing Enterprises, Inc (2010). Retrieved March 22, 2014 from <http://www.aquaflo.com/downloads/Residential%20Water%20Products%20Tech%20Manual.pdf>.
44. B. A. Hands and V. D. Arp, "A Correlation of Thermal Conductivity Data for Helium," *Cryogenics*, 21(12): 697-703 (1981).

45. "Evaluation of Shielding Analysis Methods in Spent Fuel Cask Environments," Electric Power Research Institute, Oak Ridge National Laboratory (1995). Retrieved May 9, 2014 from <http://www.epri.com/abstracts/Pages/ProductAbstract.aspx?ProductId=TR-104329>.
46. A. A. Simpkins, "Spent Nuclear Fuel: An Environmental and Regulatory Perspective," Dade Moeller & Associates (February 18, 2011). Retrieved May 5, 2014 from http://www.moellerinc.com/docstore/Ali_Simpkins_AAS_SNF_Risk_2_18_presentation.pdf.
47. J. E. Turner, Atoms, Radiation, and Radiation Protection, 3rd ed., p.232, 477, 480, 498, Wiley-VCH, Weinheim (2012).
48. W. D. Callister, D. G. Rethwisch, Materials Science and Engineering: An Introduction, 8th ed., Appendix C, WileyPLUS (2009).
49. P. J. Loferski, Mineral Commodity Summaries: Zirconium and Hafnium, USGS Mineral Commodity Specialists (2013). Retrieved April 15, 2014 from <http://minerals.usgs.gov/minerals/pubs/commodity/zirconium/mcs-2013-zirco.pdf>.
50. N. Pacheco, Mineral Commodity Summaries: Helium, USGS Mineral Commodity Specialists (2011). Retrieved April 15, 2014 from <http://minerals.er.usgs.gov/minerals/pubs/commodity/helium/mcs-2011-heliu.pdf>.
51. "Drinking Water Costs & Federal Funding," Office of Water, EPA (2004). Retrieved April 15, 2014 from http://water.epa.gov/lawsregs/guidance/sdwa/upload/2009_08_28_sdwa_fs_30ann_dwsrf_web.pdf.
52. C. S. Wiley, "Synergistic methods for the production of high-strength and low-cost boron carbide," Dissertation (2011). Retrieved April 17, 2014 from <http://udini.proquest.com/view/synergistic-methods-for-the-pqid:2417078201/>.
53. "99.5% Purity Boric Acid, 325 lb drum," Fisher Chemicals (2014). Retrieved April 22, 2014 from <http://www.fishersci.com/ecom/servlet/fsproductdetail?storeId=10652&productId=772155&catalogId=29104>.
54. M. Corradini, "Uranium Conversion and Enrichment," NEEP 571 Environmental and Economic Aspects of Nuclear Power (2014).
55. M. Corradini, "Nuclear Power: Nuclear Fuel Cycle – Mining-Milling," NEEP 571 Environmental and Economic Aspects of Nuclear Power (2014).

56. R. L. Loftness, Nuclear Power Plants: Design, Operating Experience, & Economics, 1st ed, p. 514, 523, D. Van Nostrand Company, Inc: Princeton (1964).
57. C. J. Winder, R. L. Sizmann, L. L. Vant-Hull (eds.), Solar Power Plants: Fundamentals, Technology, Systems, Economics, 1st ed, p. 373, 380, 387, 388, Springer-Verlag: Berlin (1991).
58. "Point Beach Nuclear Power Plant Fact Sheet," NextEra Energy Resources (2014). Retrieved April 25, 2014 from the Point Beach Energy Center.
59. "Fact Sheet on Reactor License Renewal," U. S. Nuclear Regulatory Commission, Office of Public Affairs (2012). Retrieved April 26, 2014 from <http://www.nrc.gov/reading-rm/doc-collections/fact-sheets/fs-reactor-license-renewal.pdf>.
60. "Super-Safe, Small and Simple Reactor (4S, Toshiba Design)," Toshiba Corporation and Central Research Institute of Electric Power Industry (CRIEPI), Japan (2013). Retrieved May 2, 2014 from <http://www.iaea.org/nuclearenergy/nuclearpower/Downloadable/aris/2013/1.4S.pdf>.
61. "34 Watt Solar Panel Kit Instructions," Parallax, Inc (2012). Retrieved April 30, 2014 from <http://www.parallax.com/sites/default/files/downloads/33000-34-Watt-Solar-Kit-v1.1.pdf>.
62. "Semi-Trailer Dimensions," YRC Freight (2014). Retrieved May 5, 2014 from <http://www.yrc.com/shippers/semi-trailer-dimensions.html>.
63. "Maximum Legal Truck Loadings and Dimensions," Michigan Department of Transportation (2007). Retrieved May 5, 2014 from http://www.michigan.gov/documents/Loads_dim_87014_7.pdf.
64. "747 Family: 747-8 Technical Characteristics," Boeing (2014). Retrieved May 6, 2014 from http://www.boeing.com/boeing/commercial/747family/747-8_fact_sheet.page.
65. "Application Notes & Product Data Sheet: Primary Batteries – Alkaline & Heavy Duty," Rayovac OEM (1999). Retrieved April 21, 2014 from [http://www.rayovac.com/~media/Rayovac/Files/Product%20Guides/pg_battery.ashx](http://www.rayovac.com/~/media/Rayovac/Files/Product%20Guides/pg_battery.ashx).

66. "Energizer NH15-2300 product datasheet," Energizer (2008). Retrieved April 21, 2014 from <http://data.energizer.com/PDFs/nh15-2300.pdf>.
67. "Battery Model TLH-5903," Tadiran Lithium Batteries (2006). Retrieved April 21, 2014 from <http://www.tadiranbat.com/pdf.php?id=TLH-5903>
68. "PowerStor Supercapacitors: XV Series," Cooper Bussmann (2012). Retrieved April 21, 2014 from <http://www.cooperindustries.com/content/dam/public/bussmann/Electronics/Resources/product-datasheets/bus-elx-ds-4424-xv-series.pdf>.
69. R. A. Serway, Physics for Scientists and Engineers, 6th ed., p. 670, 807, Brooks Cole., Stamford (2003).
70. "Well-to-Wheels Analysis of Future Automotive Fuels and Powertrains in the European Context," European Commission Directorate-General Joint Research Centre, Version 2c (March 2007).
71. D. J. Schlossberg, et. al., "A Thomson scattering diagnostic on the Pegasus Toroidal experiment," Review of Scientific Instruments, 83, 10E335 (2012).
72. Chart of the Nuclides: Nuclides and Isotopes, Knolls Atomic Power Laboratory, Inc., 16th ed, p. 40, 89, Lockheed Martin: Bethesda (2002).
73. "Centurion 'M' Series Model 2000 CM & CM3," Generator Joe (2014). Retrieved April 30, 2014 from <http://www.generatorjoe.net/html/genjoe/TA/GJCM-2000D333.pdf>.
74. "Energizer NH15-VP Ordering Information," Digikey Corporation (2014). Retrieved April 21, 2014 from <http://www.digikey.com/product-detail/en/NH15VP/N703-ND/1040723a>.
75. "PowerStor Supercapacitor Ordering Information," Digikey Corporation (2014). Retrieved April 21, 2014 from <http://www.digikey.com/product-detail/en/XV3560-2R7407-R/283-4209-ND/3878067>.
76. "Tadrian Lithium Battery Ordering Information," Digikey Corporation (2014). Retrieved April 21, 2014 from <http://www.digikey.com/product-detail/en/TL-5903%2FT/439-1016-ND/512518>.
77. "Petroleum & Other Liquids: Gasoline and Diesel Fuel Update," U. S. Energy Information Administration (April 21, 2014). Retrieved April 21, 2014 from <http://www.eia.gov/petroleum/gasdiesel/>.

78. “Natural Gas Weekly Update,” U. S. Energy Information Administration (April 24, 2014). Retrieved April 30, 2014 from <http://www.eia.gov/naturalgas/weekly/#tabs-prices-2>.
79. B. Steigerwald, “New and Improved Antimatter Spaceship for Mars Missions,” Positronics Research, LLC (2006). Retrieved April 30, 2014 from http://www.nasa.gov/exploration/home/antimatter_spaceship.html.
80. C. J. Winder, R. L. Sizmann, L. L. Vant-Hull (eds.), Solar Power Plants: Fundamentals, Technology, Systems, Economics, 1st ed, p. 373, 380, 387, 388, Springer-Verlag: Berlin (1991).
81. “Frequently Asked Questions: How much electricity does an American home use?,” U. S. Energy Information Administration (2014). Retrieved May 9, 2014 from <http://www.eia.gov/tools/faqs/faq.cfm?id=97&t=3>.

6 Design Specifications

Table 35: DREAM Design Specifications Overview

<i>Parameter</i>	<i>Specification</i>
Thermal Power Output	100 MW _{th}
Thermodynamic Efficiency (Carnot/Ideal/Non-Ideal)	42.62% / 33.0% / 29.24%
Electrical Power Output	29.2 MWe
Estimated Levelized Cost of Electricity Range	39 to 110 mills/kWh
Construction Cost	\$196.4 million
Operation Cost (Including 1/3 of a refueling)	\$8.706 million
Refueling Cost (2013 USD)	\$6.214 million
Refueling Interval	3 years
Refueling and Maintenance Time	1 week.
Maximum System Weight	1,356 metric tons
Maximum System Volume	2,716 m ³
Maximum System land area	6,216 m ²

Table 36: DREAM Thermodynamics System Overview

<i>Parameter</i>	<i>Specification</i>
Primary and Secondary Loop Working Fluid	Light Water (H ₂ O)
Primary Loop Pressure	75 atm
Primary Loop High Temperature	290 °C
Primary Loop Low Temperature	260 °C
Primary Loop Mass Flow rate	666.8 kg/s
Secondary Loop High Pressure	47 atm
Secondary Loop Reheat Pressure	11.5 atm
Secondary Loop Condenser Pressure	0.28 atm
HP and Reheat TTD	10 °C
Condenser TTD	10 °C
Maximum Cold Sink Temperature	50 °C
Secondary Loop Mass Flow rate	33.0 kg/s
HP Steam Generator ΔP	105.9 kPa
Reheat Steam Generator ΔP	243.3 kPa
Condenser ΔP	8.64 kPa
HP Turbine Efficiency	92 %
LP Turbine Efficiency	92 %
Pump Efficiency	80 %
Condenser Fan Power (at full power)	8.92 kWe (40% efficient fans)
Pump Power (at full power)	203.0 kWe
HP Turbine Exit Quality	0.905
LP Turbine Exit Quality	0.904
Total Cost	\$80 million

Table 37: DREAM Steam Generator Specifications

<i>Parameter</i>	<i>Specification</i>
Number of Tubes (Main / Reheat)	3,130 / 1,870
Tube Material	Sanicro 69
Tube inner radius	1 cm
Tube thickness	0.25 cm
Tube spacing	1 cm
Tube Height (Main / Reheat)	4.50 m / 0.405 m
Total Cost (2013 USD)	\$1.338 million

Table 38: DREAM Condenser Specifications

<i>Parameter</i>	<i>Specification</i>
Design	SPX ModuleAir™ Dry Condenser
Maximum Thermal Dissipation	70.8 MWth
Input Quality	0.90
Maximum Input Temperature	70 °C
Maximum Outside Temperature	50 °C
Land Area Required (Full Power)	6,070 m ² (1.5 acres)
Transportation Volume	1,525 m ³
Condenser Cost	\$48 thousand

Table 39: DREAM Reactor Pressure Vessel Specifications

<i>Parameter</i>	<i>Specification</i>
Total Height	11.02 m
Total Mass (Excluding primary water & core) (Includes top and bottom lids and both shells)	103.97 metric tons
Primary Water Mass	6.70 metric tons
Pressurizer Height	0.20 m
Core Height	1.63 m
Chimney Height	8.4 m
Steam Generator Maximum Height	4.5 m
Turnaround Height	0.395 m
Outer Radius (not including thickness)	1.614 m
Outer Shell Thickness	8.94 cm
Outer Shell Material	316 Stainless Steel, Standard Grade
Outer Shell Construction	3 forgings with bolted flanges.
Maximum Pressure Rating	112 atm
Inner Flow Barrier Radius	75 cm
Inner Flow Barrier Thickness	2 cm
Inner Flow Barrier Material	316 Stainless Steel, Standard Grade
Inner Flow Barrier Construction	Cold rolled, welded.
System Pumps	0
Natural Circulation Excess Buoyancy	833.5 Pa
Control Rod Locations	Below the core, external drives, gravity-driven.
Vessel Cost (Excluding RCMS, 2013 USD)	\$975 thousand

Table 40: DREAM Reactor Core Specifications

<i>Parameter</i>	<i>Specification</i>
Total Fuel Rod Height	1.63 m
Total Active Height	1.34 m
Total Fuel Rod Radius	0.485 cm
Fuel	UO ₂
Fuel Enrichment	4.95%
New Pellet Radius	0.41 cm
Gap Fill Gas	He
New Gap Fill Pressure	30 atm
Gap Thickness	0.015 cm
Cladding Material	Zircaloy-4
Cladding Thickness	0.060 cm
Fuel Rod Reflector Material	Natural C
Fuel Rod Reflector Sides	Top and Bottom
Fuel Rod Reflector Height	14.4 cm
Assembly Pitch	1.60 cm
Assembly Fuel Rod Arrangement	Hexagonal
Assembly Fuel Rods	217, 9 per side.
Arrangement of Assemblies	Hexagonal
Number of Assemblies	19
Assembly Spacing	1 Fuel Rod apart
Total Core Radius	75 cm
Core Mass (Fuel elements only)	5.79 metric tons
Radial Fill Reflector Material	Natural C
Control Blade Active Material	Boron Carbide
Control Blades	19
Control Blade Shape	Hexagonal outline
Control Blade Locations	One per assembly
Total Module Mass	8.04 metric tons
Total Module Cost (2013 USD)	\$6.214 million

Table 41: DREAM Reactor Core Operation Specifications

<i>Parameter</i>	<i>Specification</i>
Average Heat Flux (Full power)	0.703 MW/m ²
Critical Heat Flux	2.114 W/m ²
Combined Hot-Spot Factor	2.83
Minimum DNBR	1.19 (with hotspot factors)
Total Neutron Flux (past RPV, Full power)	4.31*10 ¹³ n/cm ² -s
Total Gamma Flux (past RPV, Full power)	4.22*10 ¹¹ γ/cm ² -s

Table 42: DREAM Reactor Core Operational Criticality

<i>Core State</i>	<i>Operation History</i>	<i>Run Conditions</i>	<i>Criticality</i>
New Core	Full Power	Normal Operation	1.154
New Core	Full Power	SCRAM	0.887
New Core	Full Power	SCRAM w/ 1 stuck blade	0.961
3 Year Core	Full Power	Normal Operation	0.979
2.75 Year Core	Full Power	Normal Operation	1.008
New Core	Shutdown	All-In	0.916
New Core	Shutdown	Full-Out	1.440
2.75 Year Core	Shutdown	All-In	0.638
2.75 Year Core	Shutdown	Full-Out	1.018

Table 43: DREAM Containment Specifications

<i>Parameter</i>	<i>Specification</i>
Material	SS-316
Height	15 m
Inner Radius	4.10 m
Thickness	6 cm
Fill Materials	Water to 5 m.
Designed/Maximum Pressure Rating	20 atm / 35 atm
Outside Radiation Dose (Sides)	< 2.5 mR/hr
Outside Radiation Dose (Top & Bottom)	< 2.5 mR/hr
Construction Method	Forged segments, welded on-site
Weight	492.86 metric tons.
Total Containment Cost	\$4.111 million

Assembly (Fuel): A collection of several fuel pins bundled together for ease of transportation and to prevent criticality if the *Reactor Core* were shipped intact.

Boiling Water Reactor (BWR): A nuclear reactor using moderately-pressurized-water in the *Primary Loop*, in which boiling occurs in the *Reactor Core* region.

Boron Carbide: Chemically known as B_4C , boron carbide is a strong neutron absorber used for reactor control rods/blades.

Burnable Poison: A chemical introduced into the primary loop which reduces and normalizes the core neutron flux, permitting more stable operation of the *Reactor Core*.

Containment: The structure surrounding the *Reactor Pressure Vessel (RPV)*, which prevents radiation leakage in the event of the failure of the *RPV*, reduces the radiation dose from the *Reactor Core* to safe levels, and protects the reactor against terrorist incidents.

Control Blade: A component which strongly absorbs neutrons from the *Reactor Core*, permitting safe control and operation of the core. The DREAM control blades are composed of *Boron Carbide*, although other materials are available.

Decay Heat: Heat produced from delayed fissions that occur after a nuclear reactor shutdown. Because of these delayed fissions, a nuclear reactor must be cooled after shutdown to prevent core thermal damage.

DREAM: See *Modular Atomic Energy Reactor Device*.

EES Code: EES (Engineering Equation Solver) is a software package developed at the UW-Madison to assist in solving series of equations involving thermophysical fluid data.

Fast Reactor: A nuclear reactor variant which does not moderate (“slow down”) neutrons to initiate a chain reaction, but rather uses the fast neutrons resulting from fission.

Fuel Pin (Reactor Core): A long, thin cylinder containing the fissile fuel protected inside a metal cladding. For the DREAM, each fuel pin consists of *Uranium Oxide (UO₂)* at 4.95% ²³⁵U enrichment, a Helium (He) gap, and a *Zircaloy-4* cladding.

Graphite: A form of pure carbon. Because of its low atomic number, carbon is an excellent neutron reflector used to balance the neutron flux in the *DREAM Reactor Core*.

High Temperature Gas Reactor: A nuclear reactor variant which uses a high temperature gas, such as CO₂ or He to cool and potentially moderate the reactor instead of water. These reactors can reach higher temperatures than LWRs, for a higher thermal efficiency.

Low-Enriched Uranium (LEU): Uranium fuel containing a low fraction of ²³⁵U. Because weapons-grade uranium is typically more than 90% enriched ²³⁵U, LEU is more proliferation resistant than high-enriched uranium.

Light-Water Reactor (LWR): A reactor using normal water as the coolant and moderator. At the current time, all nuclear power plants in the U. S. are *BWR* or *PWR* light-water reactors.

Levelized Cost of Electricity: The price a utility would charge for each unit of energy produced to pay for construction and operation expenses and provide a return-on-investment.

Mega-Watts: A unit of power. This unit is usually expressed as MWth, for thermal power, or MWe for electrical power. Because converting thermal energy to electrical energy is inherently inefficient, the DREAM device operates at 100 MWth, but only provides 29.2 MWe. For comparison, 1 MWe could power approximately 800 U. S. homes in 2013.⁸⁰

Modular Atomic Energy Reactor Device (DREAM): A pressurized-light-water small, modular reactor (PWR SMR) designed for the authors NE 412 Senior Design Course. This design operates with a 3 year refueling cycle and at a power level of 29.2 MWe.

Monte Carlo N-Particle (MCNP): A nuclear particle transport and physics simulation software package, supported by Los Alamos National Laboratory.

Pressurized Water Reactor (PWR): A nuclear reactor using highly-pressurized-water in the *Primary Loop*, to prevent boiling in the *Reactor Core* region.

Phase change: For metals, when the solid changes its internal structural arrangement. This process can cause mechanical stresses and failures, if repeated.

Primary Loop (Thermodynamic cycle): The portion of a nuclear power plant's thermodynamic cycle containing the *Reactor Core*. This loop never leaves the *Containment* to avoid leaking radioactive material to the outside environment.

Reactor Core: The component producing power in the DREAM design, shaped as a cylinder, containing axial and radial *Reflectors* along with 4,123 individual *Fuel Pins* in *Assemblies*. Along with the *Burnable Poison*, the reactor core is controlled with 19 hexagonal *Control Blades*.

Reactor Pressure Vessel (RPV): The structure containing the entire *Primary Loop* for a small, modular reactor. This structure also contains the *Steam Generator*, *Reactor Core*, and *Removable Core Module Structure*.

Removable Core Module Structure (RCMS): The component which supports the *Reactor Core* and easily-removes the core for refueling. The RCMS also contains the holes guiding the control rods out of the core, allowing the control rod drives to be outside of the RPV.

Reflector (Reactor Core): The component of the reactor core, made of *Graphite* in the DREAM design, which reflects neutrons back towards the core, reducing leakage and smoothing out the core neutron flux profile.

Saturation Temperature: Also known as boiling point.

Sanicro 69: An austenitic nickel-chromium-iron alloy designed for use in nuclear power plant steam generators.

SCRAM: An emergency shutdown of a nuclear reactor.

Secondary Loop (Thermodynamic Cycle): The portion of a nuclear power plant's thermodynamic cycle containing the power generation components, such as the turbines. This loop contains no radioactive material in normal operation.

Steam Generator: The component which transfers energy from the *Primary Loop* to the *Secondary Loop*, converting liquid water in the *Secondary Loop* to slightly-superheated steam.

SolidWorks: A 3D engineering modeling package.

SS-316: A corrosion-resistant austenitic stainless steel, used in the *Reactor Pressure Vessel* and *Containment*.

Uranium Oxide (UO₂): The active fuel material in the DREAM design. For standard light-water reactors, the ²³⁵U isotope is typically enriched from its natural fraction of 0.711% to 3-5% to permit a nuclear chain reaction.

Zircaloy-4: A zirconium-based alloy used as cladding for the *Fuel Pins* in the *Reactor Core*. Zircaloy-4 combines high-strength with low thermal neutron absorption, unlike the higher absorption from standard stainless steels.

A: Portable Power Supplies Economic Analysis

Analysis of the portable power supplies was accomplished by researching the per-unit volume, prices, and power density of each power supply. After determining these results and applying reasonable approximations, the authors used simple unit analyses and equivalences to compare each portable power supply.

Per-Unit Volumes

The unit volume of the AA battery used for the NiMH and lithium batteries was determined from the average diameter of 1.4 cm and height of 4.98 cm.⁶⁵ Although the voltage of an NiMH battery fluctuates slightly during discharge, the author used the average rated voltage of 1.2 V and rated amperage delivery of 2300 mAh for analysis.⁶⁶ For the lithium battery, the author used a rated voltage of 3.6 V and rated amperage delivery.⁶⁷ Interestingly, although the voltage of this battery far exceeds that of a standard AA, the lithium battery analyzed is packaged inside an AA case.⁶⁷

The unit volume of the ultracapacitor was also determined from the average diameter of 3.5 cm and height of 6.3 cm.⁶⁸ For the ultracapacitor, the author used a design voltage of 2.7 V and capacitance of 400 F.⁶⁸ To determine the energy stored in the capacitor, the author used **Equation 38**, below.

$$E = \frac{1}{2} CV^2 \quad \text{Equation 38: Capacitor stored energy.}^{69}$$

Although the voltage of a capacitor drops during discharge, making energy retrieval more difficult, the author assumed complete discharge of the capacitors.

The unit volume for diesel, natural gas, and antimatter was taken to be 1 US gallon. For diesel, the energy stored in one gallon was determined from an energy density of 43 MJ/kg and a volumetric density of 835 kg/m³.⁷⁰ For natural gas, the energy stored in one gallon was determined in part from an energy density of 45.1 MJ/kg.⁷⁰ By assuming a majority of methane (CH₄) comprising the natural gas at 25 °C and 25 MPa, EES computed the volumetric density to be 188.2 kg/m³. For antimatter, the energy stored per gallon was determined from a number density of 10¹⁹ #/cm³ by assuming plasma storage in a device similar to the Pegasus experiment⁷¹ and an atomic weight per particle of 1.00783 amu⁷² by assuming an anti-hydrogen plasma. The author doubled the resulting energy/gallon by assuming the power supply system would react the antimatter with ordinary air.

Because the 4S SMR uses solid U-10Zr fuel pins 0.70 cm in radius⁶⁰, the unit volume was taken to be 1 cm in height of a fuel pin. The energy stored for each unit volume was backtracked from the total core energy of 900 MWth-yr with 250 fuel units per fuel pin and 3,042 total fuel pins in the reactor core.⁶⁰ Although the 4S fuel lasts for 40 years⁶⁰, the author only analyzed 3 years of fuel use to permit a fair comparison with the other fuel sources. For the DREAM SMR, the unit volume was taken to be one fuel pellet 0.41 cm in radius, 1 cm in height. The energy stored per fuel pellet was backtracked from the total core energy of 300 MWth-yr with 134 fuel pellets per fuel pin and 4,123 total fuel pins in the reactor core.

Finally, the unit volume of the solar PV battery backup system was determined by first calculating the volume of NiMH batteries required to provide 29 MWe for 24 hours. This value was divided by 86,400, making each unit volume of battery backup capable of supplying 29 MWe-s. For ease of analysis, the author assumed negligible losses in charging and discharging the battery backup system.

Total Volumes

For the NiMH batteries, lithium batteries, ultracapacitors, and solar battery backup, the author simply divided 87 MWe-yr (or 29 MWe for 3 yr) by the total Wh each unit could supply, assuming negligible discharge losses.

For the diesel generators, the author used a thermal-to-electric efficiency of 30%.⁶⁹ For the CCGT, the author used a thermal-to-electric efficiency of 40%.⁶⁹ For the 4S SMR, the author used a thermal-to-electric efficiency of 33%.⁶⁰ For the DREAM SMR, the author used a thermal-to-electric efficiency of 29%. Because less fuel is burned at a lower capacity factor, the capacity factor does not factor in to this part analysis.

To simplify the analysis, the author assumed the cases for the NiMH batteries, lithium batteries, and ultracapacitors to be included in the fuel. Therefore, there was no non-fuel volume for these portable power supplies.

For the diesel generator, the authors used 15 generators providing 2 MW each, having dimensions of 5.99 m by 2.72 m by 2.90 m.⁷³

For the DREAM SMR, the author took the entire system size as the non-fuel volume. Because the author did not find any estimated system sizes for an antimatter system, the antimatter system was assumed to be the same size as the DREAM SMR. For the 4S SMR, the author used the volume of the guard vessel⁶⁰ and the volume of the containment vessel⁶⁰ in combination with the thermodynamic component volume computed for the DREAM SMR. Finally, for the CCGT system, the author estimated the system volume to be only that of the thermodynamic components of the DREAM SMR.

For the solar PV system, the author used a solar cell efficiency of 18.5%,⁶¹ a capacity factor of 25%,¹⁰ and a solar insolation of 4.5 kWh/m²/day³⁵ to determine the area of solar cells required. By estimating the solar cells to be at most 1 cm in thickness, the author determined the total volume of solar cells required.

Per-Unit and Total Prices

The per-unit prices for the NiMH batteries, lithium batteries, and ultracapacitors were determined by researching bulk prices for new units (orders > 5,000 units) from Digikey.^{74,75,76} The author also used these prices to determine the cost of the solar PV battery backup system. The per-unit prices for diesel and natural gas were determined from EIA's weekly price updates for these fuels.^{77,78} Finally, for the DREAM SMR the author used the refueling price determined previously for that design.

Because the 4S SMR does not refuel during its entire 40 year lifespan, the fuel price for this design was combined into the total system price.^{60,11}

For the antimatter system, the author used an estimated price as provided from Positronics Research, a company promoting space travel via antimatter.⁷⁹ However, the authors consider this estimated price very uncertain, due to the limited amount of antimatter production which has been done.

Because the cases for the NiMH batteries, lithium batteries, and ultracapacitors were included in the fuel, no non-fuel prices for these systems were considered. For the diesel generator, the author determined the price for each individual generator and scaled that by the number of generators required.⁷³ For the CCGT system, the author took a per-unit construction cost of \$300/kWe (1991 USD), scaled that to 29 MW, and corrected for inflation.⁸⁰ For the solar PV system, the author scaled down an estimate for a 100 MWe solar PV plant.⁸⁰

For the 4S SMR, the author took a high-end estimate of \$80 million per 10 MWe plant lasting 40 years¹¹, and linearly-sliced this cost for 2.9 plants operating 3 years. Although a more precise analysis would consider the financing done to fund construction costs, this form of analysis results in an overestimate of the required costs by neglecting the interest rate.

For the DREAM SMR, the author took the financial analysis done previously in this report. Because of the uncertainty in constructing an antimatter power plant, the author estimated the antimatter construction cost to be 10 times that of the DREAM SMR's construction cost.

B: Thermodynamic Cycle State and Solution Results

Table 44: Thermodynamic properties at states of the DREAM thermodynamic cycle.

<i>State</i>	<i>h</i> [kJ/kg]	<i>h_{rev}</i> [kJ/kg]	<i>P</i> [kPa]	<i>s</i> [kJ/kg-K]	<i>s_{rev}</i> [kJ/kg-K]	<i>T</i> [°C]
1	257.3	256.1	4,868	0.835	0.831	60.5
2	2,869	<i>N/A</i>	4,762	6.13	<i>N/A</i>	280.
3	2,582	2,557	921.9	6.19	6.13	176
4	3,004	<i>N/A</i>	1,165	6.97	<i>N/A</i>	280.
5	2,398	2,345	28.59	7.13	6.97	68.0
6	251.2	<i>N/A</i>	19.95	0.831	<i>N/A</i>	60.0

Table 45: Summary of results from the DREAM thermodynamic analysis EES code.

<i>Parameter</i>	<i>Specification</i>	<i>Parameter</i>	<i>Specification</i>
x (LP turbine)	90.39 %	Volumetric Flow Rate	0.0335 m ³ /s
x (HP turbine)	90.52 %	Mass Flow Rate	32.96 kg/s
W (LP turbine)	19.97 MW	Carnot Efficiency	42.6 %
W (HP turbine)	9.476 MW	Ideal Efficiency	33.3 %
W (pump)	0.203 MW	Actual Efficiency	29.2 %
Main ΔP Loss	105.9 kPa	Reheat ΔP Loss	243.3 kPa
Condenser ΔP Loss	8.64 kPa	Q (condenser)	70.8 MW

Note: All computer codes are available upon request.

C: Thermodynamic Cycle EES Code

D: Steam Generator Analysis EES Code

E: Homogeneous Reactor Core MCNP Code

F: Infinite 2D Square Lattice MCNP Code

G: Initial 3D Hexagonal Reactor Core MCNP Code

H: DREAM Reactor Core MCNP Code (with commented-out Burnup Code)
I: Condenser pressure loss EES Code
J: Condenser land area and energy use EES Code
K: Critical Heat Flux Analysis EES Code
L: Natural Circulation Analysis EES Code
M: Uranium Fuel Price Optimization EES Code
N: 19 Assembly Spent Fuel Cask MCNP Code